

## **XFT Upgrade Options and Studies**

Benjamin J. Kilminster, Kevin P. Lannon,  
Brian L. Winer, Richard E. Hughes  
*Ohio State University*

Gregory Veramendi, Kevin Pitts  
*University of Illinois at Urbana*

### Abstract

The demands of increasing luminosity require an XFT upgrade. This note examines a number of upgrade possibilities to determine which meet the needs CDF's needs. The criteria considered include reducing the 7 GeV single-track trigger cross section by a factor of 3-4 and reducing the scenario C two-track trigger by a factor of 2-4, while maintaining the high  $P_T$  physics program. Although several upgrade possibilities meet these requirements, the option of keeping the existing XFT axial system and adding a stereo upgrade involving COT superlayers 3, 5, and 7 provides the greatest gains for the smallest amount of risk and difficulty.

## Contents

<b>1</b>	<b>Introduction to XFT</b>	<b>1</b>
<b>2</b>	<b>Axial Upgrade Details</b>	<b>3</b>
<b>3</b>	<b>Stereo Upgrade Details</b>	<b>4</b>
<b>4</b>	<b>Data Simulation at High Luminosities</b>	<b>6</b>
4.1	Luminosity Extrapolation . . . . .	6
4.2	COT Performance Degradation . . . . .	7
4.3	XFT Simulation . . . . .	8
4.4	XFT Simulation Validation . . . . .	8
<b>5</b>	<b>Track Trigger Rates at High Luminosities</b>	<b>11</b>
5.1	7 GeV Single-Track Trigger . . . . .	12
5.2	Scenario A and C Two-Track Trigger . . . . .	12
<b>6</b>	<b>Electron Trigger Rates at High Luminosities</b>	<b>45</b>
6.1	Simulated Electron Selection . . . . .	46
6.2	Simulated Scenarios . . . . .	46
6.3	Summary of electron trigger rates . . . . .	68
<b>7</b>	<b>Conclusions</b>	<b>70</b>

## List of Figures

1	The range of variations in equivalent bunch luminosities for data with an overall luminosity of $9 \times 10^{32} \text{cm}^{-2} \text{s}^{-1}$ . As can be seen, some bunches have a higher effective luminosity while others are lower. Using the bunch luminosity increase the range of luminosities accessible to these studies. . . . .	7
2	A comparison between the number of XFT hits predicted for each superlayer by the simulation as a function of luminosity versus the number measured in data. Prompt and delayed hits are counted separately, so the maximum number of XFT hits per COT wire is two. The offset in SL8 is due to one wire in an entire quadrant of the COT being marked dead for the data used to simulate the higher luminosity environment. . . . .	9
3	A comparison between the number of XFT pixels predicted for each superlayer by the simulation as a function of luminosity versus the number measured in data. . . . .	10
4	A comparison between the number of XFT tracks predicted by the simulation as a function of luminosity versus the number measured in data. . . . .	10
5	Comparison of the 7 GeV single-track trigger cross sections for the 2-bin XFT with minimum $p_T$ thresholds of 1.5 GeV and 2.0 GeV. . . . .	14
6	Comparison of the scenario A two-track trigger cross sections for the 2-bin XFT with minimum $p_T$ thresholds of 1.5 GeV and 2.0 GeV. . . . .	15

7	Comparison of the scenario C two-track trigger cross sections for the 2-bin XFT with minimum $p_T$ thresholds of 1.5 GeV and 2.0 GeV. . . . .	16
8	Comparison of the 7 GeV single-track trigger cross sections for the 2-bin XFT with minimum $p_T$ thresholds of 1.5 GeV and 2.5 GeV. . . . .	17
9	Comparison of the scenario A two-track trigger cross sections for the 2-bin XFT with minimum $p_T$ thresholds of 1.5 GeV and 2.5 GeV. . . . .	18
10	Comparison of the scenario C two-track trigger cross sections for the 2-bin XFT with minimum $p_T$ thresholds of 1.5 GeV and 2.5 GeV. . . . .	19
11	Comparison of the 7 GeV single-track trigger cross sections for the 2-bin XFT with minimum $p_T = 1.5$ GeV and the 6-bin XFT finder-only upgrade with minimum $p_T = 2.0$ GeV. . . . .	20
12	Comparison of the scenario A two-track trigger cross sections for the 2-bin XFT with minimum $p_T = 1.5$ GeV and the 6-bin XFT finder-only upgrade with minimum $p_T = 2.0$ GeV. . . . .	21
13	Comparison of the scenario C two-track trigger cross sections for the 2-bin XFT with minimum $p_T = 1.5$ GeV and the 6-bin XFT finder-only upgrade with minimum $p_T = 2.0$ GeV. . . . .	22
14	Comparison of the 7 GeV single-track trigger cross sections for the 2-bin XFT with minimum $p_T = 1.5$ GeV and the 6-bin XFT finder + linker upgrade with minimum $p_T = 2.0$ GeV. . . . .	23
15	Comparison of the scenario A two-track trigger cross sections for the 2-bin XFT with minimum $p_T = 1.5$ GeV and the 6-bin XFT finder + linker upgrade with minimum $p_T = 2.0$ GeV. . . . .	24
16	Comparison of the scenario C two-track trigger cross sections for the 2-bin XFT with minimum $p_T = 1.5$ GeV and the 6-bin XFT finder + linker upgrade with minimum $p_T = 2.0$ GeV. . . . .	25
17	Comparison of the 7 GeV single-track trigger cross sections for the 2-bin XFT with minimum $p_T = 1.5$ GeV and the 2-bin XFT (minimum $p_T = 1.5$ GeV) + stereo (minimum $p_T = 2.0$ GeV). . . . .	26
18	Comparison of the scenario A two-track trigger cross sections for the 2-bin XFT with minimum $p_T = 1.5$ GeV and the 2-bin XFT (minimum $p_T = 1.5$ GeV) + stereo (minimum $p_T = 2.0$ GeV). . . . .	27
19	Comparison of the scenario C two-track trigger cross sections for the 2-bin XFT with minimum $p_T = 1.5$ GeV and the 2-bin XFT (minimum $p_T = 1.5$ GeV) + stereo (minimum $p_T = 2.0$ GeV). . . . .	28
20	Comparison of the 7 GeV single-track trigger cross sections for the 2-bin XFT with minimum $p_T = 1.5$ GeV and the 2-bin XFT (minimum $p_T = 2.0$ GeV) + stereo (minimum $p_T = 2.0$ GeV). . . . .	29
21	Comparison of the scenario A two-track trigger cross sections for the 2-bin XFT with minimum $p_T = 1.5$ GeV and the 2-bin XFT (minimum $p_T = 2.0$ GeV) + stereo (minimum $p_T = 2.0$ GeV). . . . .	30
22	Comparison of the scenario C two-track trigger cross sections for the 2-bin XFT with minimum $p_T = 1.5$ GeV and the 2-bin XFT (minimum $p_T = 2.0$ GeV) + stereo (minimum $p_T = 2.0$ GeV). . . . .	31

23	Comparison of the 7 GeV single-track trigger cross sections for the 2-bin XFT with minimum $p_T = 1.5$ GeV and the 2-bin XFT (minimum $p_T = 2.5$ GeV) + stereo (minimum $p_T = 2.5$ GeV). . . . .	32
24	Comparison of the scenario A two-track trigger cross sections for the 2-bin XFT with minimum $p_T = 1.5$ GeV and the 2-bin XFT (minimum $p_T = 2.5$ GeV) + stereo (minimum $p_T = 2.5$ GeV). . . . .	33
25	Comparison of the scenario C two-track trigger cross sections for the 2-bin XFT with minimum $p_T = 1.5$ GeV and the 2-bin XFT (minimum $p_T = 2.5$ GeV) + stereo (minimum $p_T = 2.5$ GeV). . . . .	34
26	Comparison of the 7 GeV single-track trigger cross sections for the 2-bin XFT with minimum $p_T = 1.5$ GeV and the 6-bin XFT finder + linker + stereo upgrade with minimum $p_T = 2.0$ GeV. . . . .	35
27	Comparison of the scenario A two-track trigger cross sections for the 2-bin XFT with minimum $p_T = 1.5$ GeV and the 6-bin finder + linker + stereo XFT upgrade with minimum $p_T = 2.0$ GeV. . . . .	36
28	Comparison of the scenario C two-track trigger cross sections for the 2-bin XFT with minimum $p_T = 1.5$ GeV and the 6-bin finder + linker + stereo XFT upgrade with minimum $p_T = 2.0$ GeV. . . . .	37
29	Comparison of the 7 GeV single-track trigger cross sections for the 2-bin XFT with minimum $p_T = 1.5$ GeV and the 2-bin XFT with a minimum $p_T = 2.5$ GeV for a degraded COT. . . . .	38
30	Comparison of the scenario A two-track trigger cross sections for the 2-bin XFT with minimum $p_T = 1.5$ GeV and the 2-bin XFT with a minimum $p_T = 2.5$ GeV for a degraded COT. . . . .	39
31	Comparison of the scenario C two-track trigger cross sections for the 2-bin XFT with minimum $p_T = 1.5$ GeV and the 2-bin XFT with a minimum $p_T = 2.5$ GeV for a degraded COT. . . . .	40
32	Comparison of the 7 GeV single-track trigger cross sections for the 2-bin XFT with minimum $p_T = 1.5$ GeV and the 6-bin XFT finder-only upgrade with a minimum $p_T = 2.0$ GeV for a degraded COT. . . . .	41
33	Comparison of the scenario A two-track trigger cross sections for the 2-bin XFT with minimum $p_T = 1.5$ GeV and the 6-bin XFT finder-only upgrade with a minimum $p_T = 2.0$ GeV for a degraded COT. . . . .	42
34	Comparison of the scenario C two-track trigger cross sections for the 2-bin XFT with minimum $p_T = 1.5$ GeV and the 6-bin XFT finder-only upgrade with a minimum $p_T = 2.0$ GeV for a degraded COT. . . . .	43
35	Cross-section for L1 EM8 trigger. For this analysis, the cross-section is conservatively estimated to be flat as a function of luminosity. . . . .	45
36	Cross-section for L1 EM8 PT8 trigger with real data. This is used only for comparison simulated results. . . . .	46
37	8 GeV electron trigger simulated at high luminosities with current 2-bin device. The star is a data point from the current device. Both 3-layer and 4-layer xft tracks are included. . . . .	47
38	8 GeV electron trigger simulated at high luminosities with current 2-bin device. The star is a data point from the current device. Only 4-layer tracks are included. . . . .	48

39	Simulated electron cross-section for current device with degraded COT using both 3-layer and 4-layer tracks. . . . .	50
40	Simulated electron cross-section for current device with degraded COT using only 4-layer tracks. . . . .	50
41	Simulated electron cross-section for 2-bin Finder with 2.0 GeV threshold for masks and roads. Both 3-layer and 4-layer tracks are included. . . . .	52
42	Simulated electron cross-section for 2-bin Finder with 2.0 GeV threshold for masks and roads. Only 4-layer tracks are included. . . . .	52
43	Simulated electron cross-section for 2-bin Finder with 2.5 GeV threshold for masks and roads. Both 3-layer and 4-layer tracks are included. . . . .	53
44	Simulated electron cross-section for 2-bin Finder with 2.5 GeV threshold for masks and roads. Only 4-layer tracks are included. . . . .	54
45	Simulated electron cross-section for 6-bin Finder with 2.0 GeV threshold. Both 3-layer and 4-layer tracks are included. . . . .	55
46	Simulated electron cross-section for 6-bin Finder with 2.0 GeV threshold. Only 4-layer tracks are included. . . . .	56
47	Simulated electron cross-section for 6-bin Finder with degraded COT. Both 3-layer and 4-layer tracks are included. . . . .	57
48	Simulated electron cross-section for 6-bin Finder with degraded COT. Only 4-layer tracks are included. . . . .	58
49	Simulated electron cross-section for 6-bin Finder plus upgraded linker. Only 4-layer tracks are included. . . . .	59
50	Simulated electron cross-section for 2-bin Finder with 2.0 GeV threshold for masks and roads, with stereo rejection from SL5 and SL7. Both 3-layer and 4-layer tracks are included. . . . .	60
51	Simulated electron cross-section for 2-bin Finder with 2.0 GeV threshold for masks and roads, with stereo rejection from SL5 and SL7. Only 4-layer tracks are included. . . . .	61
52	Simulated electron cross-section for 2-bin Finder with 2.5 GeV threshold for masks and roads, with stereo rejection from SL5 and SL7. Both 3-layer and 4-layer tracks are included. . . . .	62
53	Simulated electron cross-section for 2-bin Finder with 2.5 GeV threshold for masks and roads, with stereo rejection from SL5 and SL7. Only 4-layer tracks are included. . . . .	63
54	Simulated electron cross-section for 6-bin Finder with 2.0 GeV threshold for masks and roads, with stereo rejection from SL5 and SL7. Both 3-layer and 4-layer tracks are included. . . . .	64
55	Simulated electron cross-section for 6-bin Finder with 2.0 GeV threshold for masks and roads, with stereo rejection from SL5 and SL7. Both 3-layer and 4-layer tracks are included. . . . .	65
56	Simulated electron cross-section for 6-bin Finder plus upgraded linker, with stereo rejection from SL5 and SL7. Only 4-layer tracks are included. . . . .	66
57	Simulated electron cross-section for 6-bin Finder plus upgraded linker, with stereo rejection from SL7. Only 4-layer tracks are included. . . . .	67

# List of Tables

1	The increase in the number of masks required to accommodate the switch to 6-bin axial finder operation and additional slopes in the XFT linker. . . . .	3
2	The number of masks necessary to do stereo finding in the XFT with six time bins. This number can be reduced by increasing the minimum segment $p_T$ . . . . .	4
3	The 7 GeV single-track trigger cross sections for the 2-bin XFT with minimum $p_T$ of 1.5 GeV and 2.0 GeV. . . . .	14
4	The scenario A two-track trigger cross sections for the 2-bin XFT with minimum $p_T$ of 1.5 GeV and 2.0 GeV. . . . .	15
5	The scenario C two-track trigger cross sections for the 2-bin XFT with minimum $p_T$ of 1.5 GeV and 2.0 GeV. . . . .	16
6	The 7 GeV single-track trigger cross sections for the 2-bin XFT with minimum $p_T$ of 1.5 GeV and 2.5 GeV. . . . .	17
7	The scenario A two-track trigger cross sections for the 2-bin XFT with minimum $p_T$ of 1.5 GeV and 2.5 GeV. . . . .	18
8	The scenario C two-track trigger cross sections for the 2-bin XFT with minimum $p_T$ of 1.5 GeV and 2.5 GeV. . . . .	19
9	The 7 GeV single-track trigger cross sections for the 2-bin XFT with minimum $p_T = 1.5$ GeV and the 6-bin XFT finder-only upgrade with minimum $p_T = 2.0$ GeV. . . . .	20
10	The scenario A two-track trigger cross sections for the 2-bin XFT with minimum $p_T = 1.5$ GeV and the 6-bin XFT finder-only upgrade with minimum $p_T = 2.0$ GeV. . . . .	21
11	The scenario C two-track trigger cross sections for the 2-bin XFT with minimum $p_T = 1.5$ GeV and the 6-bin XFT finder-only upgrade with minimum $p_T = 2.0$ GeV. . . . .	22
12	The 7 GeV single-track trigger cross sections for the 2-bin XFT with minimum $p_T = 1.5$ GeV and the 6-bin XFT finder + linker upgrade with minimum $p_T = 2.0$ GeV. . . . .	23
13	The scenario A two-track trigger cross sections for the 2-bin XFT with minimum $p_T = 1.5$ GeV and the 6-bin XFT finder + linker upgrade with minimum $p_T = 2.0$ GeV. . . . .	24
14	The scenario C two-track trigger cross sections for the 2-bin XFT with minimum $p_T = 1.5$ GeV and the 6-bin XFT finder + linker upgrade with minimum $p_T = 2.0$ GeV. . . . .	25
15	The 7 GeV single-track trigger cross sections for the 2-bin XFT with minimum $p_T = 1.5$ GeV and the 2-bin XFT (minimum $p_T = 1.5$ GeV) + stereo (minimum $p_T = 2.0$ GeV). . . . .	26
16	The scenario A two-track trigger cross sections for the 2-bin XFT with minimum $p_T = 1.5$ GeV and the 2-bin XFT (minimum $p_T = 1.5$ GeV) + stereo (minimum $p_T = 2.0$ GeV). . . . .	27
17	The scenario C two-track trigger cross sections for the 2-bin XFT with minimum $p_T = 1.5$ GeV and the 2-bin XFT (minimum $p_T = 1.5$ GeV) + stereo (minimum $p_T = 2.0$ GeV). . . . .	28
18	The 7 GeV single-track trigger cross sections for the 2-bin XFT with minimum $p_T = 1.5$ GeV and the 2-bin XFT (minimum $p_T = 2.0$ GeV) + stereo (minimum $p_T = 2.0$ GeV). . . . .	29

19	The scenario A two-track trigger cross sections for the 2-bin XFT with minimum $p_T = 1.5$ GeV and the 2-bin XFT (minimum $p_T = 2.0$ GeV) + stereo (minimum $p_T = 2.0$ GeV). . . . .	30
20	The scenario C two-track trigger cross sections for the 2-bin XFT with minimum $p_T = 1.5$ GeV and the 2-bin XFT (minimum $p_T = 2.0$ GeV) + stereo (minimum $p_T = 2.0$ GeV). . . . .	31
21	The 7 GeV single-track trigger cross sections for the 2-bin XFT with minimum $p_T = 1.5$ GeV and the 2-bin XFT (minimum $p_T = 2.5$ GeV) + stereo (minimum $p_T = 2.5$ GeV). . . . .	32
22	The scenario A two-track trigger cross sections for the 2-bin XFT with minimum $p_T = 1.5$ GeV and the 2-bin XFT (minimum $p_T = 2.5$ GeV) + stereo (minimum $p_T = 2.5$ GeV). . . . .	33
23	The scenario C two-track trigger cross sections for the 2-bin XFT with minimum $p_T = 1.5$ GeV and the 2-bin XFT (minimum $p_T = 2.5$ GeV) + stereo (minimum $p_T = 2.5$ GeV). . . . .	34
24	The 7 GeV single-track trigger cross sections for the 2-bin XFT with minimum $p_T = 1.5$ GeV and the 6-bin finder + linker + stereo XFT upgrade with minimum $p_T = 2.0$ GeV. . . . .	35
25	The scenario A two-track trigger cross sections for the 2-bin XFT with minimum $p_T = 1.5$ GeV and the 6-bin finder + linker + stereo XFT upgrade with minimum $p_T = 2.0$ GeV. . . . .	36
26	The scenario C two-track trigger cross sections for the 2-bin XFT with minimum $p_T = 1.5$ GeV and the 6-bin finder + linker + sterep with minimum $p_T = 2.0$ GeV. . . . .	37
27	The 7 GeV single-track trigger cross sections for the 2-bin XFT with minimum $p_T = 1.5$ GeV and the 2-bin XFT with a minimum $p_T = 2.5$ GeV for a degraded COT. . . . .	38
28	The scenario A two-track trigger cross sections for the 2-bin XFT with minimum $p_T = 1.5$ GeV and the 2-bin XFT with a minimum $p_T = 2.5$ GeV for a degraded COT. . . . .	39
29	The scenario C two-track trigger cross sections for the 2-bin XFT with minimum $p_T = 1.5$ GeV and the 2-bin XFT with a minimum $p_T = 2.5$ GeV for a degraded COT. . . . .	40
30	The 7 GeV single-track trigger cross sections for the 2-bin XFT with minimum $p_T = 1.5$ GeV and the 6-bin XFT finder-only upgrade with a minimum $p_T = 2.0$ GeV for a degraded COT. . . . .	41
31	The scenario A two-track trigger cross sections for the 2-bin XFT with minimum $p_T = 1.5$ GeV and the 6-bin XFT finder-only upgrade with a minimum $p_T = 2.0$ GeV for a degraded COT. . . . .	42
32	The scenario C two-track trigger cross sections for the 2-bin XFT with minimum $p_T = 1.5$ GeV and the 6-bin XFT finder-only upgrade with a minimum $p_T = 2.0$ GeV for a degraded COT. . . . .	43
33	A summary of the track-trigger cross sections for the various XFT upgrade options quoted at a luminosity of $3 \times 10^{32} \text{cm}^{-2} \text{s}^{-1}$ . Numbers for the degraded COT are given in square brackets. . . . .	44

34	Trigger Cross-sections for the current, 2-bin, axial layer device, sorted by triggers from 3-Layer (3L) and 4-Layer (4L) XFT tracks. Missed refers to the fraction of the actual trigger cross-section which is not found using XFT tracks. . . . .	47
35	Trigger Cross-sections for degraded current, 2-bin, Axial Layer Device, sorted by triggers from 3-Layer (3L) and 4-Layer (4L) XFT tracks. Missed refers to the fraction of the actual trigger cross-section which is not found using XFT tracks. . . . .	49
36	Trigger Cross-sections for 2-bin, Axial Layer Device, with $ P_T  > 2.0$ GeV, sorted by triggers from 3-Layer (3L) and 4-Layer (4L) XFT tracks. Missed refers to the fraction of the actual trigger cross-section which is not found using XFT tracks. . . . .	51
37	Trigger Cross-sections for 2-bin, Axial Layer Device, with $ P_T  > 2.5$ GeV sorted by triggers from 3-Layer (3L) and 4-Layer (4L) XFT tracks. Missed refers to the fraction of the actual trigger cross-section which is not found using XFT tracks. . . . .	53
38	Trigger cross-sections for the XFT with all 4 axial layers upgraded to 6 time bins of xft hit information. The $P_T$ threshold is 2.0 GeV. . . . .	55
39	Trigger cross-sections for the XFT with all 4 axial layers upgraded to 6 time bins of xft hit information subject to degraded COT. The $P_T$ threshold is 2.0 GeV. . . . .	57
40	Trigger Cross-sections for 6-bin, Axial Layer Device, with $ P_T  > 2.0$ GeV, and an upgraded linker which uses additional slope information about the segments. Tracks with 3 layers are not considered for the upgraded linker. . . . .	59
41	The 2-Bin Axial Finder with $P_T$ threshold of 2.0 GeV, using stereo rejection from SL5 and SL7. . . . .	60
42	The 2-Bin Axial Finder with $P_T$ threshold of 2.5 GeV, using stereo rejection from SL5 and SL7. . . . .	62
43	6-bin Finder + stereo rejection in SL5 and SL7. The $P_T$ threshold used is 2.0 GeV. . . . .	64
44	Cross-sections for the 6-bin finder with upgraded linker and stereo rejection in SL5 and SL7. Tracks with 3 layers are not considered for the upgraded linker. . . . .	66
45	These are the results for the baseline upgrade which is a 6-Bin Finder, plus an upgraded linker, and Stereo Segment track rejection in SL7. . . . .	67
46	Summary of trigger cross-sections for various upgrade scenarios, sorted by triggers from 3-Layer (3L) and 4-Layer (4L) XFT tracks. The scenarios in bold are the current device, the re-scoped upgrade, and the nominal baseline upgrade. . . . .	68
47	A comparison of the predicted performance of the XFT stereo upgrade to the performance of the current XFT at a luminosity of $3 \times 10^{32} \text{cm}^{-2} \text{s}^{-1}$ . . . . .	71

# 1 Introduction to XFT

As the Tevatron luminosities increases, it will be necessary to upgrade the XFT in order to deal with the higher fake rates caused by increased luminosity. In the face of increased luminosities, the CDF physics goals are as follows:

- Maintain the high  $p_T$  physics program to a luminosity of  $3 \times 10^{32} \text{ cm}^{-2}\text{s}^{-1}$ .
- Maintain the scenario C two-track triggers to a luminosity of  $1.5 \times 10^{32} \text{ cm}^{-2}\text{s}^{-1}$ . Beyond this, the rate of real two-track triggers becomes so high that no amount of fake rate reduction can make this trigger feasible.

In order for the XFT upgrade to accommodate the above goals, it must meet the following requirements:

- Maintain the current XFT efficiency for high  $p_T$  tracks. Specifically, the XFT efficiency for tracks with  $p_T > 7 \text{ GeV}$  should be at least 90%.
- Maintain the current XFT  $p_T$  and  $\phi_0$  resolutions. For the current XFT device,  $\sigma_{p_T}/p_T^2 < 2.0\%/ \text{GeV}$  and  $\sigma_{\phi_0} < 8 \text{ mR}$ .
- Reduce the 7 GeV single-track trigger by a factor of three to four.
- Reduce the scenario C two-track trigger by a factor of two to four.

There are a number of possible upgrade options with the potential to meet these requirements:

**Option 0: Firmware Upgrade** In this option, the actual XFT hardware is left unchanged, and only the details of the XFT algorithm implemented in the firmware are changed. The primary change being considered is increasing  $p_T$  threshold of the XFT from its current value of 1.5 GeV to something higher, like 2.0 GeV to 2.5 GeV. In addition, the option to require both XFT slope bits to be fired for high  $p_T$  tracks is being explored.

**Option 1: 6-Bin Finder-Only Upgrade** For this option, the number of time bins sent up to the XFT from the TDC cards is tripled, from two to six. This allows better resolution for the segment finding portion of the XFT algorithm. This upgrade option requires new XTC cards (or a new TDC) and new XFT finder boards.

**Option 2: 6-Bin Finder+Linker Upgrade** This option is identical to the one above except that finder uses its increased segment finding resolution to pass on additional segment slope information to the linker boards. The main advantage of this upgrade is that the linker can use the additional segment slope information to reduce the number of fake tracks resulting from the linking of segments from multiple low- $p_T$  tracks into one high- $p_T$  fake. This upgrade option requires new XFT linker boards in addition to the boards listed above.

**Option 3: Stereo Upgrade** Another approach is to implement some of the COT stereo layers in the XFT system. Currently, we are considering adding stereo information to the XFT from superlayers 3, 5, and 7. Stereo segments would be found using a new 6-time-bin finder board. Association of stereo segments with tracks would occur at level 1 in the "Stereo Linker

Association Module" (or SLAM) board. More detailed information is passed on to Level 2. This upgrade option would require the construction of new XTC cards (or new TDC), stereo finder boards for the finder layers, the SLAM boards, and any hardware required to do the stereo association at level 2.

It should be noted that the actual upgrade will likely consist of some combination of the above options. For example, one possible approach would be to combine the stereo upgrade (option 3) with increased XFT  $p_T$  thresholds (option 1). It would also be possible to include all options in one upgrade plan (upgrading the axial XFT finders and linkers, building new stereo hardware, and increasing the XFT  $p_T$  threshold from 1.5 GeV to something higher).

The original plan proposed in the Run IIb TDR included both the 6-bin finder+linker and stereo (SL 7 only) upgrade options. However, improved predictions of the high luminosity environment bring into question whether such an extensive upgrade is truly needed to meet CDF's requirements at  $3 \times 10^{32} \text{ cm}^{-2}\text{s}^{-1}$ . In addition, time constraints and limits on person-power make it unlikely that this entire upgrade can be achieved. Therefore, in this note, we evaluate the various upgrade options (and combinations of options) to determine which approaches are capable of meeting the future needs of CDF. In making the evaluation, we consider how each upgrade option performs in terms of efficiency, resolutions, track-trigger cross sections, and electron cross sections.

## 2 Axial Upgrade Details

The XFT was originally designed to operate with a bunch spacing of 132 ns. However, the Tevatron will not be operated in this mode, but rather will remain at a bunch spacing of 396 ns. The key idea behind the XFT axial upgrade options is to use the extra time allowed by the 396 ns bunch spacing to send more information at each stage of the track finding process.

At the hit finding stage, which involves the communication between the TDC/XTC and the XFT Finder boards, the additional time allows us to send six bits of timing information, rather than the two bits that are sent in the current system. This means that hit times can be reported in 6 bins, allowing better drift distance resolution. Currently, our investigations of the 6-bin axial upgrade options have all used six time bins evenly spaced between 0 ns and 210 ns (after  $t_0$  corrections). Further optimization of the 6-bin algorithms may be possible by choosing different time bin spacings.

The additional time bins mean that the segment finding algorithms have to search through a larger number of hit patterns to find track segments. Table 1 shows the increase in the number of masks required to find tracks with six time bins.

Although upgrading the XFT finder to use six time bins produces an improvement by itself, XFT performance can be further improved by using the better resolution to make a better measurement of the slope of the XFT track segments. The XFT segment slope is related to the segment  $p_T$  and can be used by the linker to limit the linking of low  $p_T$  segments from multiple tracks into a higher  $p_T$  fake track.

For the linker upgrade studies presented in this note, we assume that the 396 bunch spacing allows transmission of three times the pixel information between the XFT finder and linker. The current XFT transmits twelve bits of information. For the inner two axial COT layers, all twelve bits are used to specify the pixel position. The outer two layers currently use 6 bits of position information with two bits of slope information at each position. For the upgraded linker, we would allow three bits of slope information for the inner two axial layers and five slope bits for the outer axial layers. It may be possible, by upgrading the technology used to transfer information between the finder and the linker to send somewhat more information, but such options have not been investigated in this note.

Incorporating additional slope information in the linker stage leads to an increase in the number of roads required for track finding in the linker. Table 1 shows the increase in the number of roads for approach considering in this note.

	Original XFT	Axial Upgrade	Ratio
Masks SL 2	166	1343	8.1
Masks SL 4	227	2053	9.0
Masks SL 6	292	2511	8.6
Masks SL 8	345	2780	8.1
Roads	1228	3658	3.0

Table 1: The increase in the number of masks required to accommodate the switch to 6-bin axial finder operation and additional slopes in the XFT linker.

### 3 Stereo Upgrade Details

In the XFT stereo upgrade option, new finder boards are added to find track segments in the stereo superlayers of the COT. Fake axial tracks can be rejected by requiring associated stereo segments. The stereo upgrade option also allows the XFT to measure the tracks  $\cot\theta$  and  $z_0$ . This additional information allows new ways of reducing XFT fakes not available to an axial-only system, such as requiring consistency between the XFT track pointing in the  $z$ -direction and the calorimeter tower or muon stub involved in electron or muon triggers. The ability to reconstruct XFT tracks in three-dimensions opens the possibility for mass-based triggers for  $B$  physics. In addition, having a good resolution measurement of track  $z_0$  may make it possible to distinguish tracks from different interactions, reducing the growth term in triggers rates from pile-up interactions.

The COT stereo superlayers permit a measurement of the  $z$  position of a track segment because the stereo angle of the wires causes an apparent displacement of the stereo track segment from the azimuthal position that would be expected based on the measurement of the track in the axial layers. For small stereo angles, the amount of the apparent displacement of the stereo track is roughly proportional to the  $z$  position of the track segment at that superlayer. Combining stereo information from multiple layers with an XFT track reconstructed in the axial layers (and optionally, assuming that the track originates from  $z = 0$  at the origin) allows a measurement of the complete three-dimensional trajectory of a particle. For more information on using the stereo XFT layers to make three-dimensional track measurements, consult ref [1].

In this note, we examine the simplest, most straight-forward implementation of the XFT stereo upgrade, focusing on the power of the stereo layers to reject fakes through the requirement of stereo track segments associated with the XFT axial track. The XFT stereo finder implementation is based on the current XFT finder boards as configured for the outer axial superlayers, with the exception that six time-bins are used for XFT stereo hits. The stereo track segments are reported with a six-pixel per cell position resolution and two slopes, just as in the current system in the outer axial superlayers. Further gains possible from using more pixels per cell or finer segment slope distinctions are not considered in this note. The number of masks required to implement the stereo XFT layers in this fashion are shown in Table 2. The XFT stereo upgrade option studied here involves using only the outer two COT stereo superlayers (referred to as SL5 and SL7). Recent studies show that additional benefits result from including the next innermost stereo layer (SL3) as well, so the stereo upgrade proposal includes the implementation of SL3. Studies of how to best incorporate information from stereo SL3 are ongoing and performance predictions of the XFT stereo upgrade including SL3 will be presented in a separate note. The innermost stereo superlayer (SL1).

	Stereo Upgrade
Masks SL 3	1670
Masks SL 5	2312
Masks SL 7	2602

Table 2: The number of masks necessary to do stereo finding in the XFT with six time bins. This number can be reduced by increasing the minimum segment  $p_T$ .

In this scheme, the XFT track is reconstructed first in the current axial-only XFT system. The stereo track segment finding proceeds independently from the current axial XFT system and

stereo track segments are associated with the axial XFT track after the fact. This association takes place at two different points in the CDF trigger. To make the stereo association available as soon as possible for rejection of fake XFT tracks, a new board, known as the stereo linker association module (SLAM) board takes the axial XFT tracks from the current XFT and determines whether any XFT stereo segments from the stereo finder boards are associated with these tracks before passing them onto the XTRP. The primary purpose of the association at this point is to reject fake XFT tracks that are not matched to stereo segments. Although the exact implementation of the SLAM board is still under development, the studies here use a number of simple algorithms consistent with what may be possible to implement in the final SLAM board as shown below:

**Option 1** ( $\Delta\text{pixel}(\text{SL5}) < 18$  and  $\Delta\text{pixel}(\text{SL7}) < 18$ ): Because of the stereo angle of the COT, no stereo track segment will be displaced by more than 3 cells or 18 pixels from the position extrapolated from the axial track. The simplest algorithm of stereo association merely requires the presence of a stereo segment in both superlayers 5 and 7 in the maximum allowed window.

**Option 2** ( $|\Delta\text{pixel}(\text{SL5}) + \Delta\text{pixel}(\text{SL7})| < 9$ ): Because the stereo angle in superlayers 5 and 7 is opposite, the displacement of the track segment in superlayer 7 should be in the opposite direction as the displacement in superlayer 5, although the magnitude of the displacements should be roughly equal. (The displacement in SL5 will always be slightly less than SL7 because SL5 is at a smaller radius.) This requirements represent a loose implementation of a consistency check between the stereo track segment displacement in the two stereo layers.

**Option 3** ( $|\Delta\text{pixel}(\text{SL5}) + \Delta\text{pixel}(\text{SL7})| < 6$ ,  $|1.25 \times \Delta\text{pixel}(\text{SL5}) + \Delta\text{pixel}(\text{SL7})| < 5$ ): This requirement represents an even tighter constraint on stereo segment consistency than the previous one. The first cut ( $|\Delta\text{pixel}(\text{SL5}) + \Delta\text{pixel}(\text{SL7})| < 6$ ) is equivalent to requiring  $|\cot\theta| < 2.2$ , while the second requirement equates to demanding that  $|z_0| < 175$  cm. Both these cuts equate to requiring that the track pass through the fiducial volume of the COT to within the resolution of these track parameters as predicted for measurements with this implementation of the XFT stereo upgrade.

Each of the above requirements gives comparable overall performance with Option 2 representing an incremental improvement over Option 1 and the same for Option 3. The studies in this note use Option 2 or 3. In addition to using stereo information via the SLAM board in Level 1, it is also expected that the stereo information will be passed to the Level 2 trigger where more complicated algorithms may make use of it. Level 2 provides the opportunity for more detailed analysis of the stereo information including such possibilities as fitting multiple stereo segments to get an improved measurement of the three-dimensional track and fitting the  $z_0$  of the primarily interaction vertex based on the all the stereo segments reconstructed in the event. The more sophisticated uses of stereo information in Level 2 will be the subject of a future note.

## 4 Data Simulation at High Luminosities

The choice of XFT upgrade options depends requires accurate simulation of the XFT performance in a high luminosity environment. Obtaining these performance predictions involved two steps: It is first necessary to simulate  $p\bar{p}$  collisions in a high luminosity environment. This was accomplished through an event mixing procedure that combines multiple events from data taken at the current Tevatron luminosities in a way that appropriately reflects the high luminosity environment. At this stage, we also considered the possible effects of degrading the COT performance as a result of possible wire aging. Once the high luminosity data has been generated, it must be passed through a simulation of the XFT upgrade options (as well as the current XFT device) in order to get an idea of the performance gains possible from each upgrade option. Details of these individual steps are given below:

### 4.1 Luminosity Extrapolation

In order to evaluate the performance of the current XFT device as well as various upgrade options for the remainder of Run II, we need a model for high luminosity collisions (up to  $3 \times 10^{32} \text{ cm}^{-2}\text{s}^{-1}$ ) at a 396 ns bunch spacing. Rather than using a Monte Carlo simulation, which may give an undesirably idealized picture of such an environment, we choose to model high luminosity collisions by mixing together data from several lower luminosity events. With this approach, the effects of actual detector response can be reflected in the projections. Also, it is not necessary to rely on any theoretical description for the physics of soft  $p\bar{p}$  collisions.

The procedure for mixing events from lower luminosity data to model a higher luminosity environment is as follows: First, an event from the current data that represents the main physics process of interest is selected. For the track trigger studies presented here, this event is a minimum-bias event. For the electron trigger studies, the main event is selected from the EM8 trigger, meaning the event contained at least one 8 GeV energy deposit in a single tower of the electromagnetic calorimeter. In either case, the main event is combined with one or more zero-bias events. It should be noted that zero-bias events may contain data from zero, one, or multiple  $p\bar{p}$  collisions, depending on the luminosity at which they are taken. Combining the minimum-bias or EM8 event with one or more zero bias events entails the following procedure:

- The COT hits from the main event and the additional zero-bias events are merged. Overlapping hits are combined to form a single hit with leading and trailing edge times adjusted accordingly.
- Reconstructed offline tracks from the main event and the zero-bias events are collected into a single list. Offline tracking is not re-run for the merged events. Keeping the offline tracks reconstructed in the separate events before merging avoids dealing with issues of offline track reconstruction performance at higher luminosities. This approach allows us to continue to use offline tracks to define the XFT efficiency and fake rates at all luminosities.
- For other event data (such as calorimeter energy deposits), only the quantities from the main event are used. No information from the additional zero-bias events are added. This approximation make no difference to the track trigger studies since no quantities beyond the COT hits and offline tracks are necessary. It is a reasonable approximation for the EM8 data

used in the electron trigger studies because the additional zero-bias interactions added has a negligible chance of addition additional 8 GeV calorimeter energy deposits.

The equivalent luminosity of the merged event is determined by summing the luminosities of main event (minimum-bias or EM8) and the individual zero-bias events. The luminosities of the unmerged events are determined on a bunch-by-bunch basis from CLC data. This increases the range of luminosities accessible to our studies because the intensity of each bunch varies, as illustrated in figure 1.

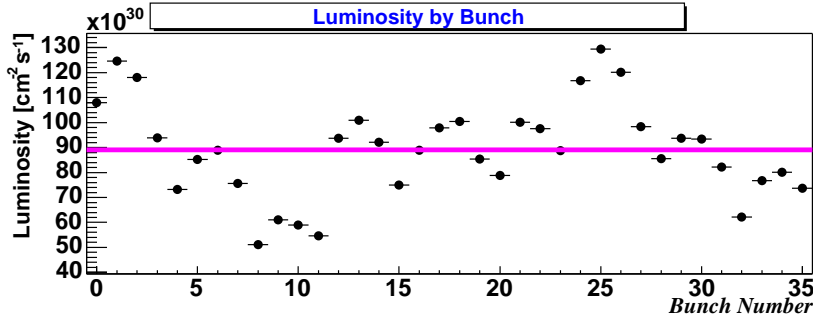


Figure 1: The range of variations in equivalent bunch luminosities for data with an overall luminosity of  $9 \times 10^{32} \text{cm}^{-2} \text{s}^{-1}$ . As can be seen, some bunches have a higher effective luminosity while others are lower. Using the bunch luminosity increase the range of luminosities accessible to these studies.

## 4.2 COT Performance Degradation

When these studies were started, there was serious concerns that the COT performance would be significantly degraded by unexpectedly high amounts of wire aging. This loss of COT performance translate directly to a degradation in the XFT performance and caused concern that the XFT upgrade should incorporate features to offset the COT aging. However, recent developments indicate that the COT aging can be controlled and reversed by introducing a small amount of oxygen into the chamber gas mixture. Although there no longer seems much concern that COT aging will present an obstacle to the XFT upgrade, we still present a limited number of studies of the performance of some upgrade options subject to degraded COT conditions to indicate the robustness of certain options.

The degraded COT scenario shown here is rather extreme. It supposes that the innermost axial superlayer has been so severely aged that it can no longer be used. This is handled by treating all wires in that superlayer as dead. The XFT handles dead wires by setting all possible hit time bins for that wire on. Doing this for a whole superlayer is equivalent to removing the requirement for finding a track segment in that superlayer. In other words, the current XFT goes from being a four-layer device to a three layer device. In addition, we assume that the second axial superlayer is degraded to the point that the single hit efficiency is reduced to 80%. These running conditions are comperable to those seen with the “compromised” COT running from February to May of 2004.

Implementation of this performance degradation is handled during the event merging stage. Before hits are merged a random number generator is used to discard a set fraction of the hits.

The fraction can be different for each superlayer. Table ?? shows the hit efficiencies applied to the data before merging for the degraded COT studies presented here.

### 4.3 XFT Simulation

After event merging, the simulated high-luminosity data is passed through specialized XFT simulation code to predict the performance of various XFT upgrade options. The XFT simulation would perhaps be better referred to as an emulation because there is no randomness involved. Instead, the code duplicates the functionality of the XFT hardware precisely, all the way to the chip level. The agreement between the simulation of the current XFT device and actual data taken with the hardware is outstanding, leading to high confidence in our ability to simulate the various upgrade options.

Simulation of the current XFT device and the various upgrade options proceeds along the following lines:

- The first step is to take COT hits with 1 ns resolution and convert them to XFT hits in the appropriate number of time bins (2 or 6). This simulates the action of the XTC cards from the current XFT system as well as the new 6-bin XTC cards or upgraded TDC operation for the XFT upgrade. For the current XFT, this step produces results that are very similar to the actual hardware output, although very small timing differences in the hardware itself prevent an exact emulation at this stage.
- Next, the XFT hits are passed to a simulation of the XFT finder boards. The simulation replicates the action of the XFT hardware at the chip level. The final result of this stage of simulation is a set of XFT pixels line segments for each layer, output in the appropriate format (number of pixels per cell and slopes) for the XFT option in question. The results of this stage and all the following stages match the output of the hardware exactly when starting from the same set of XFT hits.
- Once the XFT pixels have been found, an XFT linker simulation links the pixels into XFT tracks. Again, the linker simulation replicates the actions of the linker board down to the chip level, including the generation of duplicate XFT tracks at linker board boundaries.

The XFT simulation code has been committed to the CDF software repository under the `XFTSim` (for the current XFT) and `XFT2Sim` (for the XFT upgrade simulations) packages. The `XFTSim` code runs either as a compiled AC++ executable or as a ROOT script for quick development and turnaround time. The `XFT2Sim` code runs only as a ROOT script.

### 4.4 XFT Simulation Validation

The following plots show the simulation of the current XFT device for high luminosities compared to recent XFT data taken with the actual hardware. The agreement, over the range of luminosities where the data and the simulation overlap, is excellent.

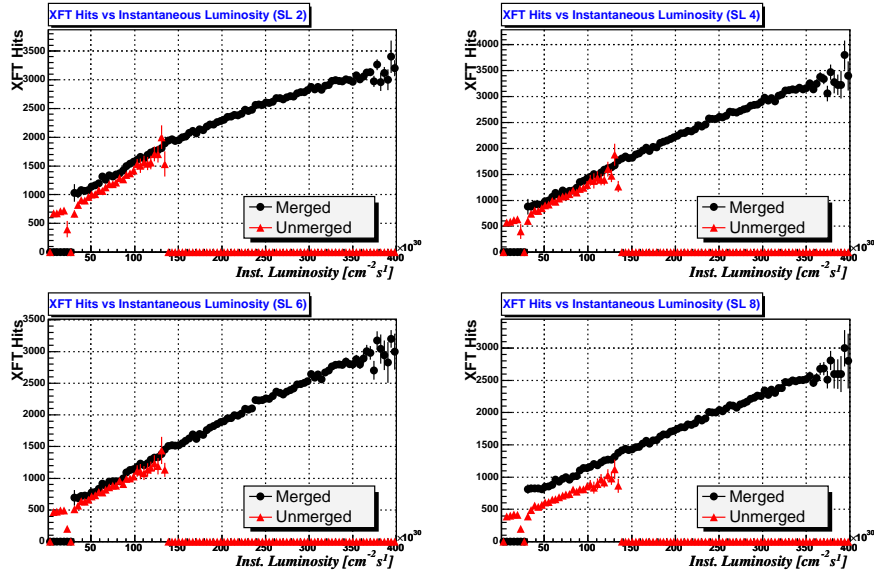


Figure 2: A comparison between the number of XFT hits predicted for each superlayer by the simulation as a function of luminosity versus the number measured in data. Prompt and delayed hits are counted separately, so the maximum number of XFT hits per COT wire is two. The offset in SL8 is due to one wire in an entire quadrant of the COT being marked dead for the data used to simulate the higher luminosity environment.

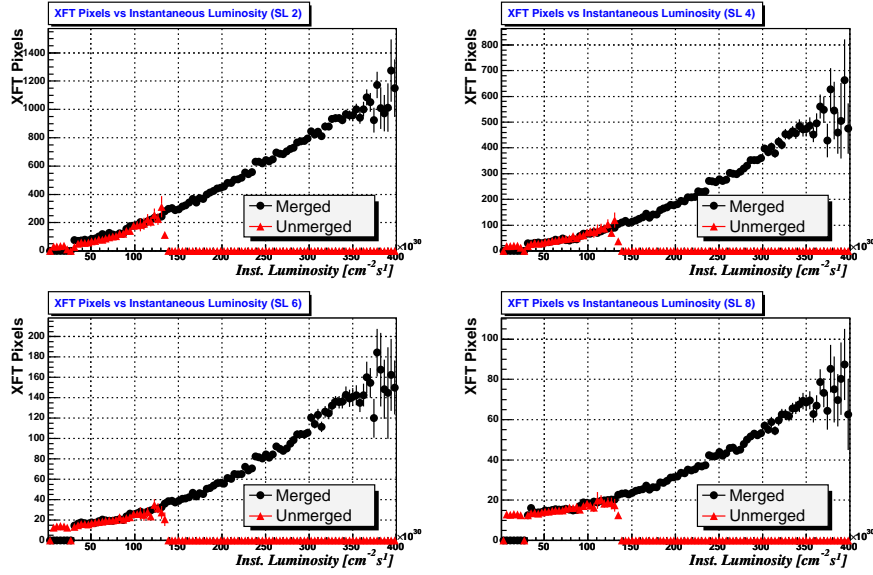


Figure 3: A comparison between the number of XFT pixels predicted for each superlayer by the simulation as a function of luminosity versus the number measured in data.

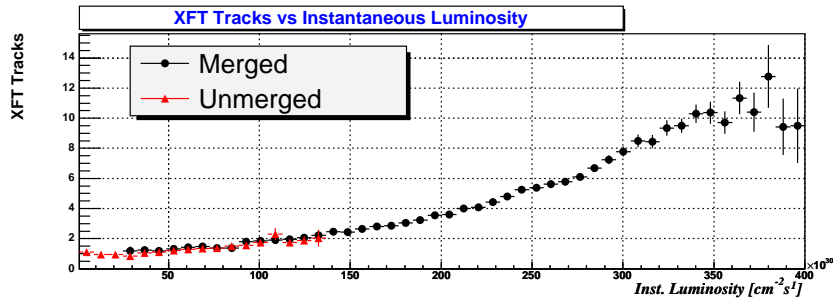


Figure 4: A comparison between the number of XFT tracks predicted by the simulation as a function of luminosity versus the number measured in data.

## 5 Track Trigger Rates at High Luminosities

Track triggers provide a fundamental insight into the performance of the XFT at high luminosities because no information from other detector systems (like the muon chambers or calorimeter) can be used to control XFT rates. In this way, they represent a worst-case scenario for XFT performance while the electro trigger, discussed in Section 6, represents the best case of combining an XFT track with a high purity calorimeter signal. Furthermore, the track triggers, especially those requiring two low  $p_T$  tracks, are a pivotal part of the CDF  $B$  physics program.

The following track triggers will be considered here:

- **7 GeV Single-Track Trigger:** This trigger requires that only a single XFT track with measured  $p_T$  be present in the event. It is a useful trigger to study because we have data on the rate produced by this trigger over a range of luminosities. In addition, this trigger should indicate the general behavior of XFT-only portion of the electron and muon triggers that make up a large part of CDF's high  $p_T$  physics program.
- **Scenario A Two-Track Trigger:** This is the preferred trigger for doing studies of hadronic  $B$  decays. This trigger requires two tracks of opposite charge that have  $p_T > 2.0$  GeV. In addition, the two tracks are required to be separated by an azimuthal angle of no greater than  $135^\circ$ , and the scalar sum of the two track's  $p_T$  must be greater than 5.5 GeV. Although this trigger is currently the preferred  $B$  physics two-track trigger because it has the best purity, it also has a higher yield than other two-track triggers, making it's continued use at high luminosities impractical.
- **Scenario C Two-Track Trigger:** Although this trigger is not as pure as Scenario A, it also has a smaller cross section, making it more likely that this trigger could remain viable at high luminosities. This trigger requires two tracks with opposite charge, each having  $p_T > 2.5$  GeV. Again, the two tracks must be separated by no more than  $135^\circ$ , and the scalar sum of the track  $p_T$  must be greater than 6.5 GeV.

In order to compute a trigger cross section for each of the track triggers above, we need a data sample that is unbiased with respect to track triggers. The only data set that meets the requirements in this case is the minimum-bias data set. After merging additional zero-bias events into the minimum bias data to simulate a higher luminosity environment, the track trigger cross sections can be calculated as follows:

$$\sigma_{track} = \sigma_{mb}(\mathcal{L}) \frac{N_{pass}}{N_{mb}}, \quad (1)$$

where  $\sigma_{track}$  is the cross section of the track trigger of interest,  $\sigma_{mb}$  is the cross section for the minimum bias trigger,  $N_{mb}$  is the total number of minimum bias events considered, and  $N_{pass}$  are the number of minimum bias events satisfying the requirements for the track trigger of interest. As noted in the equation, the minimum bias trigger cross section varies with luminosity. For these studies, we use the following parameterization for the minimum bias trigger cross section [2]:

$$\sigma_{mb}(\mathcal{L}) = \frac{R}{\mathcal{L}} \left[ 1 - \exp\left(-\sigma_{mb,phys} \frac{\mathcal{L}}{R}\right) \right], \quad (2)$$

where  $R$  is the beam crossing rate (in this case 1.7 MHz), and  $\sigma_{mb,phys}$  is the physics cross section (as opposed to a trigger cross section) for a minimum bias interaction. For these studies, we use  $\sigma_{mb,phys} = 50$  mb. At high luminosities, this trigger cross section reduces to  $\sigma_{mb}(\mathcal{L}) = \frac{R}{\mathcal{L}}$  as a simple consequence of the fact that the maximum trigger rate is equal to the beam crossing rate  $R$ . Once this trigger rate is saturated, as the luminosity increases, the trigger cross section has to decrease to keep the rate constant. However, at lower luminosities, this behavior changes, as reflected by the exponential term in Eq. 2 which represents the probability that a given interaction has no min bias collision.

The plots that follow show a comparison of the track trigger cross sections mentioned above between the current XFT device and various upgrade options, extrapolated over a range of luminosities from approximately  $5 \times 10^{31} \text{ cm}^{-2}\text{s}^{-1}$  to  $4 \times 10^{32} \text{ cm}^{-2}\text{s}^{-1}$ . For each upgrade option, the absolute trigger cross section is plotted in comparison with the cross section produced by the current device. In addition the ratio of the trigger cross section with the given up grade option to the trigger cross section predicted for the current device is shown. Finally, a table tallies the individual cross sections and the ratio for each upgrade option. In this table, the cross section values are extracted by fitting a second-order polynomial to each cross section plot and using this fit to extract cross sections for particular luminosities. The ratio entries in this table are obtained from a linear fit to the ratio plot. Because the two fits are not always in agreement, the ratio value in the table is not always equal to the ratio of the cross sections in the table. This is primarily a noticeable effect at low luminosities, when the linear model for the ratio is not such a good approximation. At high luminosities, the linear fit to the ratio produces results in much closer agreement to the quadratic fits to the cross section plots.

The following sections provide a brief overview of some of the features of the following plots:

### 5.1 7 GeV Single-Track Trigger

The cross section plots for this trigger are presented as follows: The black line shows the total 7 GeV single-track trigger rate as a function of luminosity, with the error bars indicating the statistical uncertainty in each bin. The green shaded region shows the fraction of the trigger cross section coming from fake XFT tracks where “fake” means that the XFT track was not matched to an offline-reconstructed track. The purple shaded region shows the fraction of the trigger cross section coming from real XFT tracks, where “real” means that the XFT track was matched to an offline track. The red points indicate the 7 GeV single track cross section calculated from the offline reconstructed tracks. One would expect the true 7 GeV single track cross section to be constant as a function of luminosity, as indicated from the cross section computed with offline tracks. The discrepancy between the real XFT cross section and the cross section calculated from offline tracks results from the worse momentum resolution of the XFT tracks, which allows lower momentum tracks to satisfy the 7 GeV cut. As the luminosity increases, the XFT resolution gets worse, leading to an increase in real XFT tracks that satisfy the trigger momentum threshold.

### 5.2 Scenario A and C Two-Track Trigger

These plots use the same definition of a fake XFT track as the single-track trigger plots; in other words, a fake track is an XFT track that is not matched to an offline track. The black line with error bars again shows the total two-track trigger rate. The dark-purple region represents the fraction of the total trigger rate in which both XFT tracks in the pair were matched to offline

tracks (no fakes). The light-purple region of the plot shows the fraction of the events in which one of the XFT tracks was matched to an offline track and one was not (one fake). Finally, the green portion of the plot shows the fraction of the trigger cross section coming from events in which neither XFT track in the two-track pair is matched to an offline track (two fakes). For comparison, one cross section measurement from data is shown in each plot. For the Scenario A two-track trigger cross section, the reference value is 0.35 mb at  $5 \times 10^{31} \text{cm}^{-2} \text{s}^{-1}$ . For scenario C, the reference value is 0.13 mb at  $5 \times 10^{31} \text{cm}^{-2} \text{s}^{-1}$ .

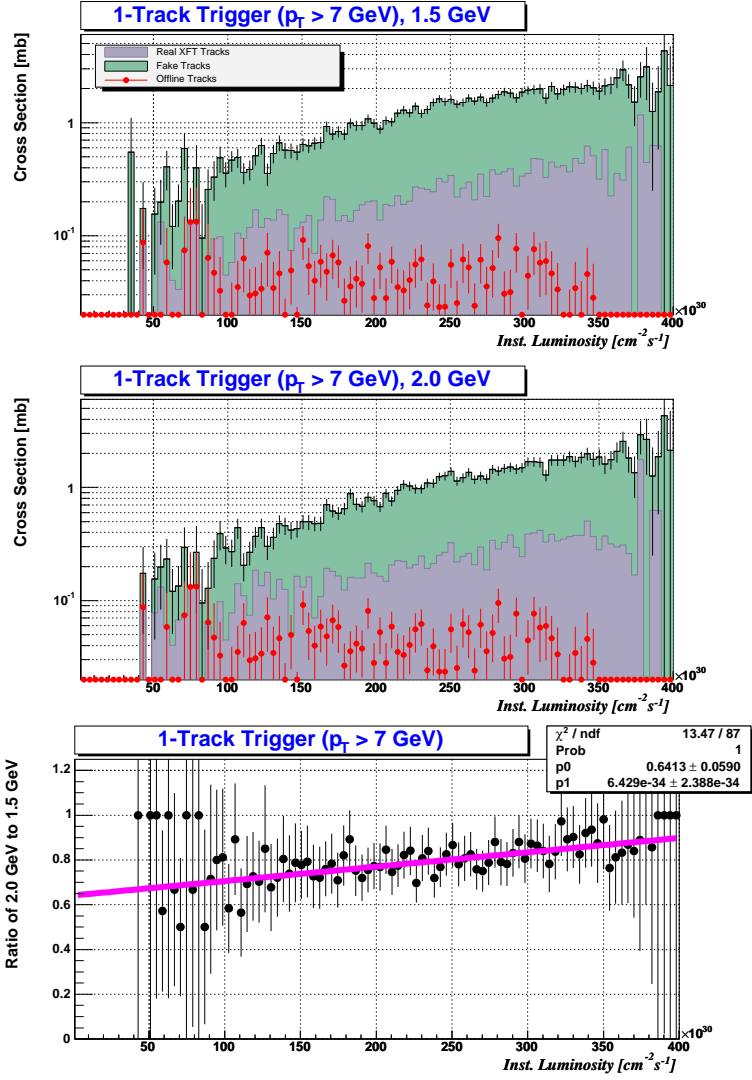


Figure 5: Comparison of the 7 GeV single-track trigger cross sections for the 2-bin XFT with minimum  $p_T$  thresholds of 1.5 GeV and 2.0 GeV.

Luminosity [ $1 \times 10^{32} \text{ cm}^{-2} \text{ s}^{-1}$ ]	0.5	1.0	1.5	2.0	3.0
1.5 GeV $\sigma$ [mb]	0.09	0.37	0.68	1.0	1.8
2.0 GeV $\sigma$ [mb]	0.08	0.27	0.50	0.79	1.5
ratio	0.67	0.71	0.74	0.77	0.83

Table 3: The 7 GeV single-track trigger cross sections for the 2-bin XFT with minimum  $p_T$  of 1.5 GeV and 2.0 GeV.

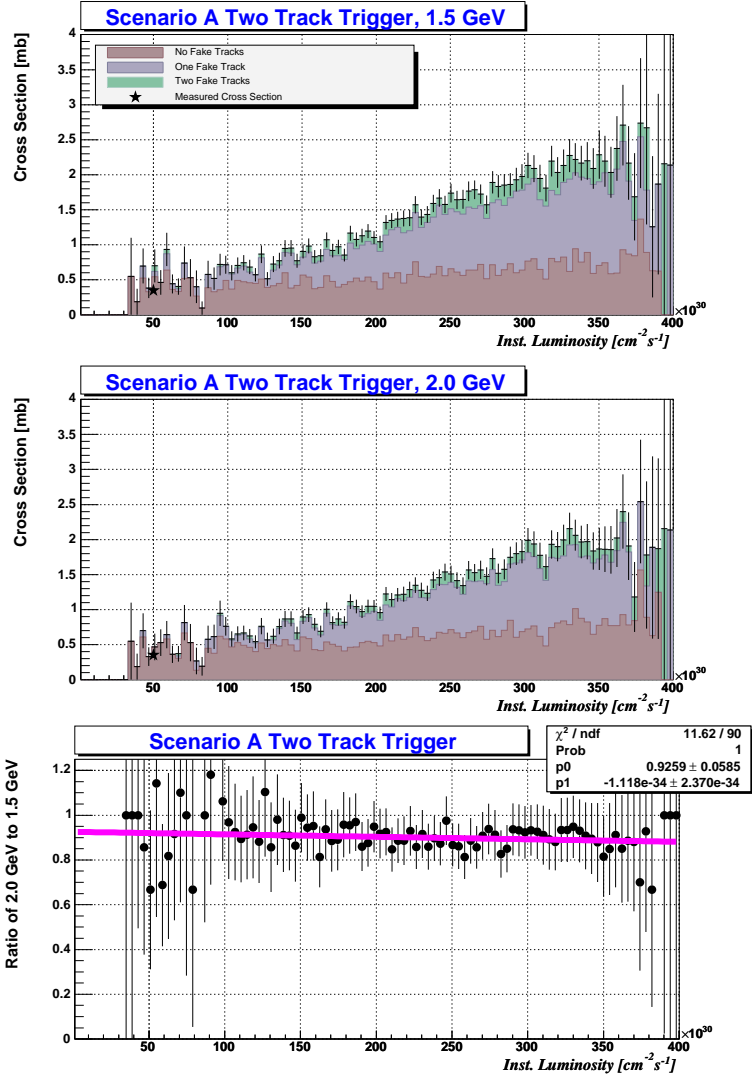


Figure 6: Comparison of the scenario A two-track trigger cross sections for the 2-bin XFT with minimum  $p_T$  thresholds of 1.5 GeV and 2.0 GeV.

Luminosity [ $1 \times 10^{32} \text{ cm}^{-2} \text{ s}^{-1}$ ]	0.5	1.0	1.5	2.0	3.0
1.5 GeV $\sigma$ [mb]	0.33	0.59	0.88	1.2	1.9
2.0 GeV $\sigma$ [mb]	0.36	0.57	0.81	1.1	1.7
ratio	0.92	0.91	0.91	0.90	0.89

Table 4: The scenario A two-track trigger cross sections for the 2-bin XFT with minimum  $p_T$  of 1.5 GeV and 2.0 GeV.

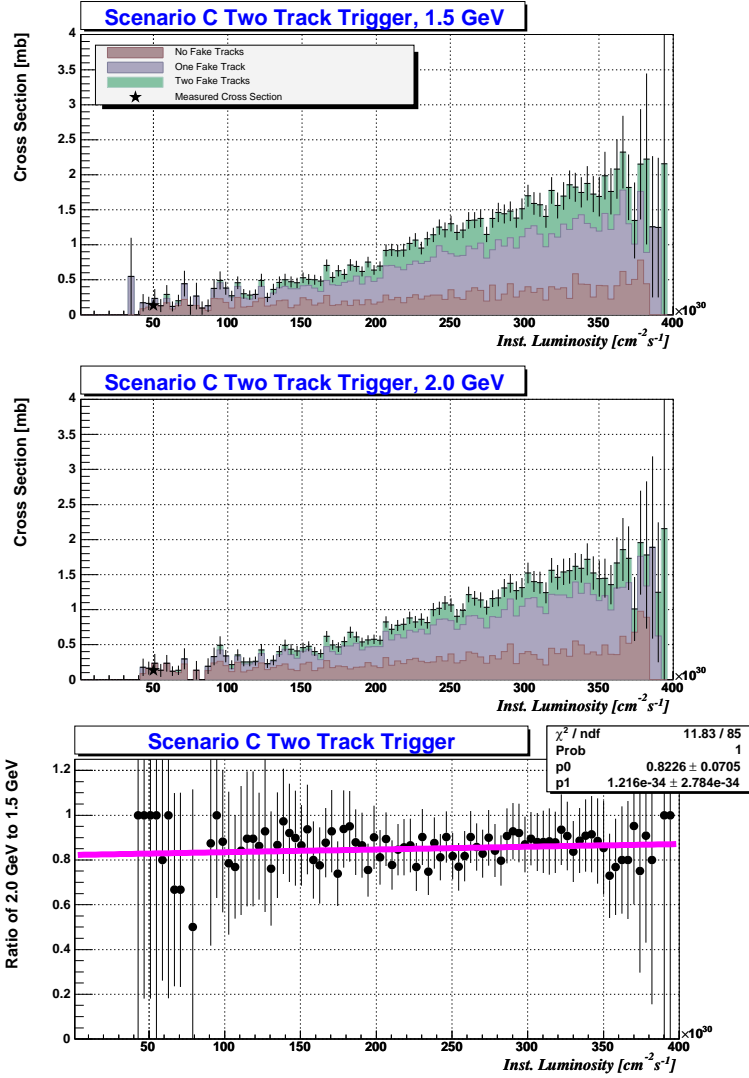


Figure 7: Comparison of the scenario C two-track trigger cross sections for the 2-bin XFT with minimum  $p_T$  thresholds of 1.5 GeV and 2.0 GeV.

Luminosity [ $1 \times 10^{32} \text{ cm}^{-2} \text{ s}^{-1}$ ]	0.5	1.0	1.5	2.0	3.0
1.5 GeV $\sigma$ [mb]	0.12	0.28	0.50	0.78	1.5
2.0 GeV $\sigma$ [mb]	0.13	0.25	0.43	0.66	1.3
ratio	0.83	0.83	0.84	0.85	0.86

Table 5: The scenario C two-track trigger cross sections for the 2-bin XFT with minimum  $p_T$  of 1.5 GeV and 2.0 GeV.

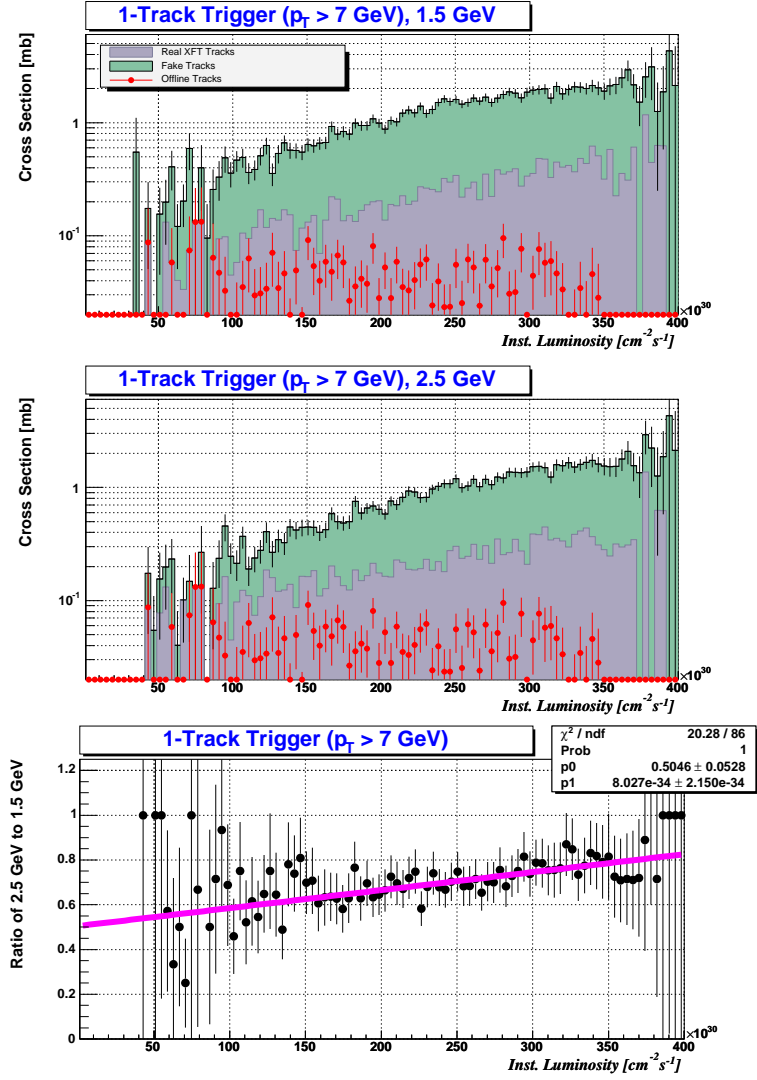


Figure 8: Comparison of the 7 GeV single-track trigger cross sections for the 2-bin XFT with minimum  $p_T$  thresholds of 1.5 GeV and 2.5 GeV.

Luminosity [ $1 \times 10^{32} \text{ cm}^{-2} \text{ s}^{-1}$ ]	0.5	1.0	1.5	2.0	3.0
1.5 GeV $\sigma$ [mb]	0.09	0.37	0.68	1.0	1.8
2.5 GeV $\sigma$ [mb]	0.06	0.22	0.43	0.69	1.4
ratio	0.54	0.58	0.63	0.67	0.75

Table 6: The 7 GeV single-track trigger cross sections for the 2-bin XFT with minimum  $p_T$  of 1.5 GeV and 2.5 GeV.

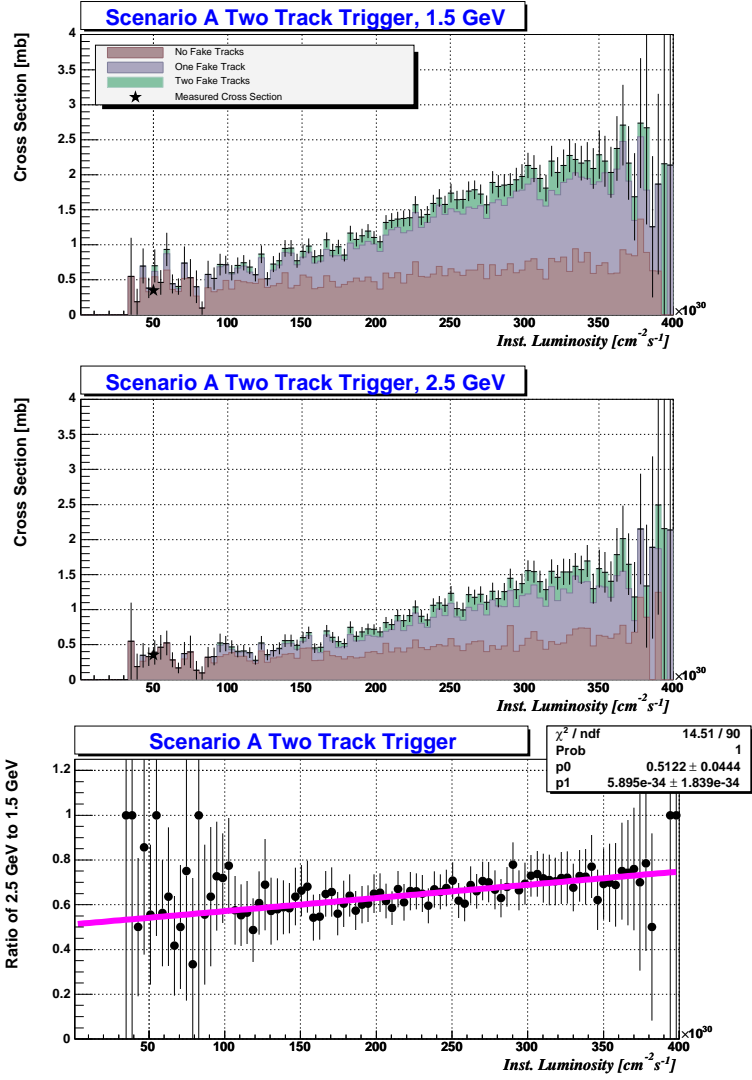


Figure 9: Comparison of the scenario A two-track trigger cross sections for the 2-bin XFT with minimum  $p_T$  thresholds of 1.5 GeV and 2.5 GeV.

Luminosity [ $1 \times 10^{32} \text{ cm}^{-2} \text{ s}^{-1}$ ]	0.5	1.0	1.5	2.0	3.0
1.5 GeV $\sigma$ [mb]	0.33	0.59	0.88	1.2	1.9
2.5 GeV $\sigma$ [mb]	0.23	0.35	0.52	0.75	1.3
ratio	0.54	0.57	0.60	0.63	0.69

Table 7: The scenario A two-track trigger cross sections for the 2-bin XFT with minimum  $p_T$  of 1.5 GeV and 2.5 GeV.

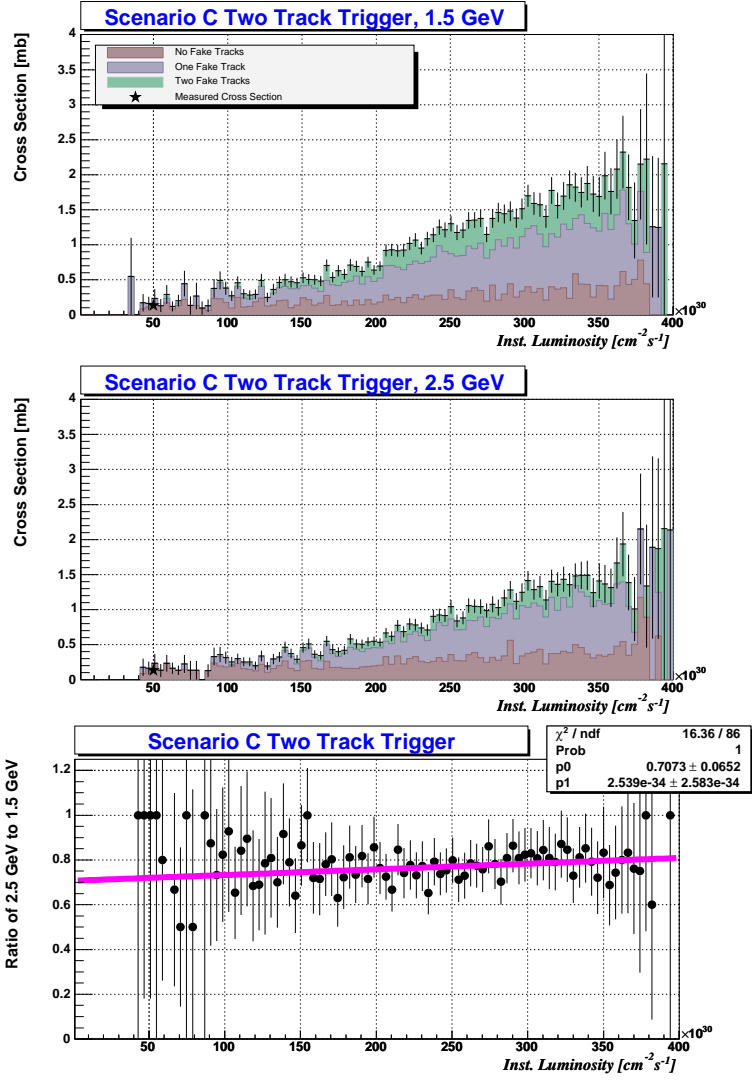


Figure 10: Comparison of the scenario C two-track trigger cross sections for the 2-bin XFT with minimum  $p_T$  thresholds of 1.5 GeV and 2.5 GeV.

Luminosity [ $1 \times 10^{32} \text{ cm}^{-2} \text{ s}^{-1}$ ]	0.5	1.0	1.5	2.0	3.0
1.5 GeV $\sigma$ [mb]	0.12	0.28	0.50	0.78	1.5
2.5 GeV $\sigma$ [mb]	0.14	0.23	0.38	0.59	1.2
ratio	0.72	0.73	0.75	0.76	0.78

Table 8: The scenario C two-track trigger cross sections for the 2-bin XFT with minimum  $p_T$  of 1.5 GeV and 2.5 GeV.

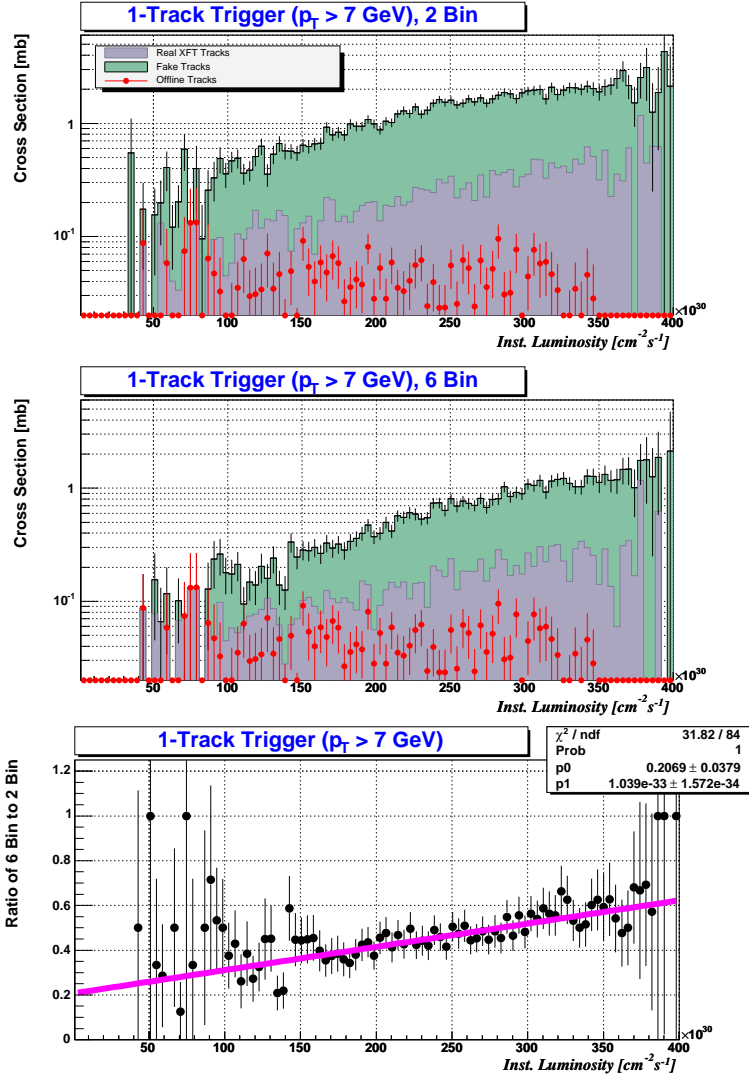


Figure 11: Comparison of the 7 GeV single-track trigger cross sections for the 2-bin XFT with minimum  $p_T = 1.5$  GeV and the 6-bin XFT finder-only upgrade with minimum  $p_T = 2.0$  GeV.

Luminosity [ $1 \times 10^{32} \text{ cm}^{-2} \text{ s}^{-1}$ ]	0.5	1.0	1.5	2.0	3.0
2-bin $\sigma$ [mb]	0.09	0.37	0.68	1.0	1.8
6-bin $\sigma$ [mb]	0.08	0.13	0.25	0.42	0.95
ratio	0.26	0.31	0.36	0.41	0.52

Table 9: The 7 GeV single-track trigger cross sections for the 2-bin XFT with minimum  $p_T = 1.5$  GeV and the 6-bin XFT finder-only upgrade with minimum  $p_T = 2.0$  GeV.

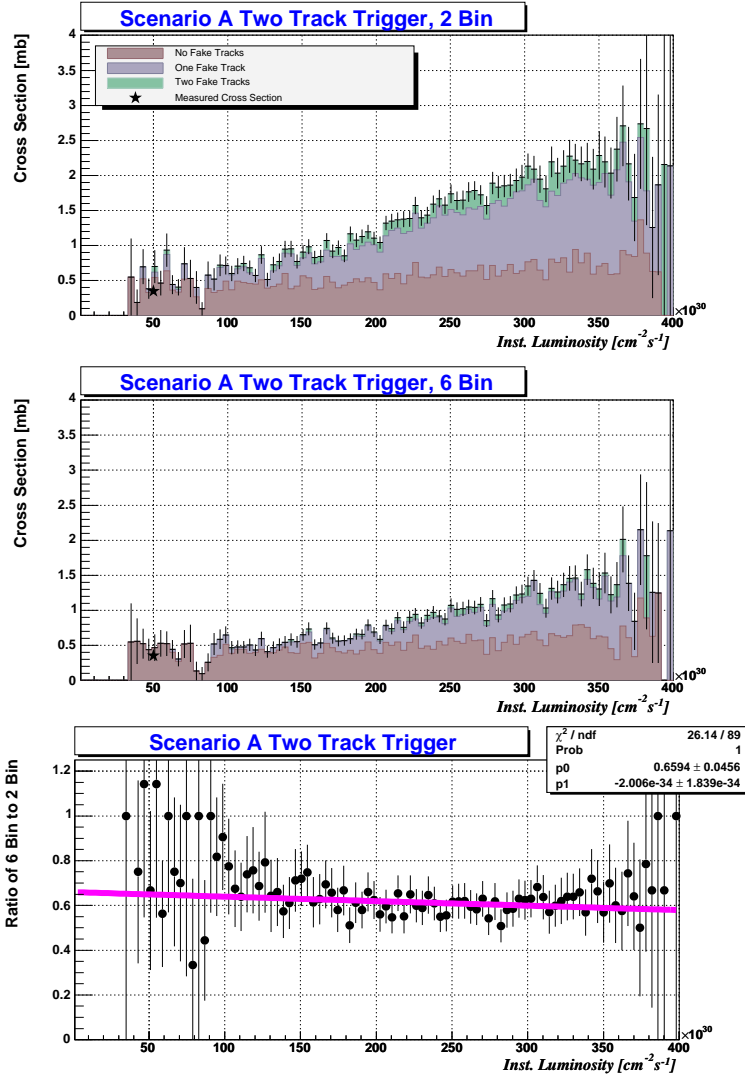


Figure 12: Comparison of the scenario A two-track trigger cross sections for the 2-bin XFT with minimum  $p_T = 1.5$  GeV and the 6-bin XFT finder-only upgrade with minimum  $p_T = 2.0$  GeV.

Luminosity [ $1 \times 10^{32} \text{ cm}^{-2} \text{ s}^{-1}$ ]	0.5	1.0	1.5	2.0	3.0
2-bin $\sigma$ [mb]	0.33	0.59	0.88	1.2	1.9
6-bin $\sigma$ [mb]	0.35	0.43	0.56	0.73	1.2
ratio	0.65	0.64	0.64	0.62	0.60

Table 10: The scenario A two-track trigger cross sections for the 2-bin XFT with minimum  $p_T = 1.5$  GeV and the 6-bin XFT finder-only upgrade with minimum  $p_T = 2.0$  GeV.

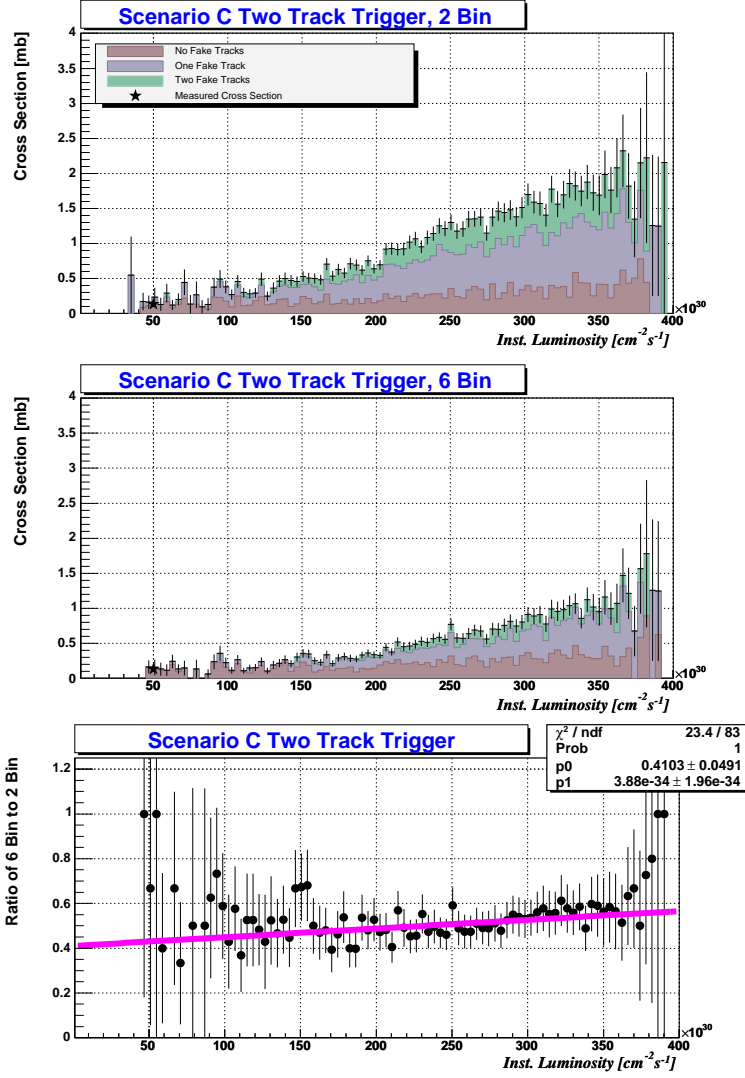


Figure 13: Comparison of the scenario C two-track trigger cross sections for the 2-bin XFT with minimum  $p_T = 1.5$  GeV and the 6-bin XFT finder-only upgrade with minimum  $p_T = 2.0$  GeV.

Luminosity [ $1 \times 10^{32} \text{ cm}^{-2} \text{ s}^{-1}$ ]	0.5	1.0	1.5	2.0	3.0
2-bin $\sigma$ [mb]	0.12	0.28	0.50	0.78	1.5
6-bin $\sigma$ [mb]	0.12	0.15	0.23	0.38	0.81
ratio	0.43	0.45	0.47	0.49	0.53

Table 11: The scenario C two-track trigger cross sections for the 2-bin XFT with minimum  $p_T = 1.5$  GeV and the 6-bin XFT finder-only upgrade with minimum  $p_T = 2.0$  GeV.

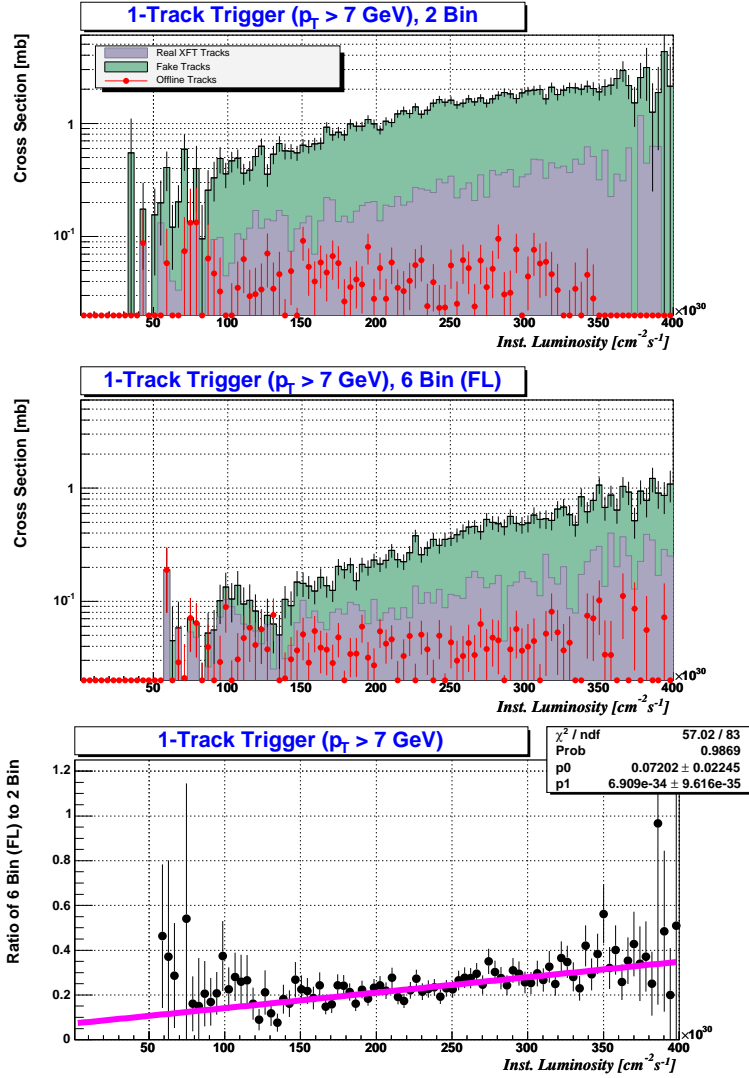


Figure 14: Comparison of the 7 GeV single-track trigger cross sections for the 2-bin XFT with minimum  $p_T = 1.5$  GeV and the 6-bin XFT finder + linker upgrade with minimum  $p_T = 2.0$  GeV.

Luminosity [ $1 \times 10^{32} \text{ cm}^{-2} \text{ s}^{-1}$ ]	0.5	1.0	1.5	2.0	3.0
2-bin $\sigma$ [mb]	0.09	0.37	0.68	1.0	1.8
6-bin (Finder+Linker) $\sigma$ [mb]	0.03	0.06	0.12	0.21	0.53
ratio	0.11	0.14	0.18	0.21	0.28

Table 12: The 7 GeV single-track trigger cross sections for the 2-bin XFT with minimum  $p_T = 1.5$  GeV and the 6-bin XFT finder + linker upgrade with minimum  $p_T = 2.0$  GeV.

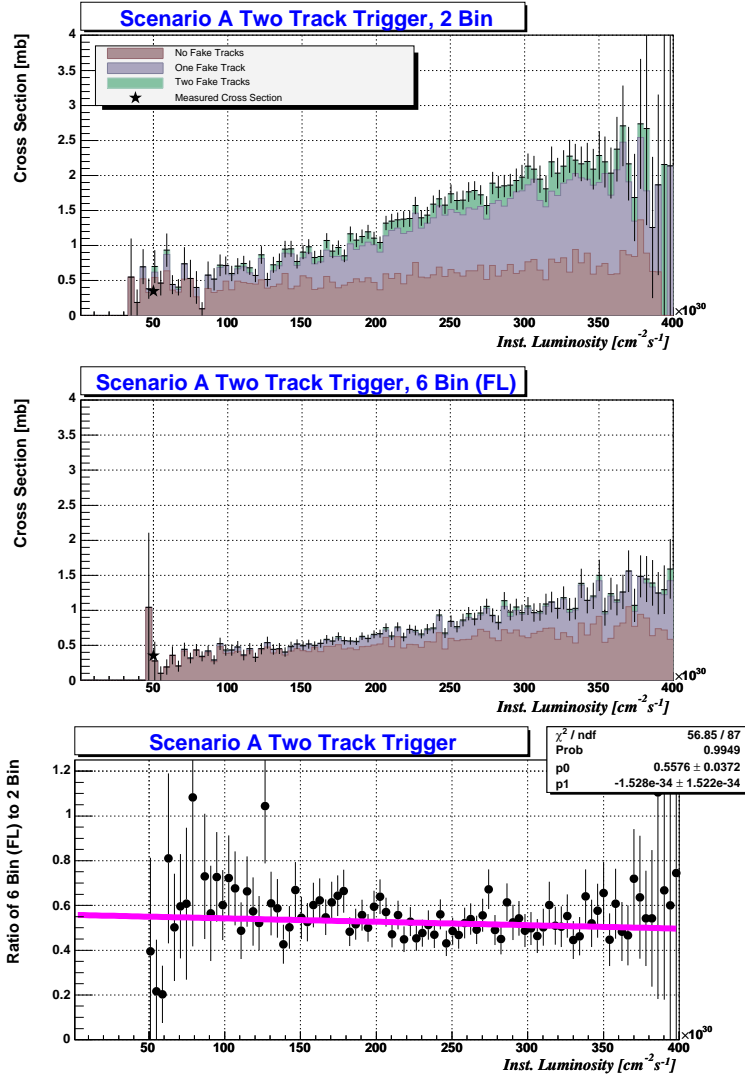


Figure 15: Comparison of the scenario A two-track trigger cross sections for the 2-bin XFT with minimum  $p_T = 1.5$  GeV and the 6-bin XFT finder + linker upgrade with minimum  $p_T = 2.0$  GeV.

Luminosity [ $1 \times 10^{32} \text{ cm}^{-2} \text{ s}^{-1}$ ]	0.5	1.0	1.5	2.0	3.0
2-bin $\sigma$ [mb]	0.33	0.59	0.88	1.2	1.9
6-bin (Finder+Linker) $\sigma$ [mb]	0.28	0.38	0.50	0.65	1.0
ratio	0.55	0.54	0.53	0.53	0.51

Table 13: The scenario A two-track trigger cross sections for the 2-bin XFT with minimum  $p_T = 1.5$  GeV and the 6-bin XFT finder + linker upgrade with minimum  $p_T = 2.0$  GeV.

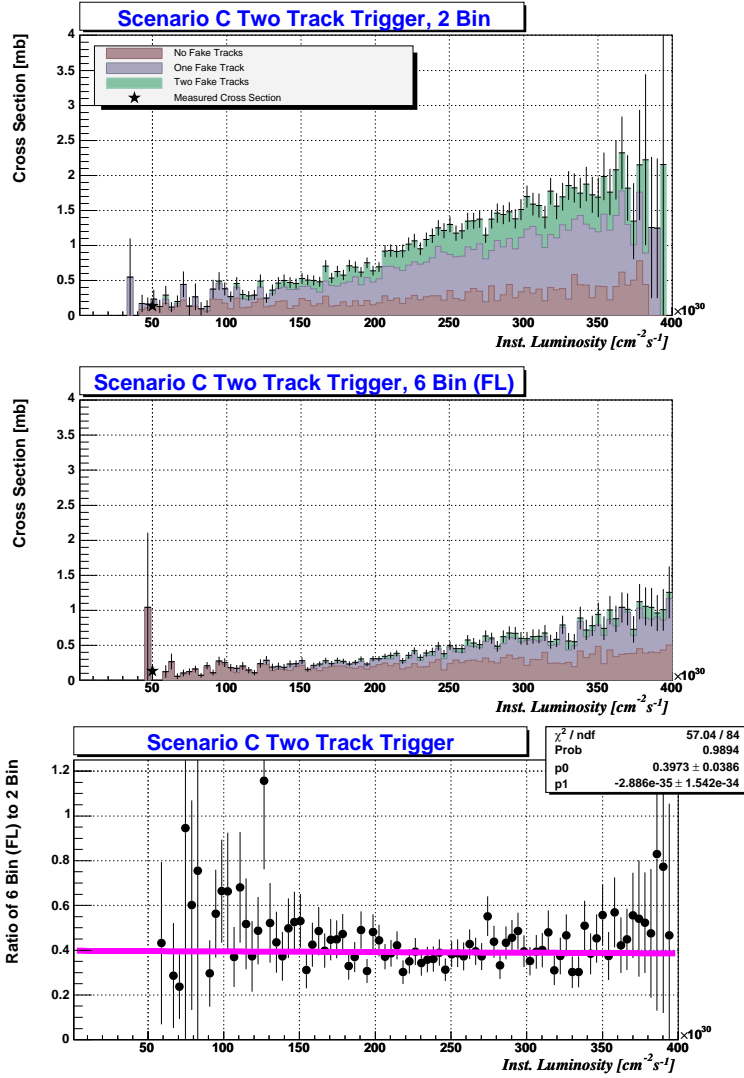


Figure 16: Comparison of the scenario C two-track trigger cross sections for the 2-bin XFT with minimum  $p_T = 1.5$  GeV and the 6-bin XFT finder + linker upgrade with minimum  $p_T = 2.0$  GeV.

Luminosity [ $1 \times 10^{32} \text{ cm}^{-2} \text{ s}^{-1}$ ]	0.5	1.0	1.5	2.0	3.0
2-bin $\sigma$ [mb]	0.12	0.28	0.50	0.78	1.5
6-bin (Finder+Linker) $\sigma$ [mb]	0.12	0.15	0.21	0.30	0.61
ratio	0.40	0.39	0.39	0.39	0.39

Table 14: The scenario C two-track trigger cross sections for the 2-bin XFT with minimum  $p_T = 1.5$  GeV and the 6-bin XFT finder + linker upgrade with minimum  $p_T = 2.0$  GeV.

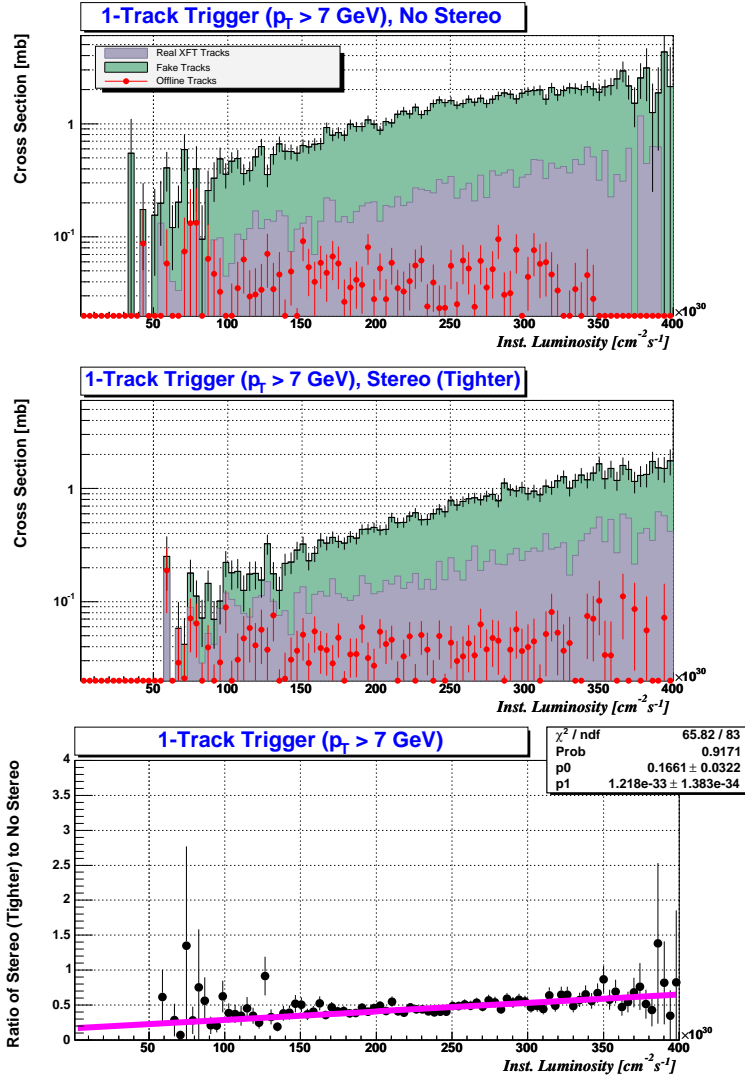


Figure 17: Comparison of the 7 GeV single-track trigger cross sections for the 2-bin XFT with minimum  $p_T = 1.5$  GeV and the 2-bin XFT (minimum  $p_T = 1.5$  GeV) + stereo (minimum  $p_T = 2.0$  GeV).

Luminosity [ $1 \times 10^{32} \text{ cm}^{-2} \text{ s}^{-1}$ ]	0.5	1.0	1.5	2.0	3.0
2-bin $\sigma$ [mb]	0.09	0.37	0.68	1.0	1.8
2-bin + stereo $\sigma$ [mb]	0.04	0.13	0.26	0.45	0.97
ratio	0.23	0.29	0.35	0.41	0.53

Table 15: The 7 GeV single-track trigger cross sections for the 2-bin XFT with minimum  $p_T = 1.5$  GeV and the 2-bin XFT (minimum  $p_T = 1.5$  GeV) + stereo (minimum  $p_T = 2.0$  GeV).

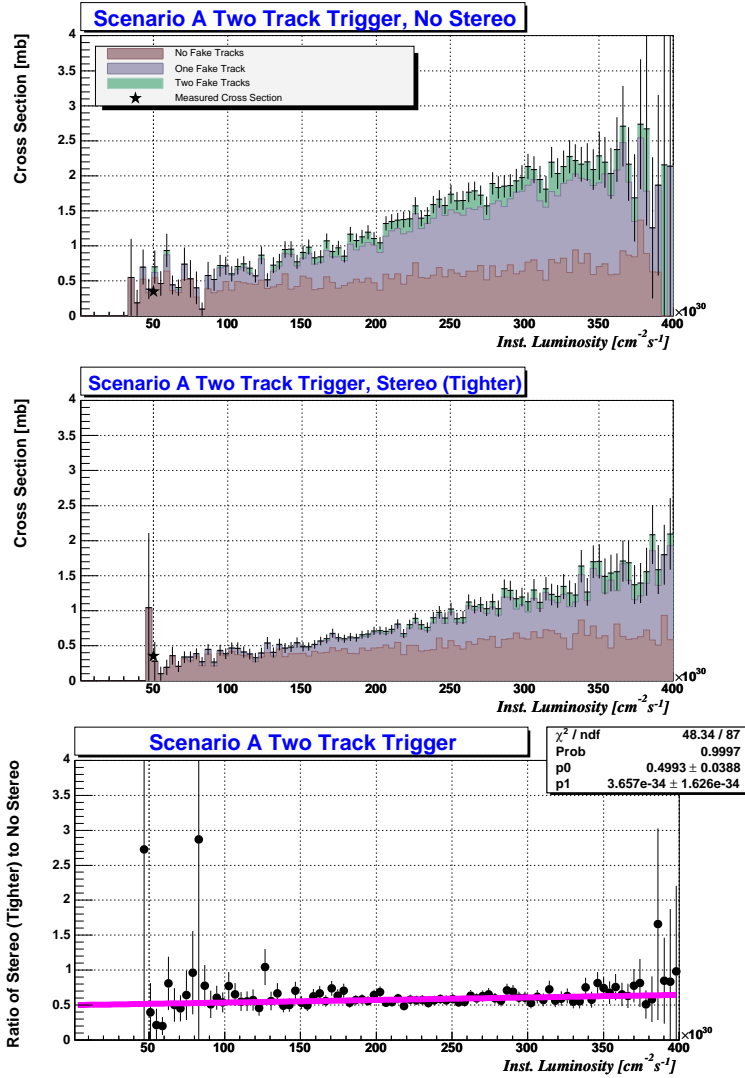


Figure 18: Comparison of the scenario A two-track trigger cross sections for the 2-bin XFT with minimum  $p_T = 1.5$  GeV and the 2-bin XFT (minimum  $p_T = 1.5$  GeV) + stereo (minimum  $p_T = 2.0$  GeV).

Luminosity [ $1 \times 10^{32} \text{ cm}^{-2} \text{ s}^{-1}$ ]	0.5	1.0	1.5	2.0	3.0
2-bin $\sigma$ [mb]	0.33	0.59	0.88	1.2	1.9
2-bin + stereo $\sigma$ [mb]	0.24	0.36	0.51	0.70	1.2
ratio	0.52	0.54	0.55	0.57	0.61

Table 16: The scenario A two-track trigger cross sections for the 2-bin XFT with minimum  $p_T = 1.5$  GeV and the 2-bin XFT (minimum  $p_T = 1.5$  GeV) + stereo (minimum  $p_T = 2.0$  GeV).

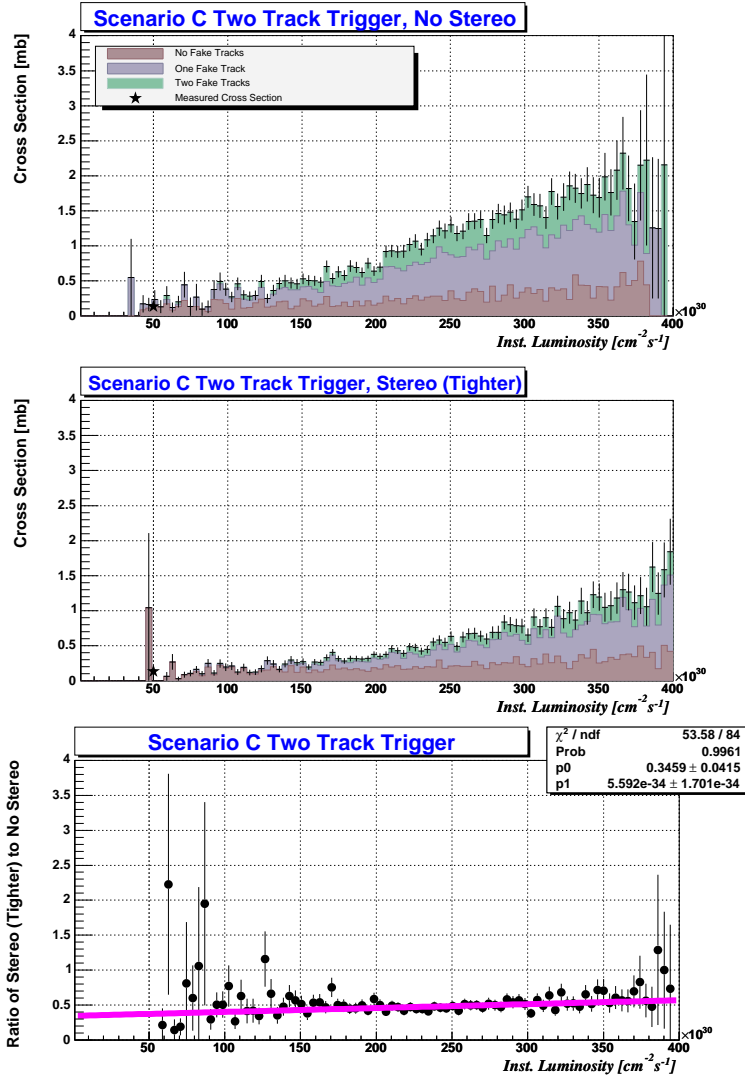


Figure 19: Comparison of the scenario C two-track trigger cross sections for the 2-bin XFT with minimum  $p_T = 1.5$  GeV and the 2-bin XFT (minimum  $p_T = 1.5$  GeV) + stereo (minimum  $p_T = 2.0$  GeV).

Luminosity [ $1 \times 10^{32} \text{ cm}^{-2} \text{ s}^{-1}$ ]	0.5	1.0	1.5	2.0	3.0
2-bin $\sigma$ [mb]	0.12	0.28	0.50	0.78	1.5
2-bin + stereo $\sigma$ [mb]	0.09	0.14	0.23	0.38	0.79
ratio	0.37	0.40	0.43	0.46	0.51

Table 17: The scenario C two-track trigger cross sections for the 2-bin XFT with minimum  $p_T = 1.5$  GeV and the 2-bin XFT (minimum  $p_T = 1.5$  GeV) + stereo (minimum  $p_T = 2.0$  GeV).

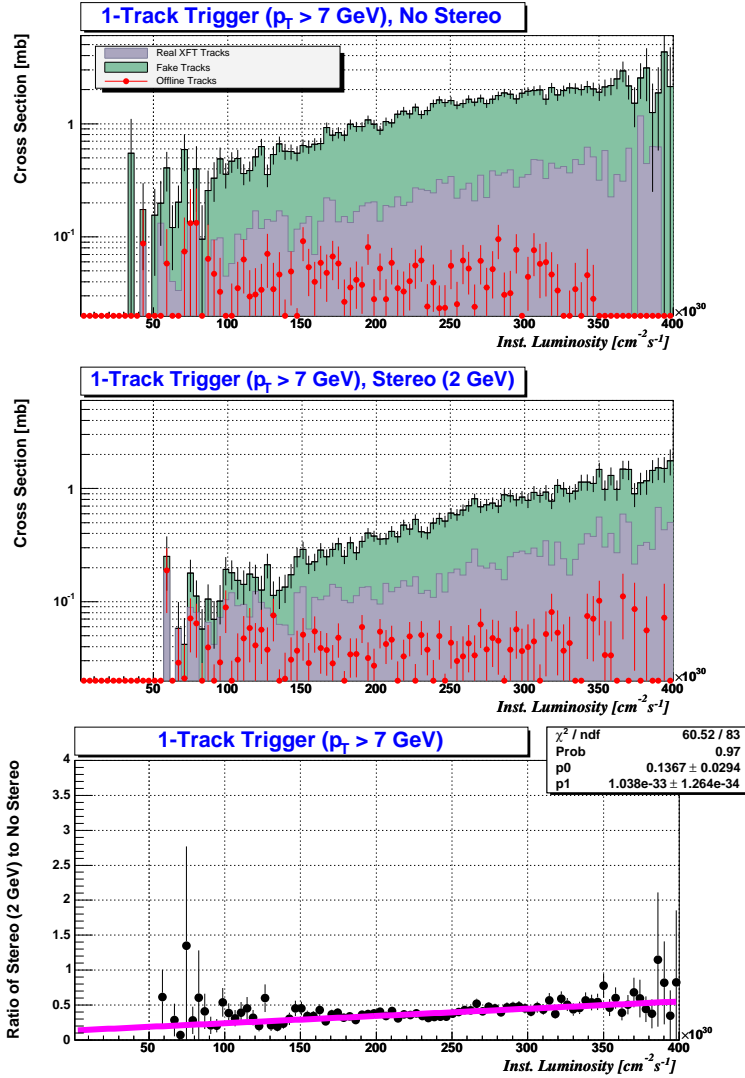


Figure 20: Comparison of the 7 GeV single-track trigger cross sections for the 2-bin XFT with minimum  $p_T = 1.5$  GeV and the 2-bin XFT (minimum  $p_T = 2.0$  GeV) + stereo (minimum  $p_T = 2.0$  GeV).

Luminosity [ $1 \times 10^{32} \text{ cm}^{-2} \text{ s}^{-1}$ ]	0.5	1.0	1.5	2.0	3.0
2-bin $\sigma$ [mb]	0.09	0.37	0.68	1.0	1.8
2-bin + stereo $\sigma$ [mb]	0.06	0.11	0.21	0.37	0.83
ratio	0.19	0.24	0.29	0.34	0.45

Table 18: The 7 GeV single-track trigger cross sections for the 2-bin XFT with minimum  $p_T = 1.5$  GeV and the 2-bin XFT (minimum  $p_T = 2.0$  GeV) + stereo (minimum  $p_T = 2.0$  GeV).

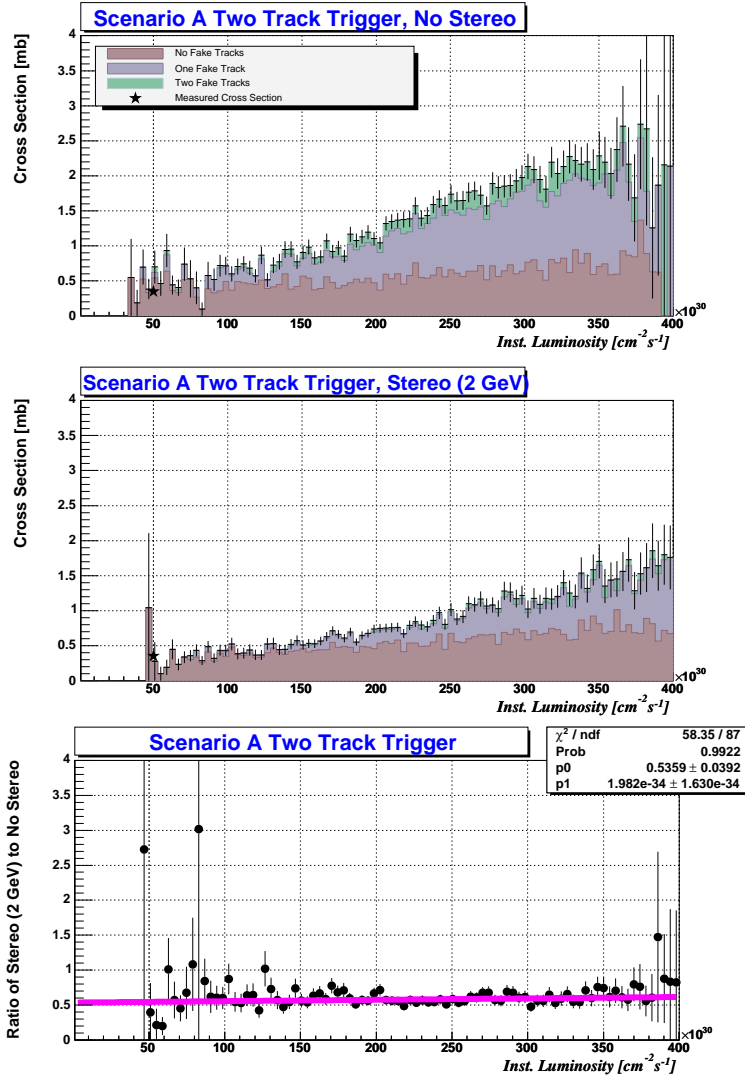


Figure 21: Comparison of the scenario A two-track trigger cross sections for the 2-bin XFT with minimum  $p_T = 1.5$  GeV and the 2-bin XFT (minimum  $p_T = 2.0$  GeV) + stereo (minimum  $p_T = 2.0$  GeV).

Luminosity [ $1 \times 10^{32} \text{ cm}^{-2} \text{ s}^{-1}$ ]	0.5	1.0	1.5	2.0	3.0
2-bin $\sigma$ [mb]	0.33	0.59	0.88	1.2	1.9
2-bin + stereo $\sigma$ [mb]	0.27	0.38	0.53	0.71	1.2
ratio	0.55	0.56	0.57	0.58	0.60

Table 19: The scenario A two-track trigger cross sections for the 2-bin XFT with minimum  $p_T = 1.5$  GeV and the 2-bin XFT (minimum  $p_T = 2.0$  GeV) + stereo (minimum  $p_T = 2.0$  GeV).

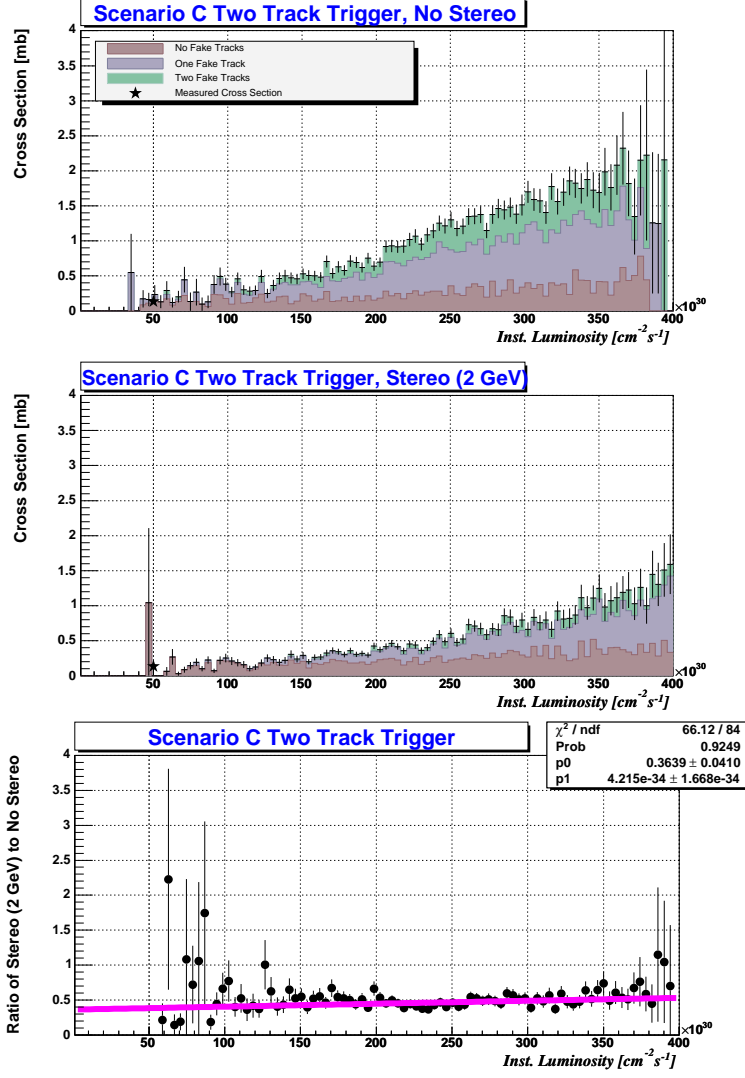


Figure 22: Comparison of the scenario C two-track trigger cross sections for the 2-bin XFT with minimum  $p_T = 1.5$  GeV and the 2-bin XFT (minimum  $p_T = 2.0$  GeV) + stereo (minimum  $p_T = 2.0$  GeV).

Luminosity [ $1 \times 10^{32} \text{ cm}^{-2} \text{ s}^{-1}$ ]	0.5	1.0	1.5	2.0	3.0
2-bin $\sigma$ [mb]	0.12	0.28	0.50	0.78	1.5
2-bin + stereo $\sigma$ [mb]	0.08	0.14	0.24	0.37	0.75
ratio	0.39	0.41	0.43	0.45	0.49

Table 20: The scenario C two-track trigger cross sections for the 2-bin XFT with minimum  $p_T = 1.5$  GeV and the 2-bin XFT (minimum  $p_T = 2.0$  GeV) + stereo (minimum  $p_T = 2.0$  GeV).

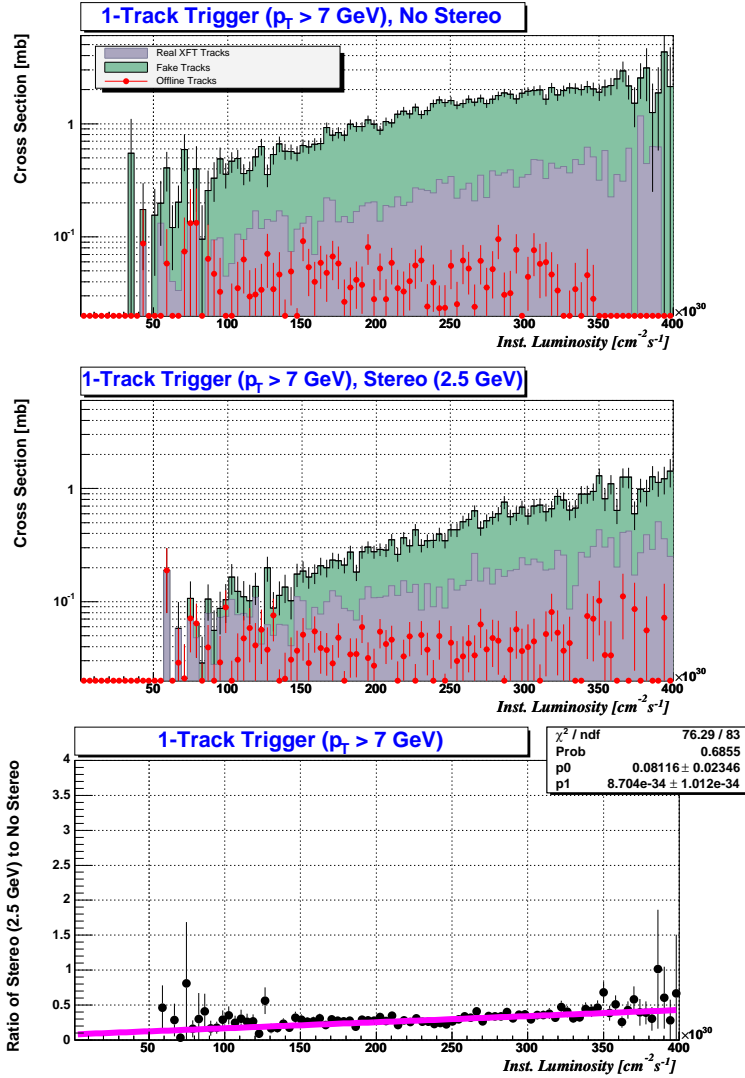


Figure 23: Comparison of the 7 GeV single-track trigger cross sections for the 2-bin XFT with minimum  $p_T = 1.5$  GeV and the 2-bin XFT (minimum  $p_T = 2.5$  GeV) + stereo (minimum  $p_T = 2.5$  GeV).

Luminosity [ $1 \times 10^{32} \text{ cm}^{-2} \text{ s}^{-1}$ ]	0.5	1.0	1.5	2.0	3.0
2-bin $\sigma$ [mb]	0.09	0.37	0.68	1.0	1.8
2-bin + stereo $\sigma$ [mb]	0.03	0.08	0.16	0.28	0.63
ratio	0.12	0.17	0.21	0.26	0.34

Table 21: The 7 GeV single-track trigger cross sections for the 2-bin XFT with minimum  $p_T = 1.5$  GeV and the 2-bin XFT (minimum  $p_T = 2.5$  GeV) + stereo (minimum  $p_T = 2.5$  GeV).

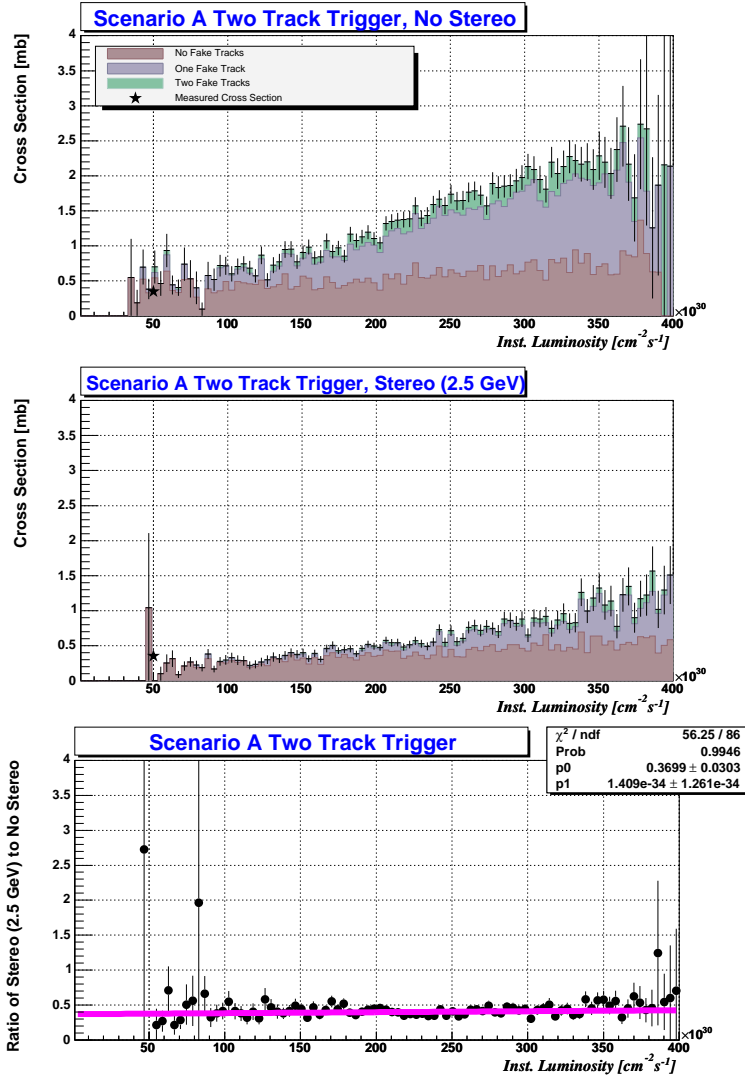


Figure 24: Comparison of the scenario A two-track trigger cross sections for the 2-bin XFT with minimum  $p_T = 1.5$  GeV and the 2-bin XFT (minimum  $p_T = 2.5$  GeV) + stereo (minimum  $p_T = 2.5$  GeV).

Luminosity [ $1 \times 10^{32} \text{ cm}^{-2} \text{ s}^{-1}$ ]	0.5	1.0	1.5	2.0	3.0
2-bin $\sigma$ [mb]	0.33	0.59	0.88	1.2	1.9
2-bin + stereo $\sigma$ [mb]	0.17	0.25	0.36	0.49	0.81
ratio	0.38	0.38	0.39	0.40	0.41

Table 22: The scenario A two-track trigger cross sections for the 2-bin XFT with minimum  $p_T = 1.5$  GeV and the 2-bin XFT (minimum  $p_T = 2.5$  GeV) + stereo (minimum  $p_T = 2.5$  GeV).

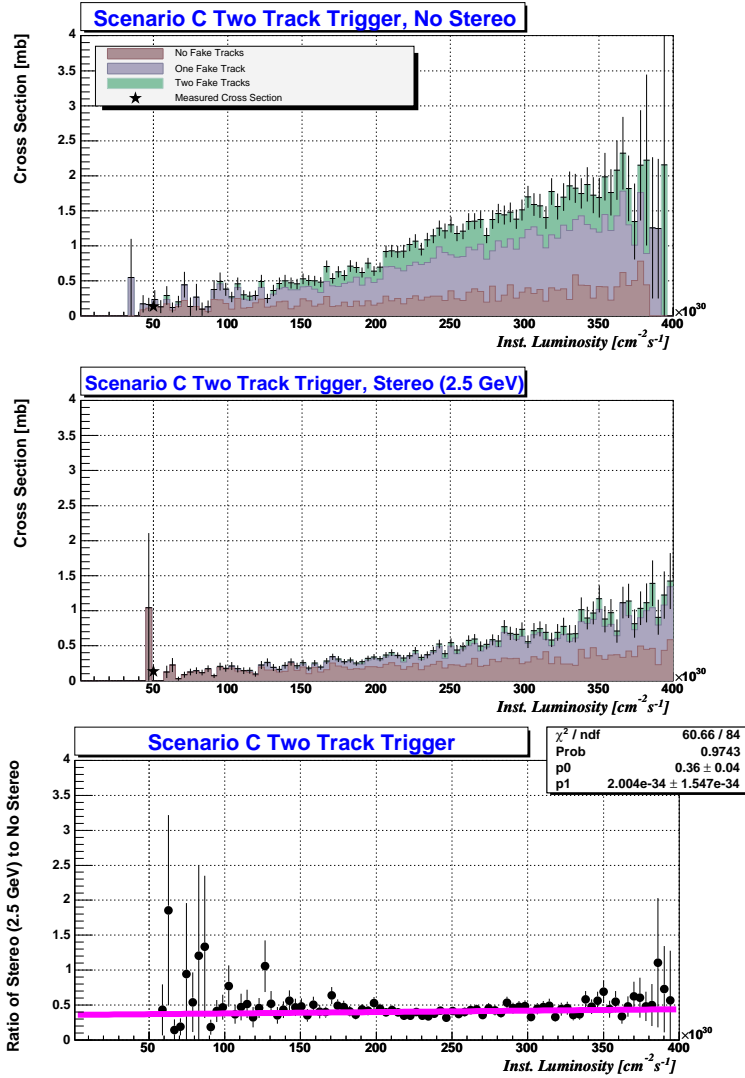


Figure 25: Comparison of the scenario C two-track trigger cross sections for the 2-bin XFT with minimum  $p_T = 1.5$  GeV and the 2-bin XFT (minimum  $p_T = 2.5$  GeV) + stereo (minimum  $p_T = 2.5$  GeV).

Luminosity [ $1 \times 10^{32} \text{ cm}^{-2} \text{ s}^{-1}$ ]	0.5	1.0	1.5	2.0	3.0
2-bin $\sigma$ [mb]	0.12	0.28	0.50	0.78	1.5
2-bin + stereo $\sigma$ [mb]	0.08	0.13	0.21	0.33	0.65
ratio	0.37	0.38	0.39	0.40	0.42

Table 23: The scenario C two-track trigger cross sections for the 2-bin XFT with minimum  $p_T = 1.5$  GeV and the 2-bin XFT (minimum  $p_T = 2.5$  GeV) + stereo (minimum  $p_T = 2.5$  GeV).

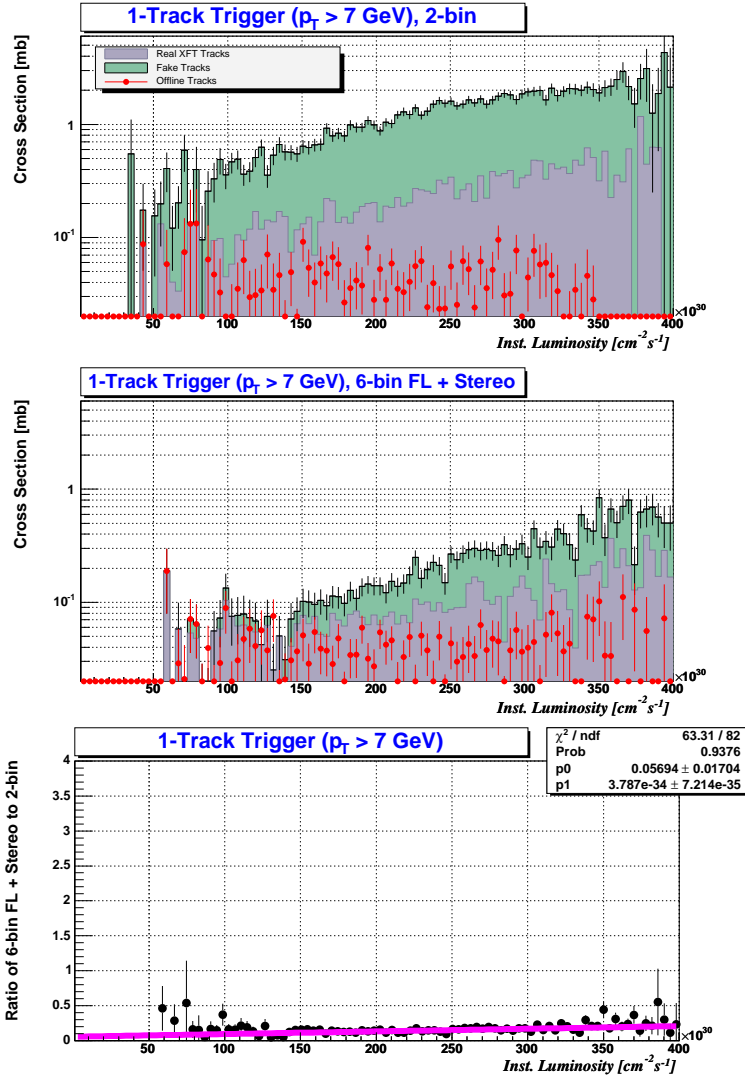


Figure 26: Comparison of the 7 GeV single-track trigger cross sections for the 2-bin XFT with minimum  $p_T = 1.5$  GeV and the 6-bin XFT finder + linker + stereo upgrade with minimum  $p_T = 2.0$  GeV.

Luminosity [ $1 \times 10^{32} \text{ cm}^{-2} \text{ s}^{-1}$ ]	0.5	1.0	1.5	2.0	3.0
2-bin $\sigma$ [mb]	0.09	0.37	0.68	1.0	1.8
6-bin finder + linker + stereo $\sigma$ [mb]	0.02	0.04	0.08	0.14	0.32
ratio	0.08	0.09	0.11	0.13	0.17

Table 24: The 7 GeV single-track trigger cross sections for the 2-bin XFT with minimum  $p_T = 1.5$  GeV and the 6-bin finder + linker + stereo XFT upgrade with minimum  $p_T = 2.0$  GeV.

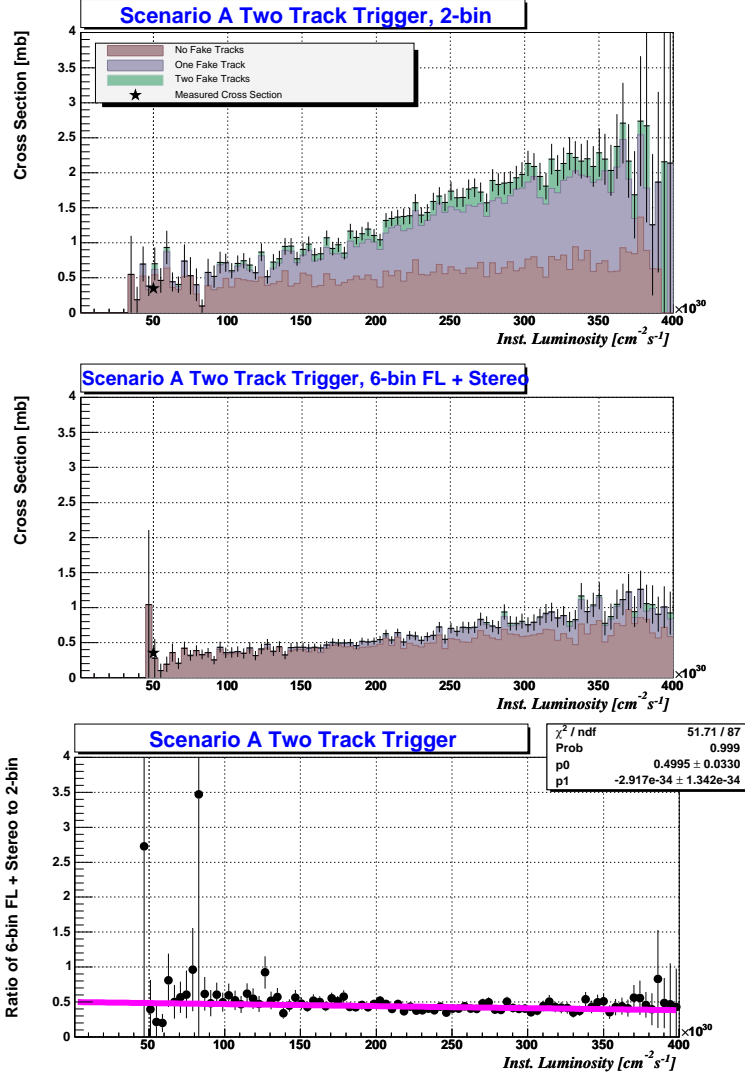


Figure 27: Comparison of the scenario A two-track trigger cross sections for the 2-bin XFT with minimum  $p_T = 1.5$  GeV and the 6-bin finder + linker + stereo XFT upgrade with minimum  $p_T = 2.0$  GeV.

Luminosity [ $1 \times 10^{32} \text{ cm}^{-2} \text{ s}^{-1}$ ]	0.5	1.0	1.5	2.0	3.0
2-bin $\sigma$ [mb]	0.33	0.59	0.88	1.2	1.9
6-bin + finder + linker + stereo $\sigma$ [mb]	0.27	0.34	0.43	0.54	0.80
ratio	0.49	0.47	0.46	0.44	0.41

Table 25: The scenario A two-track trigger cross sections for the 2-bin XFT with minimum  $p_T = 1.5$  GeV and the 6-bin finder + linker + stereo XFT upgrade with minimum  $p_T = 2.0$  GeV.

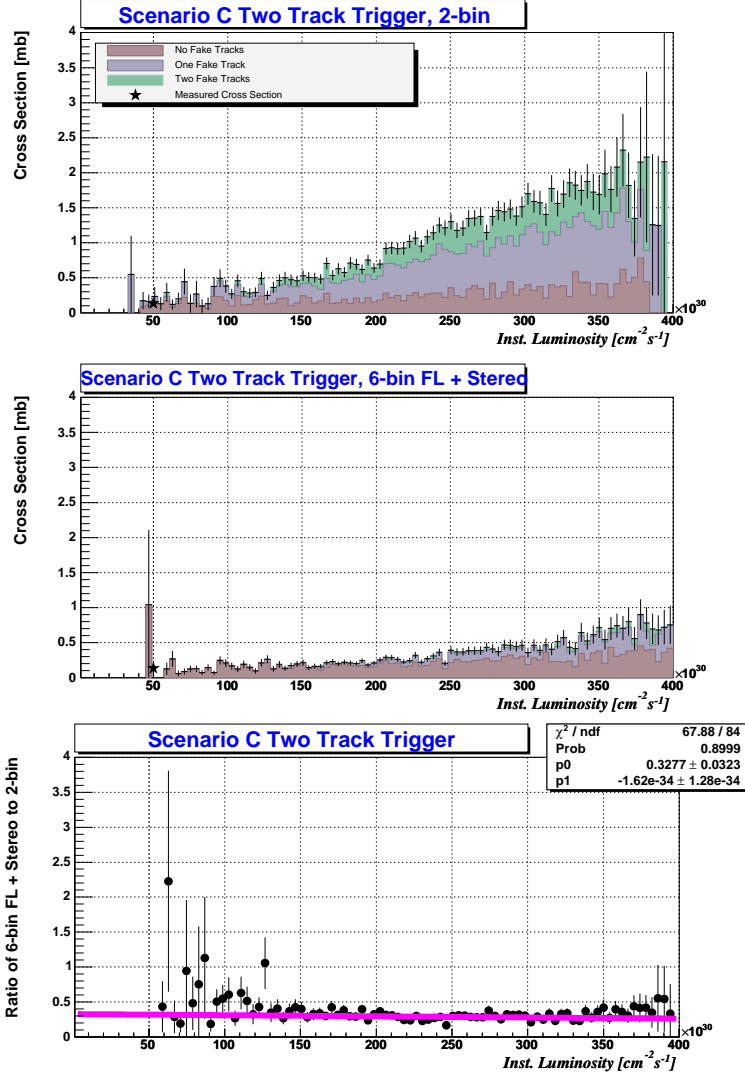


Figure 28: Comparison of the scenario C two-track trigger cross sections for the 2-bin XFT with minimum  $p_T = 1.5$  GeV and the 6-bin finder + linker + stereo XFT upgrade with minimum  $p_T = 2.0$  GeV.

Luminosity [ $1 \times 10^{32} \text{ cm}^{-2} \text{ s}^{-1}$ ]	0.5	1.0	1.5	2.0	3.0
2-bin $\sigma$ [mb]	0.12	0.28	0.50	0.78	1.5
2-bin + finder + linker + stereo $\sigma$ [mb]	0.11	0.13	0.17	0.23	0.44
ratio	0.32	0.31	0.30	0.30	0.28

Table 26: The scenario C two-track trigger cross sections for the 2-bin XFT with minimum  $p_T = 1.5$  GeV and the 6-bin finder + linker + stereo with minimum  $p_T = 2.0$  GeV.

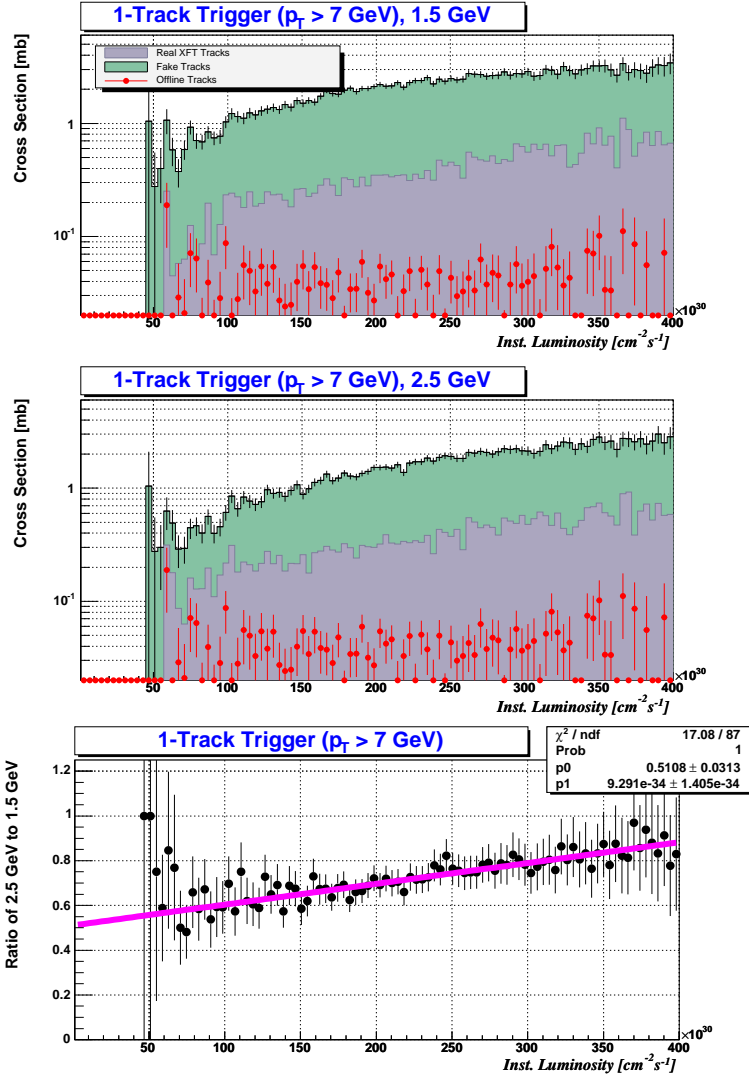


Figure 29: Comparison of the 7 GeV single-track trigger cross sections for the 2-bin XFT with minimum  $p_T = 1.5$  GeV and the 2-bin XFT with a minimum  $p_T = 2.5$  GeV for a degraded COT.

Luminosity [ $1 \times 10^{32} \text{ cm}^{-2} \text{ s}^{-1}$ ]	0.5	1.0	1.5	2.0	3.0
1.5 GeV (Degraded COT) $\sigma$ [mb]	0.29	0.99	1.6	2.1	2.8
2.5 GeV (Degraded COT) $\sigma$ [mb]	0.16	0.61	1.0	1.5	2.2
ratio	0.56	0.60	0.65	0.70	0.79

Table 27: The 7 GeV single-track trigger cross sections for the 2-bin XFT with minimum  $p_T = 1.5$  GeV and the 2-bin XFT with a minimum  $p_T = 2.5$  GeV for a degraded COT.

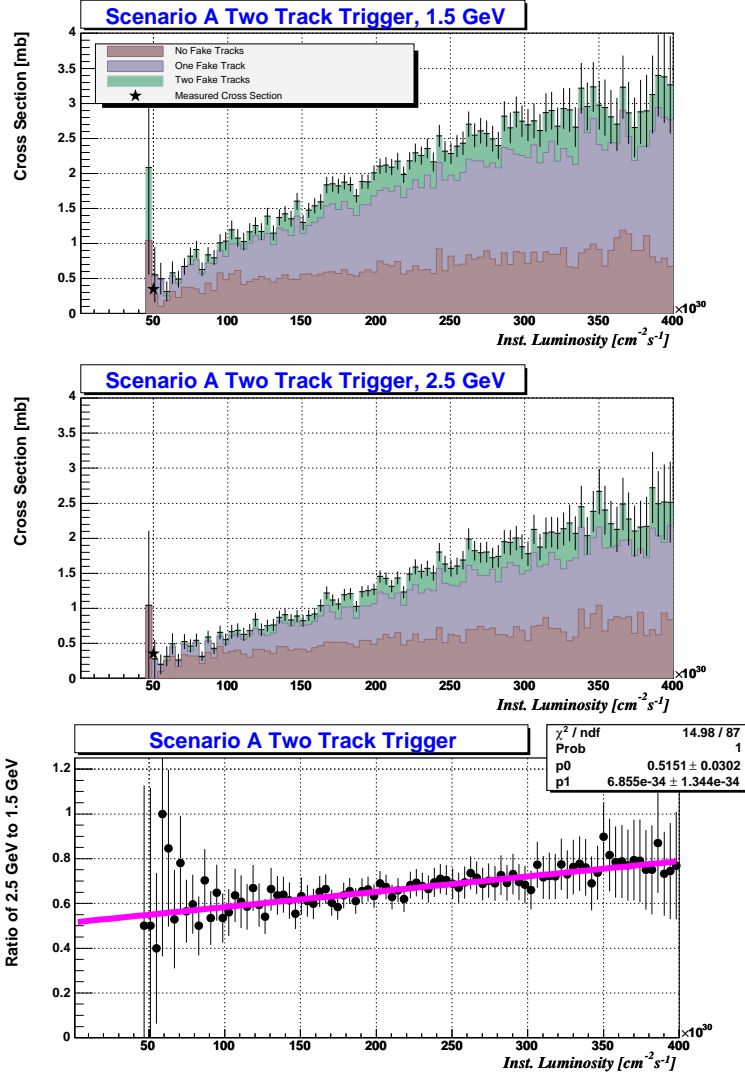


Figure 30: Comparison of the scenario A two-track trigger cross sections for the 2-bin XFT with minimum  $p_T = 1.5$  GeV and the 2-bin XFT with a minimum  $p_T = 2.5$  GeV for a degraded COT.

Luminosity [ $1 \times 10^{32} \text{ cm}^{-2} \text{ s}^{-1}$ ]	0.5	1.0	1.5	2.0	3.0
1.5 GeV (Degraded COT) $\sigma$ [mb]	0.36	0.98	1.5	2.0	2.7
2.5 GeV (Degraded COT) $\sigma$ [mb]	0.22	0.58	0.94	1.3	2.0
ratio	0.55	0.58	0.62	0.65	0.72

Table 28: The scenario A two-track trigger cross sections for the 2-bin XFT with minimum  $p_T = 1.5$  GeV and the 2-bin XFT with a minimum  $p_T = 2.5$  GeV for a degraded COT.

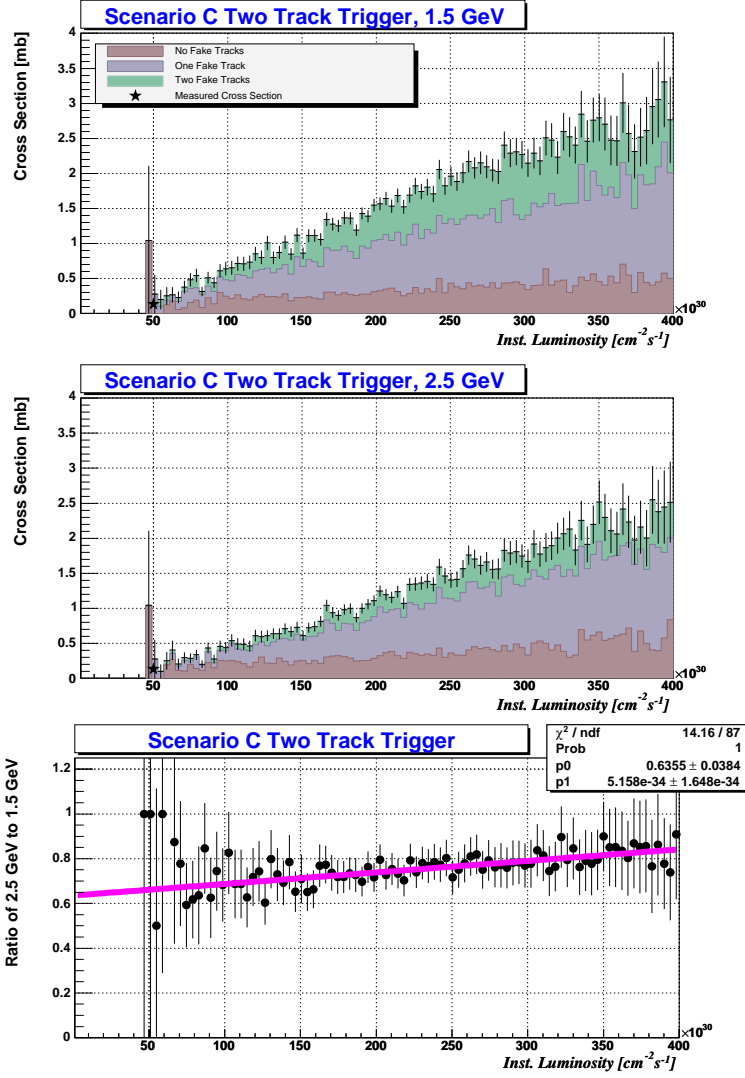


Figure 31: Comparison of the scenario C two-track trigger cross sections for the 2-bin XFT with minimum  $p_T = 1.5$  GeV and the 2-bin XFT with a minimum  $p_T = 2.5$  GeV for a degraded COT.

Luminosity [ $1 \times 10^{32} \text{ cm}^{-2} \text{ s}^{-1}$ ]	0.5	1.0	1.5	2.0	3.0
1.5 GeV (Degraded COT) $\sigma$ [mb]	0.13	0.61	1.1	1.5	2.3
2.5 GeV (Degraded COT) $\sigma$ [mb]	0.10	0.43	0.76	1.1	1.8
ratio	0.66	0.69	0.71	0.74	0.79

Table 29: The scenario C two-track trigger cross sections for the 2-bin XFT with minimum  $p_T = 1.5$  GeV and the 2-bin XFT with a minimum  $p_T = 2.5$  GeV for a degraded COT.

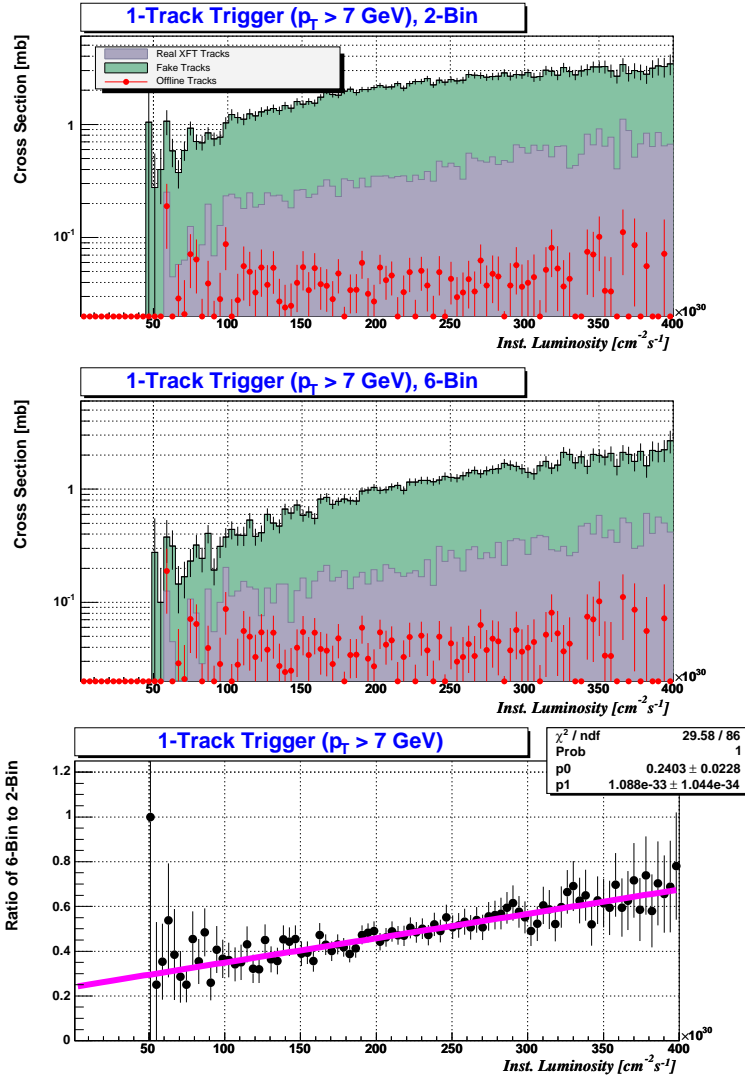


Figure 32: Comparison of the 7 GeV single-track trigger cross sections for the 2-bin XFT with minimum  $p_T = 1.5$  GeV and the 6-bin XFT finder-only upgrade with a minimum  $p_T = 2.0$  GeV for a degraded COT.

Luminosity [ $1 \times 10^{32} \text{ cm}^{-2} \text{ s}^{-1}$ ]	0.5	1.0	1.5	2.0	3.0
2-bin (Degraded COT) $\sigma$ [nb]	0.29	0.99	1.6	2.1	2.8
6-bin (Degraded COT) $\sigma$ [nb]	0.07	0.36	0.65	0.95	1.6
ratio	0.29	0.35	0.40	0.46	0.57

Table 30: The 7 GeV single-track trigger cross sections for the 2-bin XFT with minimum  $p_T = 1.5$  GeV and the 6-bin XFT finder-only upgrade with a minimum  $p_T = 2.0$  GeV for a degraded COT.

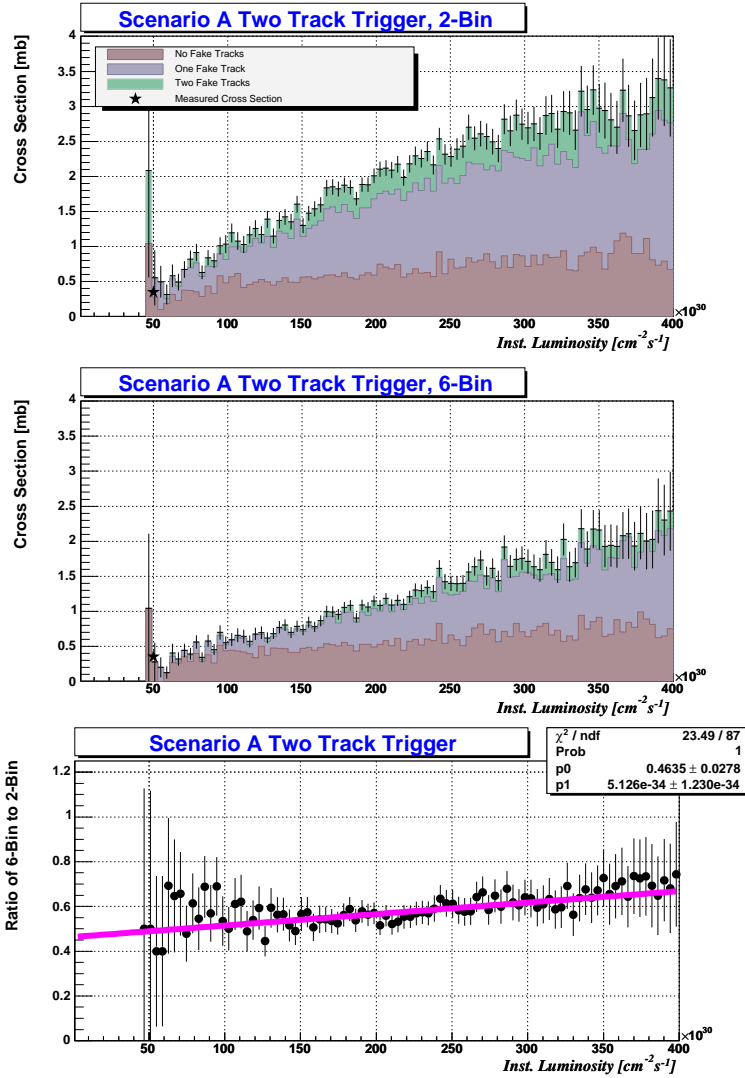


Figure 33: Comparison of the scenario A two-track trigger cross sections for the 2-bin XFT with minimum  $p_T = 1.5$  GeV and the 6-bin XFT finder-only upgrade with a minimum  $p_T = 2.0$  GeV for a degraded COT.

Luminosity [ $1 \times 10^{32} \text{ cm}^{-2} \text{ s}^{-1}$ ]	0.5	1.0	1.5	2.0	3.0
2-bin (Degraded COT) $\sigma$ [mb]	0.36	0.98	1.5	2.0	2.7
6-bin (Degraded COT) $\sigma$ [mb]	0.24	0.54	0.82	1.1	1.7
ratio	0.49	0.51	0.54	0.57	0.62

Table 31: The scenario A two-track trigger cross sections for the 2-bin XFT with minimum  $p_T = 1.5$  GeV and the 6-bin XFT finder-only upgrade with a minimum  $p_T = 2.0$  GeV for a degraded COT.

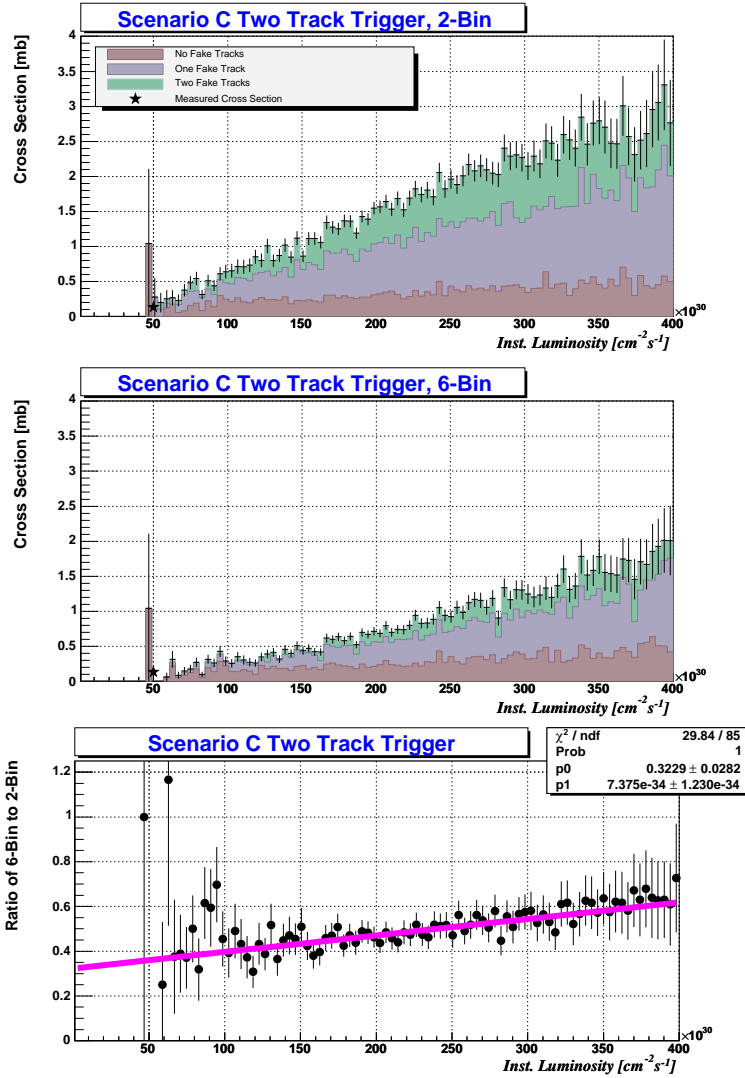


Figure 34: Comparison of the scenario C two-track trigger cross sections for the 2-bin XFT with minimum  $p_T = 1.5$  GeV and the 6-bin XFT finder-only upgrade with a minimum  $p_T = 2.0$  GeV for a degraded COT.

Luminosity [ $1 \times 10^{32} \text{ cm}^{-2} \text{ s}^{-1}$ ]	0.5	1.0	1.5	2.0	3.0
2-bin (Degraded COT) $\sigma$ [nb]	0.13	0.61	1.1	1.5	2.3
6-bin (Degraded COT) $\sigma$ [nb]	0.08	0.25	0.46	0.69	1.3
ratio	0.36	0.40	0.43	0.47	0.54

Table 32: The scenario C two-track trigger cross sections for the 2-bin XFT with minimum  $p_T = 1.5$  GeV and the 6-bin XFT finder-only upgrade with a minimum  $p_T = 2.0$  GeV for a degraded COT.

Upgrade Option	7 GeV Single-Track	Scenario A Two-Track	Scenario C Two-Track
2-Bin (1.5 GeV) (Current System)	1.8 mb [2.2 mb]	1.9 mb [2.7 mb]	1.5 mb [2.3 mb]
2-Bin (2.0 GeV)	1.5 mb (20% decrease)	1.7 mb (10% decrease)	1.3 mb (15% decrease)
2-Bin (2.5 GeV)	1.4 mb [2.2 mb] (25% decrease) [20% decrease]	1.3 mb [2.0 mb] (30% decrease) [30% decrease]	1.2 mb [1.7 mb] (20% decrease) [40% decrease]
6-Bin (2.0 GeV) Finder-Only	0.95 mb [1.6 mb] (50% decrease) [40% decrease]	1.1 mb [1.7 mb] (40% decrease) [40% decrease]	0.81 mb [1.3 mb] (50% decrease) [45% decrease]
6-Bin (2.0 GeV) Finder + Linker	0.53 mb (70% decrease)	1.0 mb (50% decrease)	0.61 mb (60% decrease)
2-Bin (1.5 GeV) + Stereo (2.0 GeV)	1.0 mb (40% decrease)	1.3 mb (35% decrease)	0.85 mb (45% decrease)
2-Bin (2.0 GeV) + Stereo (2.0 GeV)	0.83 mb (55% decrease)	1.2 mb (40% decrease)	0.75 mb (50% decrease)
2-Bin (2.5 GeV) + Stereo (2.5 GeV)	0.63 mb (65% decrease)	0.81 mb (60% decrease)	0.65 mb (60% decrease)
6-Bin Finder + Linker + Stereo (2.0 GeV)	0.32 mb (80% decrease)	0.80 mb (60% decrease)	0.44 mb (70% decrease)

Table 33: A summary of the track-trigger cross sections for the various XFT upgrade options quoted at a luminosity of  $3 \times 10^{32} \text{cm}^{-2} \text{s}^{-1}$ . Numbers for the degraded COT are given in square brackets.

## 6 Electron Trigger Rates at High Luminosities

Maintaining the performance of the high  $P_T$  physics program at high instantaneous luminosities is vital for the future of the experiment. As the growth of the track-only triggers steadily climbs, it becomes important to make certain that the high  $P_T$  trigger rates remain efficient, while minimizing the acceptance of fake high  $P_T$  objects. Electron trigger rates rise with luminosity due to an increased number of tracks pointing to a fixed number of electromagnetic energy clusters in the calorimeter.

To study high  $P_T$  electrons trigger rates at high luminosity, events from data having an 8 GeV electromagnetic cluster are selected by the level one trigger (L1 EM8), and merged with zero-bias data from the same run period according to the procedure in 4.1. Specifically, 10,000 level 1 EM triggers taken from run number 163064 are merged with zero bias from runs 164775 through 167023. During these runs, the COT and XFT are operating with standard configurations 6 months before COT aging became apparent. The COT hit information from each of the merged events is input into the XFT upgrade simulation, XFT2Sim, to produce a list of XFT tracks. The offline track lists are appended to one another and are used to identify real tracks. Only EM clusters from the L1 EM8 events are considered. This is justified since in contrast with the COT hit occupancy, the L1 EM8 trigger cross-section does not increase with luminosity as shown in the XMON plot, Figure 35.

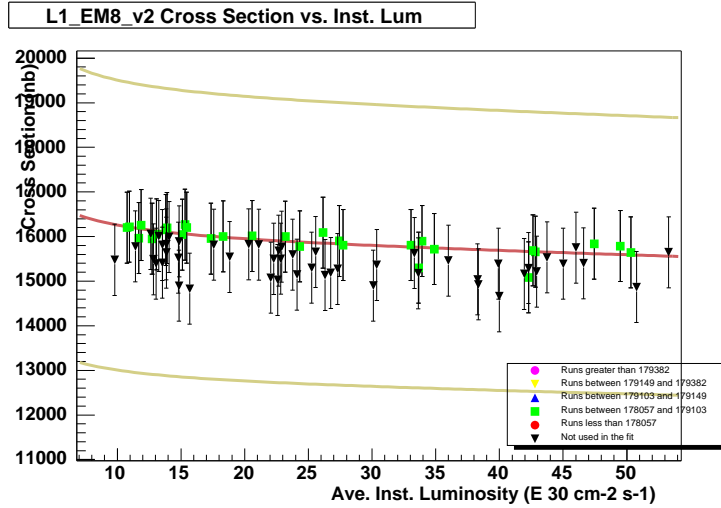


Figure 35: Cross-section for L1 EM8 trigger. For this analysis, the cross-section is conservatively estimated to be flat as a function of luminosity.

The L1 EM8 trigger cross-section is used to normalize the trigger cross-section for L1 CEM8 PT8 which is defined as

$$\sigma_{L1CEM8PT8} = \sigma_{L1EM8}(\mathcal{L}) \frac{N_{L1CEM8PT8}}{N_{L1EM8}}. \quad (3)$$

To validate XFT2Sim and the merging procedure, the L1 CEM8 PT8 trigger cross-section is

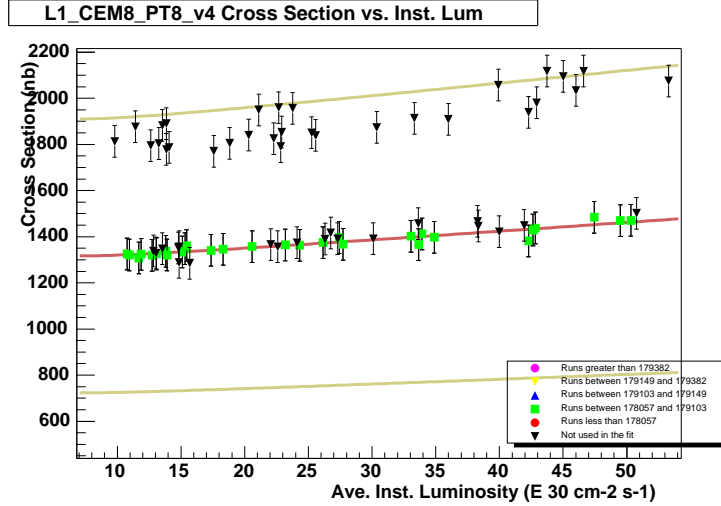


Figure 36: Cross-section for L1 EM8 PT8 trigger with real data. This is used only for comparison simulated results.

determined from the XMON plot in Figure 36 to be  $1.35 \mu \text{ b}$  at  $15 \cdot 10^{30} \text{ cm}^{-2} \text{ s}^{-1}$ , and used for reference in plots showing simulated results.

## 6.1 Simulated Electron Selection

From the sample of merged events with an EM cluster of at least 8 GeV, events are first required to have be central, mainly towers 7 through 16. An XFT track with three or four layers and having at least 8 GeV is required to match to this tower. The matching uses an algorithm similar to that of the XTRP such that tracks are extrapolated to the CES, and a  $P_T$ -dependent smearing factor determines a range of towers in which an electron would deposit its energy. Such events are considered to pass the L1 CEM8 PT8 trigger.

The event is considered to be a real electron trigger if it contains an offline track with  $P_T > 8 \text{ GeV}$ , at least 20 axial and 20 stereo hits, and pointing to an EM tower using the same CES extrapolating algorithm. Otherwise, the event is considered a fake electron. The “actual” trigger cross-section, measured using only offline tracks pointing to EM clusters, is  $1.14 \mu \text{ b}$ .

## 6.2 Simulated Scenarios

For each scenario, plots are shown with the total trigger cross-section in blue, fit with a second order polynomial, the fake trigger cross-section in red, and a star indicating the data point from Figure 36. The total cross-section at  $300 \cdot 10^{30} \text{ cm}^{-2} \text{ s}^{-1}$  is indicated on the plot. Beneath each plot is a summary of the real and fake trigger cross-sections at a range of luminosity values.

**2 Bin XFT** ... Table 34 and Figures 37 and 38 show the performance of the current XFT device simulated at a range of luminosities. Two time bins, prompt and delayed, are used to categorize each XFT hit. The  $P_T$  threshold for segments and roads is 1.5 GeV. XFT tracks may have three or four segments per track. The output for each segment is one of twelve phi positions per cell for the inner two axial layers, and one of 6 phi positions per cell plus three  $P_T$  bins for the outer two axial layers. Tracks can either be formed with a segment on all 4 layers, or in just the inner 3 layers. The current electron trigger uses both 3-layer and 4-layer tracks. However, it is clear that removing 3L tracks would reduce the fake cross-section significantly while removing very little of the real trigger rate.

Luminosity [ $1 \times 10^{32} \text{ cm}^{-2} \text{ s}^{-1}$ ]	0.5	1.0	1.5	2.0	3.0
Real 3L $\sigma$ [mb]	0.02	0.02	0.02	0.02	0.02
Fake 3L $\sigma$ [mb]	0.22	0.57	0.92	1.25	1.88
Total 3L $\sigma$ [mb]	0.24	0.59	0.93	1.26	1.89
Real 4L $\sigma$ [mb]	1.04	1.04	1.04	1.04	1.04
Fake 4L $\sigma$ [mb]	0.40	0.59	0.86	1.19	2.07
(Missed 4L) $\sigma$ [mb]	0.10	0.10	0.09	0.08	0.07
Total 4L $\sigma$ [mb]	1.44	1.63	1.90	2.23	3.11
Total 3L+4L $\sigma$ [mb]	1.67	2.22	2.83	3.49	5.00

Table 34: Trigger Cross-sections for the current, 2-bin, axial layer device, sorted by triggers from 3-Layer (3L) and 4-Layer (4L) XFT tracks. Missed refers to the fraction of the actual trigger cross-section which is not found using XFT tracks.

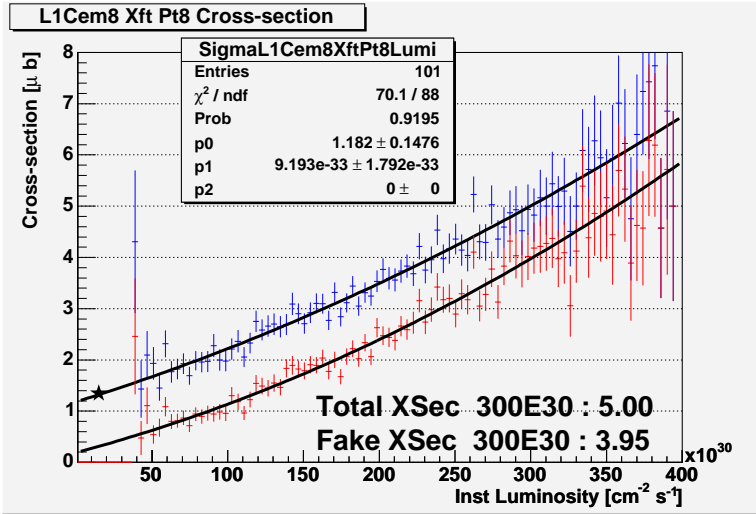


Figure 37: 8 GeV electron trigger simulated at high luminosities with current 2-bin device. The star is a data point from the current device. Both 3-layer and 4-layer xft tracks are included.

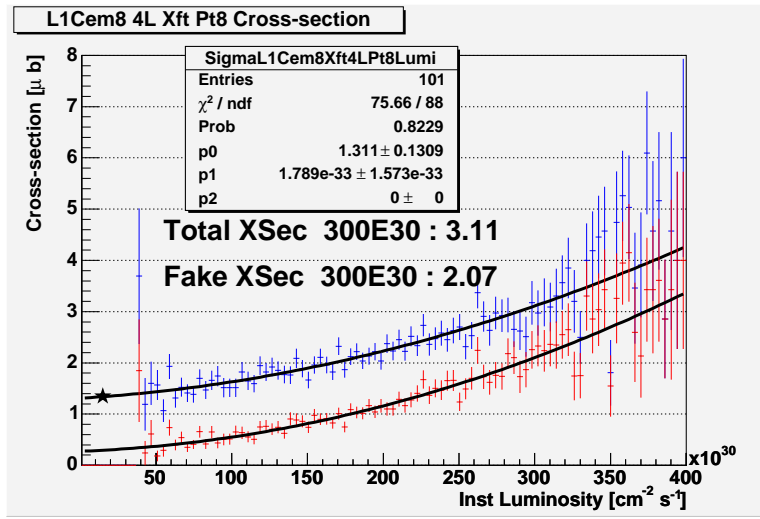


Figure 38: 8 GeV electron trigger simulated at high luminosities with current 2-bin device. The star is a data point from the current device. Only 4-layer tracks are included.

**2 Bin Degraded XFT,  $|P_T| > 1.5$  GeV ...**Table 35 and Figures 39 and 40 show simulated trigger cross-sections for the current device with degraded COT. The first axial superlayer, SL2, is masked completely on, and the second axial layer, SL4, is reduced to 80 % hit efficiency ( $\sim 50\%$  gain) before the COT hit merging is done. The number of misses allowed per layer in SL4 is increased from one to three to maintain segment finding efficiency. This scenario was evaluated after a problem was identified in the COT which was causing COT hit efficiency to decrease. Since then, the COT aging problem has been solved through the addition of air into the COT chamber. The effects of degraded COT on XFT performance will likely become largely historical.

Luminosity [ $1 \times 10^{32} \text{ cm}^{-2} \text{ s}^{-1}$ ]	0.5	1.0	1.5	2.0	3.0
Real 3L $\sigma$ [mb]	0.02	0.02	0.02	0.02	0.02
Fake 3L $\sigma$ [mb]	0.74	1.01	1.24	1.43	1.70
Total 3L $\sigma$ [mb]	0.75	1.02	1.25	1.45	1.72
Real 4L $\sigma$ [mb]	1.03	1.03	1.03	1.03	1.03
Fake 4L $\sigma$ [mb]	0.66	1.09	1.56	2.08	3.25
(Missed 4L) $\sigma$ [mb]	0.12	0.11	0.09	0.08	0.05
Total 4L $\sigma$ [mb]	1.69	2.12	2.59	3.11	4.28
Total 3L+4L $\sigma$ [mb]	2.45	3.14	3.85	4.55	5.99

Table 35: Trigger Cross-sections for degraded current, 2-bin, Axial Layer Device, sorted by triggers from 3-Layer (3L) and 4-Layer (4L) XFT tracks. Missed refers to the fraction of the actual trigger cross-section which is not found using XFT tracks.

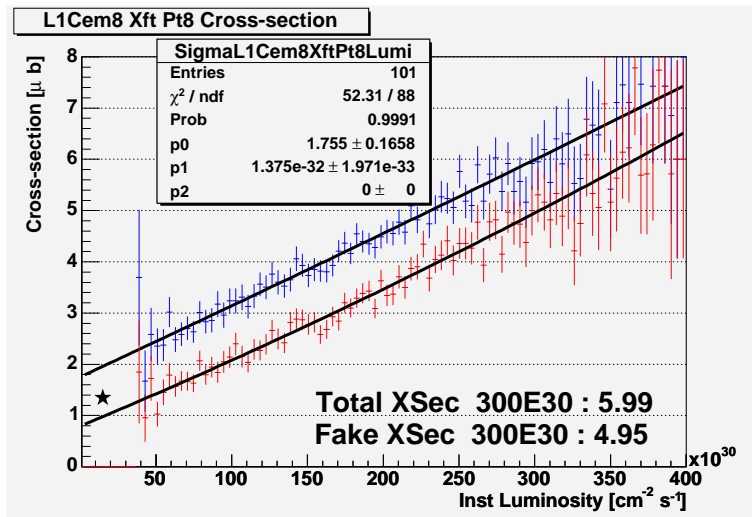


Figure 39: Simulated electron cross-section for current device with degraded COT using both 3-layer and 4-layer tracks.

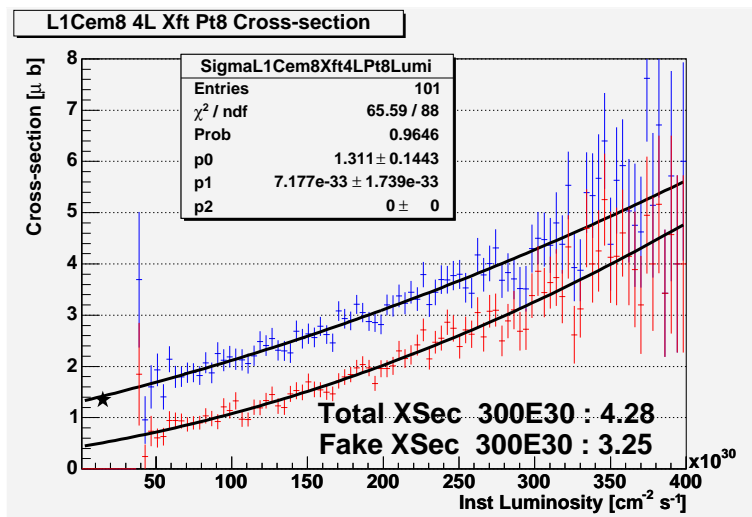


Figure 40: Simulated electron cross-section for current device with degraded COT using only 4-layer tracks.

**2 Bin XFT,  $|P_T| > 2.0$  GeV** ...Table 36 and Figures 41 and 42 show simulated trigger cross-sections with the  $P_T$  threshold for XFT segments and roads raised to 2.0 GeV. This reduces the number of fake segments which can join together to form spurious, higher  $P_T$  tracks. When raising the  $P_T$  threshold, there are several effects to be consider. The most important effect is that the trigger rate for electrons with 3-layer XFT tracks actually increases when the  $P_T$  threshold is raised. This happens because a linker will first report the highest  $P_T$  4-layer track in a 1.25 deg  $\phi$ -slice, and if none are found, will report the highest  $P_T$  3-layer track.

Luminosity [ $1 \times 10^{32}$ cm <sup>-2</sup> s <sup>-1</sup> ]	0.5	1.0	1.5	2.0	3.0
Real 3L $\sigma$ [mb]	0.02	0.02	0.02	0.02	0.02
Fake 3L $\sigma$ [mb]	0.31	0.72	1.17	1.66	2.75
Total 3L $\sigma$ [mb]	0.33	0.74	1.19	1.68	2.77
Real 4L $\sigma$ [mb]	1.02	1.02	1.02	1.02	1.02
Fake 4L $\sigma$ [mb]	0.38	0.52	0.73	0.99	1.71
(Missed 4L) $\sigma$ [mb]	0.13	0.12	0.11	0.10	0.07
Total 4L $\sigma$ [mb]	1.40	1.55	1.75	2.02	2.73
Total 3L+4L $\sigma$ [mb]	1.73	2.29	2.94	3.69	5.50

Table 36: Trigger Cross-sections for 2-bin, Axial Layer Device, with  $|P_T| > 2.0$  GeV, sorted by triggers from 3-Layer (3L) and 4-Layer (4L) XFT tracks. Missed refers to the fraction of the actual trigger cross-section which is not found using XFT tracks.

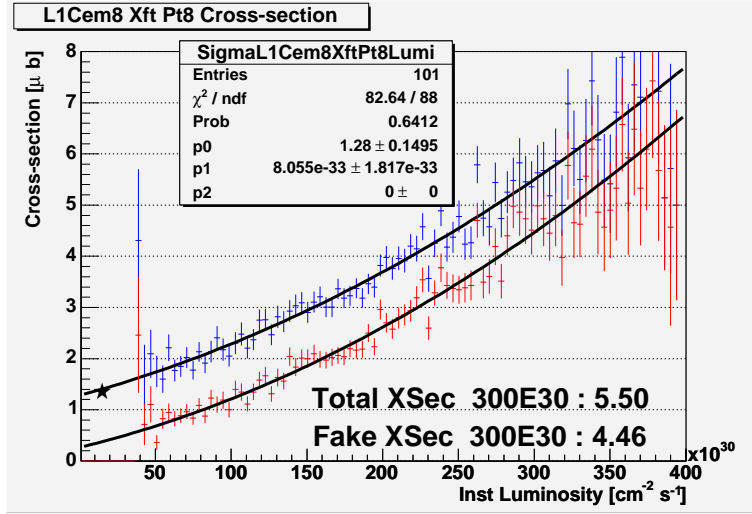


Figure 41: Simulated electron cross-section for 2-bin Finder with 2.0 GeV threshold for masks and roads. Both 3-layer and 4-layer tracks are included.

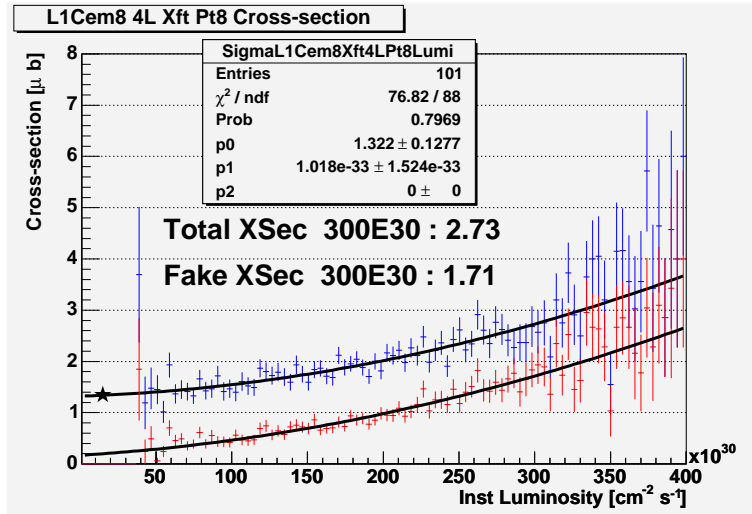


Figure 42: Simulated electron cross-section for 2-bin Finder with 2.0 GeV threshold for masks and roads. Only 4-layer tracks are included.

**2 Bin XFT,  $|P_T| > 2.5$  GeV ...** Table 37 and Figures 43 and 44 show the simulated trigger cross-sections with  $P_T$  threshold for XFT segments and roads raised to 2.5 GeV, further reducing fake segments leading to fake high  $P_T$  tracks.

Luminosity [ $1 \times 10^{32} \text{ cm}^{-2} \text{ s}^{-1}$ ]	0.5	1.0	1.5	2.0	3.0
Real 3L $\sigma$ [mb]	0.02	0.02	0.02	0.02	0.02
Fake 3L $\sigma$ [mb]	0.36	0.73	1.16	1.67	2.90
Total 3L $\sigma$ [mb]	0.38	0.74	1.18	1.69	2.91
Real 4L $\sigma$ [mb]	1.02	1.02	1.02	1.02	1.02
Fake 4L $\sigma$ [mb]	0.37	0.49	0.66	0.88	1.45
(Missed 4L) $\sigma$ [mb]	0.13	0.12	0.10	0.09	0.07
Total 4L $\sigma$ [mb]	1.40	1.52	1.69	1.90	2.47
Total 3L+4L $\sigma$ [mb]	1.77	2.26	2.87	3.59	5.39

Table 37: Trigger Cross-sections for 2-bin, Axial Layer Device, with  $|P_T| > 2.5$  GeV sorted by triggers from 3-Layer (3L) and 4-Layer (4L) XFT tracks. Missed refers to the fraction of the actual trigger cross-section which is not found using XFT tracks.

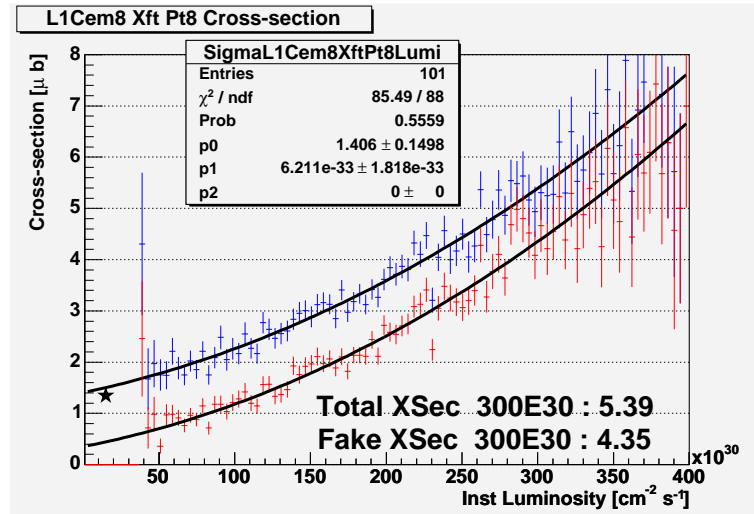


Figure 43: Simulated electron cross-section for 2-bin Finder with 2.5 GeV threshold for masks and roads. Both 3-layer and 4-layer tracks are included.

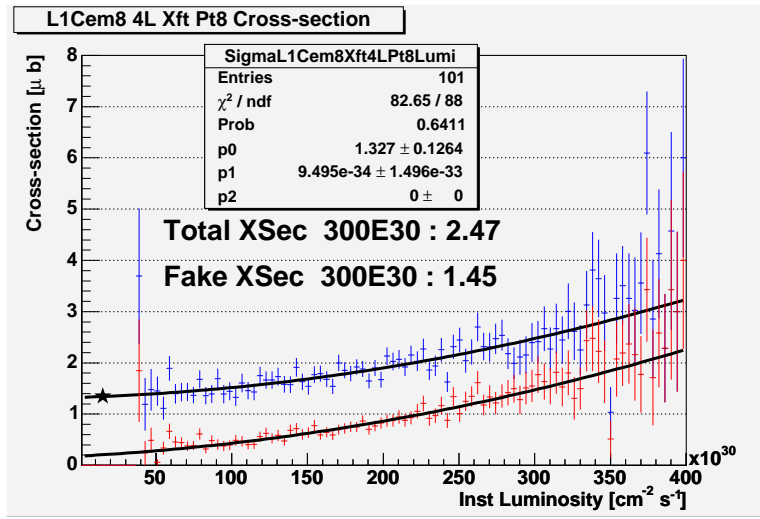


Figure 44: Simulated electron cross-section for 2-bin Finder with 2.5 GeV threshold for masks and roads. Only 4-layer tracks are included.

**6 Bin XFT, Finder-Only,  $|P_T| > 2.0$  GeV** ...Table 38 and Figures 45 and 46 show the simulated trigger cross-section for a 6 time-bin device with 4 axial layers. Each XFT hit is categorized by whether the signal is high in each of 6 equally-spaced time bins. This increased time resolution reduces fakes, but also increases the number of valid track segments by at least a factor of 7. Care is taken to use a segment finding mask set with sufficiently high efficiency which does not introduce an exorbitant amount of masks with only slight variation. By allowing one miss in the hit pattern, as in the current device, these slight variations are accommodated.

Luminosity [ $1 \times 10^{32} \text{ cm}^{-2} \text{ s}^{-1}$ ]	0.5	1.0	1.5	2.0	3.0
Real 3L $\sigma$ [mb]	0.01	0.01	0.01	0.01	0.01
Fake 3L $\sigma$ [mb]	0.19	0.33	0.51	0.73	1.30
Total 3L $\sigma$ [mb]	0.21	0.34	0.52	0.75	1.31
Real 4L $\sigma$ [mb]	1.02	1.02	1.02	1.02	1.02
Fake 4L $\sigma$ [mb]	0.35	0.45	0.57	0.72	1.11
(Missed 4L) $\sigma$ [mb]	0.10	0.10	0.09	0.09	0.08
Total 4L $\sigma$ [mb]	1.38	1.47	1.59	1.74	2.13
Total 3L+4L $\sigma$ [mb]	1.58	1.81	2.12	2.49	3.44

Table 38: Trigger cross-sections for the XFT with all 4 axial layers upgraded to 6 time bins of xft hit information. The  $P_T$  threshold is 2.0 GeV.

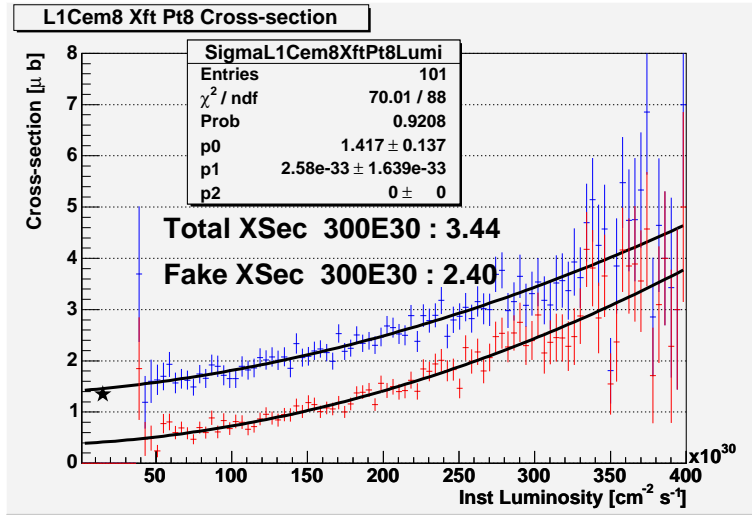


Figure 45: Simulated electron cross-section for 6-bin Finder with 2.0 GeV threshold. Both 3-layer and 4-layer tracks are included.

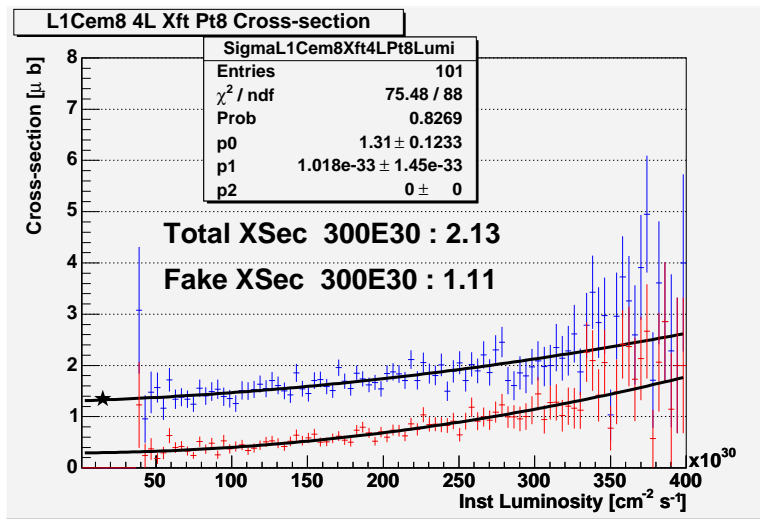


Figure 46: Simulated electron cross-section for 6-bin Finder with 2.0 GeV threshold. Only 4-layer tracks are included.

**6 Bin XFT, Finder-Only, Degraded,  $|P_T| > 2.0$  GeV ...** Table 39 and Figures 47 and 48 show the simulated trigger cross-section for a 6-Bin Finder with degraded COT.

Luminosity [ $1 \times 10^{32} \text{ cm}^{-2} \text{ s}^{-1}$ ]	0.5	1.0	1.5	2.0	3.0
Real 3L $\sigma$ [mb]	0.01	0.01	0.01	0.01	0.01
Fake 3L $\sigma$ [mb]	0.38	0.61	0.83	1.03	1.41
Total 3L $\sigma$ [mb]	0.39	0.62	0.84	1.04	1.42
Real 4L $\sigma$ [mb]	1.01	1.01	1.01	1.01	1.01
Fake 4L $\sigma$ [mb]	0.45	0.69	0.96	1.26	1.94
(Missed 4L) $\sigma$ [mb]	0.16	0.14	0.12	0.10	0.06
Total 4L $\sigma$ [mb]	1.47	1.71	1.98	2.27	2.95
Total 3L+4L $\sigma$ [mb]	1.86	2.33	2.81	3.32	4.37

Table 39: Trigger cross-sections for the XFT with all 4 axial layers upgraded to 6 time bins of xft hit information subject to degraded COT. The  $P_T$  threshold is 2.0 GeV.

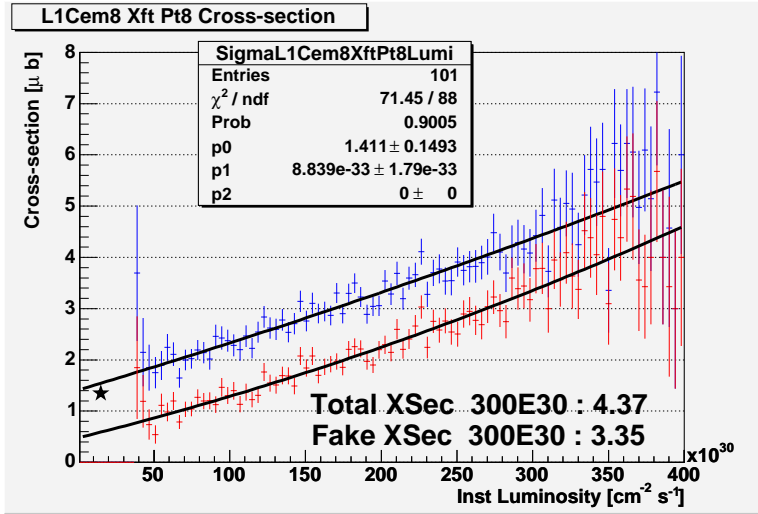


Figure 47: Simulated electron cross-section for 6-bin Finder with degraded COT. Both 3-layer and 4-layer tracks are included.

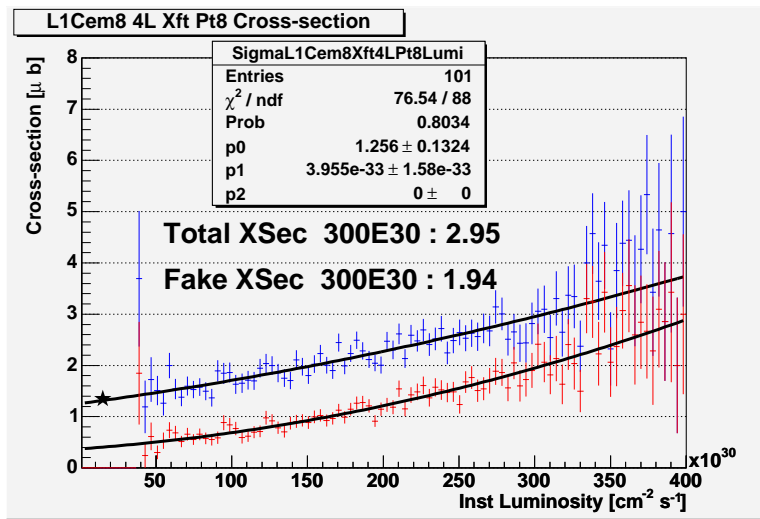


Figure 48: Simulated electron cross-section for 6-bin Finder with degraded COT. Only 4-layer tracks are included.

**6 Bin XFT, Finder+Linker,  $|P_T| > 2.0$  GeV** ...Table 40 and Figure 49 show trigger cross-sections for the Finder+Linker scenario, where segments are calculated using 6 time bins for the XFT hits, but output additional slope information to the segment linker. In the inner two layers, 3 slope bits are used for  $+P_T$ ,  $-P_T$ , and high  $P_T$  instead of no slope bits. In the outer two layers, 5 slope bits are used instead of 3. Therefore, the upgraded segment linker checks for tracks in a larger set of roads with improved resolution. The output tracks from the segment linker is still the same as in the 2-Bin and 6-Bin Finder schemes. The efficiency is lower for the upgraded linker since the large number of roads necessary to specify all the tracks cannot be all included due to the increase in fakes that would be generated.

Luminosity [ $1 \times 10^{32} \text{ cm}^{-2} \text{ s}^{-1}$ ]	0.5	1.0	1.5	2.0	3.0
Real 4L $\sigma$ [mb]	0.92	0.92	0.92	0.92	0.92
Fake 4L $\sigma$ [mb]	0.36	0.46	0.56	0.66	0.84
(Missed 4L) $\sigma$ [mb]	0.25	0.23	0.20	0.18	0.13
Total 4L $\sigma$ [mb]	1.28	1.39	1.49	1.58	1.77
Total 3L+4L $\sigma$ [mb]	1.28	1.39	1.49	1.58	1.77

Table 40: Trigger Cross-sections for 6-bin, Axial Layer Device, with  $|P_T| > 2.0$  GeV, and an upgraded linker which uses additional slope information about the segments. Tracks with 3 layers are not considered for the upgraded linker.

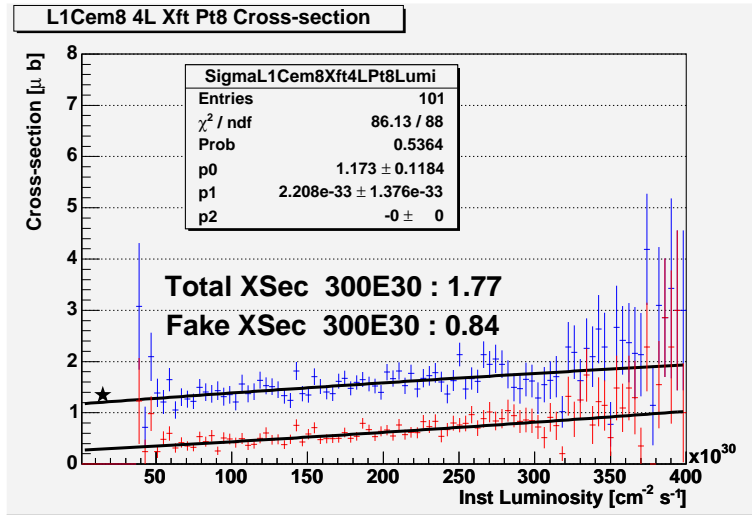


Figure 49: Simulated electron cross-section for 6-bin Finder plus upgraded linker. Only 4-layer tracks are included.

**2 Bin XFT, Stereo,  $|P_T| > 2.0$  GeV ...** Table 41 and Figures 50 and 51 show the XFT design using track rejection from segments in the two stereo superlayers, SL 5 and SL 7. A track passes the stereo rejection requirement if it extrapolates to within 3 cells of segments in the SL 5 and SL 7, and the sum of the signed displacements between the track and SL 5, and the track and SL 7 is less than 1.5 cells. This latter criterion takes advantage of the oppositely sloped stereo angles in SL 5 and SL 7. In addition, the output slopes of the segments in the stereo layers are required to be high  $P_T$  (which is true for  $|P_T| > 3.4$  GeV).

Luminosity [ $1 \times 10^{32} \text{ cm}^{-2}\text{s}^{-1}$ ]	0.5	1.0	1.5	2.0	3.0
Real 3L $\sigma$ [mb]	0.01	0.01	0.01	0.01	0.01
Fake 3L $\sigma$ [mb]	0.08	0.21	0.35	0.49	0.79
Total 3L $\sigma$ [mb]	0.09	0.22	0.36	0.50	0.80
Real 4L $\sigma$ [mb]	1.00	1.00	1.00	1.00	1.00
Fake 4L $\sigma$ [mb]	0.33	0.47	0.63	0.84	1.35
(Missed 4L) $\sigma$ [mb]	0.17	0.15	0.14	0.12	0.08
Total 4L $\sigma$ [mb]	1.33	1.47	1.64	1.84	2.35
Total 3L+4L $\sigma$ [mb]	1.42	1.69	1.99	2.34	3.15

Table 41: The 2-Bin Axial Finder with  $P_T$  threshold of 2.0 GeV, using stereo rejection from SL5 and SL7.

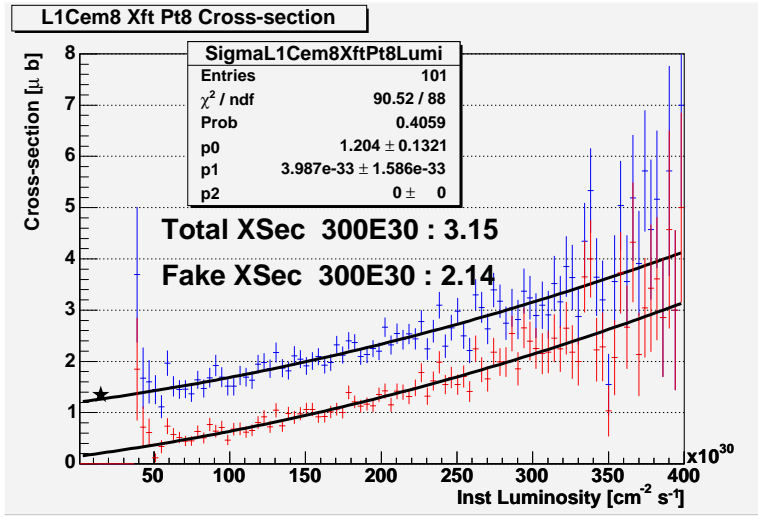


Figure 50: Simulated electron cross-section for 2-bin Finder with 2.0 GeV threshold for masks and roads, with stereo rejection from SL5 and SL7. Both 3-layer and 4-layer tracks are included.

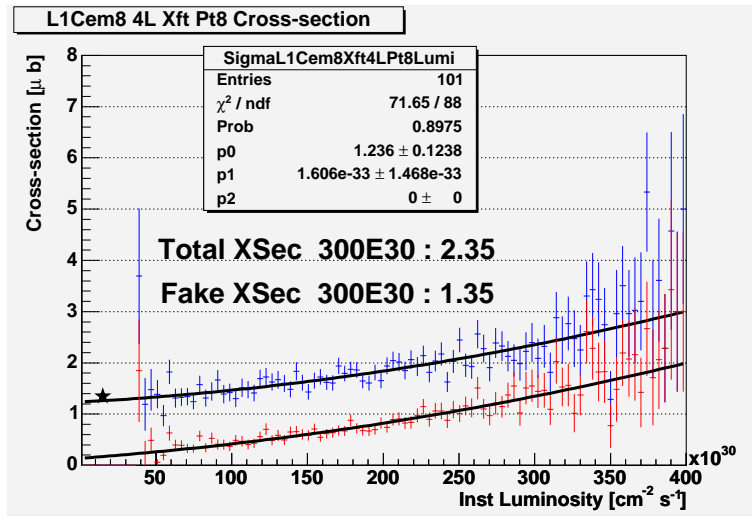


Figure 51: Simulated electron cross-section for 2-bin Finder with 2.0 GeV threshold for masks and roads, with stereo rejection from SL5 and SL7. Only 4-layer tracks are included.

**2 Bin XFT, Stereo,  $|P_T| > 2.5$  GeV** ...Table 42 and Figures 50 and 51 show the XFT design using track rejection from segments in the two stereo superlayers, SL 5 and SL 7.

Luminosity [ $1 \times 10^{32} \text{ cm}^{-2} \text{ s}^{-1}$ ]	0.5	1.0	1.5	2.0	3.0
Real 3L $\sigma$ [mb]	0.01	0.01	0.01	0.01	0.01
Fake 3L $\sigma$ [mb]	0.12	0.20	0.32	0.48	0.90
Total 3L $\sigma$ [mb]	0.13	0.21	0.33	0.49	0.91
Real 4L $\sigma$ [mb]	1.00	1.00	1.00	1.00	1.00
Fake 4L $\sigma$ [mb]	0.32	0.44	0.58	0.74	1.14
(Missed 4L) $\sigma$ [mb]	0.17	0.15	0.13	0.11	0.07
Total 4L $\sigma$ [mb]	1.33	1.44	1.58	1.74	2.14
Total 3L+4L $\sigma$ [mb]	1.46	1.65	1.91	2.23	3.05

Table 42: The 2-Bin Axial Finder with  $P_T$  threshold of 2.5 GeV, using stereo rejection from SL5 and SL7.

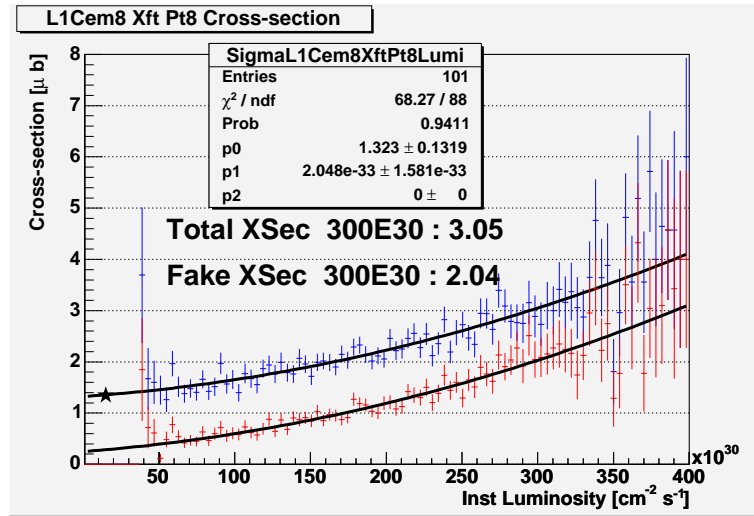


Figure 52: Simulated electron cross-section for 2-bin Finder with 2.5 GeV threshold for masks and roads, with stereo rejection from SL5 and SL7. Both 3-layer and 4-layer tracks are included.

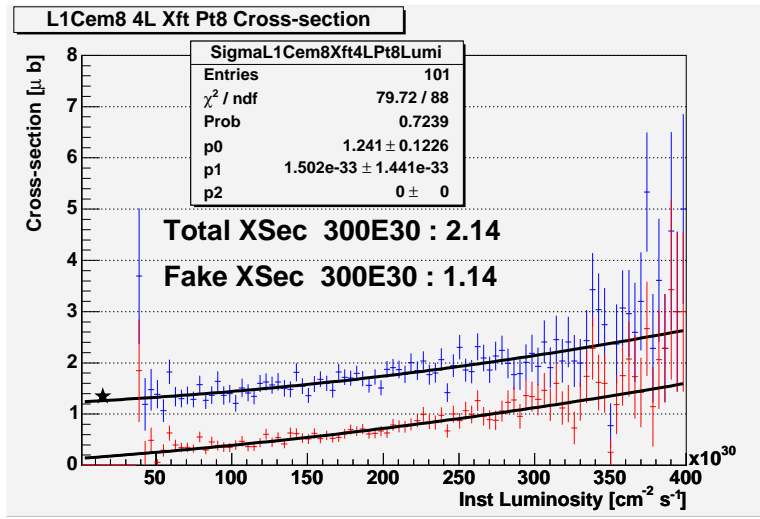


Figure 53: Simulated electron cross-section for 2-bin Finder with 2.5 GeV threshold for masks and roads, with stereo rejection from SL5 and SL7. Only 4-layer tracks are included.

**6 Bin XFT, Finder-Only, Stereo,  $|P_T| > 2.0$  GeV** ...Table 43 and Figures 54 and 55 show the 6-Bin Finder-only scheme using additional track rejection by failure to match appropriate stereo segments SL5 and SL7.

Luminosity [ $1 \times 10^{32} \text{ cm}^{-2} \text{ s}^{-1}$ ]	0.5	1.0	1.5	2.0	3.0
Real 3L $\sigma$ [mb]	0.01	0.01	0.01	0.01	0.01
Fake 3L $\sigma$ [mb]	0.07	0.13	0.19	0.25	0.41
Total 3L $\sigma$ [mb]	0.09	0.14	0.20	0.27	0.42
Real 4L $\sigma$ [mb]	1.00	1.00	1.00	1.00	1.00
Fake 4L $\sigma$ [mb]	0.33	0.41	0.51	0.64	0.97
(Missed 4L) $\sigma$ [mb]	0.13	0.12	0.11	0.10	0.08
Total 4L $\sigma$ [mb]	1.33	1.41	1.51	1.64	1.97
Total 3L+4L $\sigma$ [mb]	1.41	1.55	1.71	1.91	2.39

Table 43: 6-bin Finder + stereo rejection in SL5 and SL7. The  $P_T$  threshold used is 2.0 GeV.

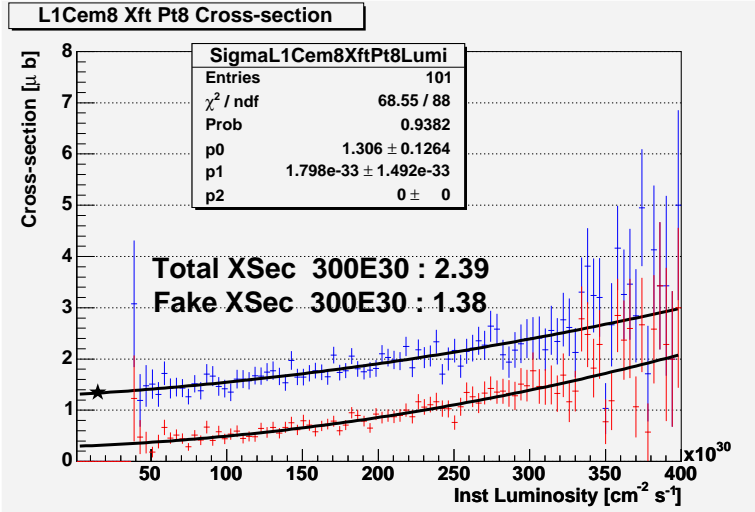


Figure 54: Simulated electron cross-section for 6-bin Finder with 2.0 GeV threshold for masks and roads, with stereo rejection from SL5 and SL7. Both 3-layer and 4-layer tracks are included.

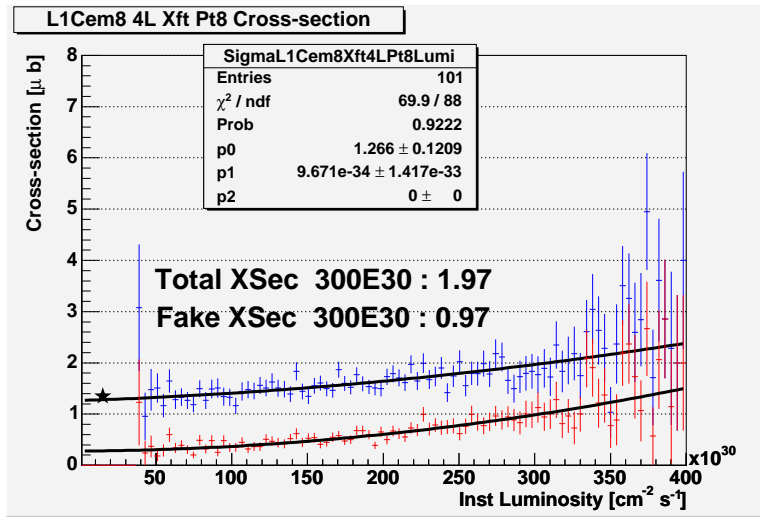


Figure 55: Simulated electron cross-section for 6-bin Finder with 2.0 GeV threshold for masks and roads, with stereo rejection from SL5 and SL7. Both 3-layer and 4-layer tracks are included.

**6 Bin XFT, Finder+Linker, 2L of Stereo,  $|P_T| > 2.0$  GeV** ...Table 44 and Figure 56 show the 6-Bin Finder+Linker scheme using additional track rejection from absence of stereo segments in SL5 and SL7.

Luminosity [ $1 \times 10^{32} \text{ cm}^{-2} \text{ s}^{-1}$ ]	0.5	1.0	1.5	2.0	3.0
Real 4L $\sigma$ [mb]	0.90	0.90	0.90	0.90	0.90
Fake 4L $\sigma$ [mb]	0.31	0.43	0.54	0.63	0.77
(Missed 4L) $\sigma$ [mb]	0.29	0.26	0.23	0.20	0.13
Total 4L $\sigma$ [mb]	1.21	1.34	1.44	1.53	1.67
Total 3L+4L $\sigma$ [mb]	1.21	1.34	1.44	1.53	1.67

Table 44: Cross-sections for the 6-bin finder with upgraded linker and stereo rejection in SL5 and SL7. Tracks with 3 layers are not considered for the upgraded linker.

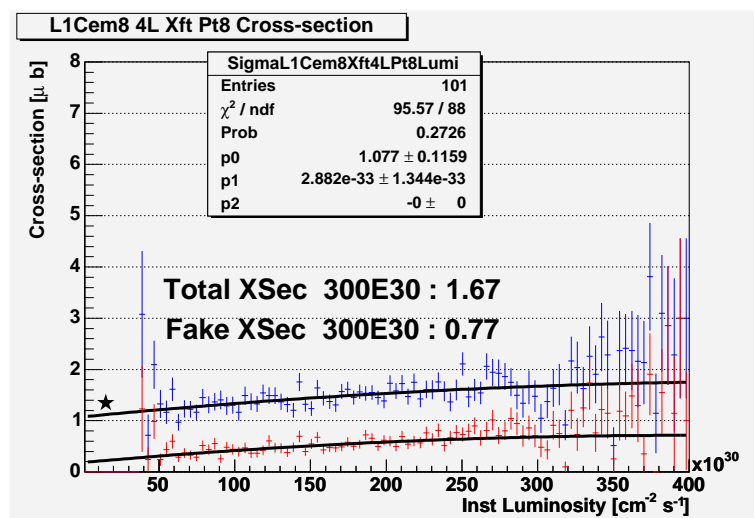


Figure 56: Simulated electron cross-section for 6-bin Finder plus upgraded linker, with stereo rejection from SL5 and SL7. Only 4-layer tracks are included.

**Baseline Upgrade: 6 Bin XFT, Finder+Linker, Stereo SL7,  $|P_T| > 2.0$  GeV ...** Table 45 and Figure 57 show trigger cross-sections for the baseline upgrade of 6 Bin Finder with upgraded Linker and stereo segment rejection in Super Layer 7.

Luminosity [ $1 \times 10^{32} \text{ cm}^{-2} \text{ s}^{-1}$ ]	0.5	1.0	1.5	2.0	3.0
Real 4L $\sigma$ [mb]	0.92	0.92	0.92	0.92	0.92
Fake 4L $\sigma$ [mb]	0.34	0.45	0.55	0.64	0.82
(Missed 4L) $\sigma$ [mb]	0.27	0.24	0.21	0.19	0.13
Total 4L $\sigma$ [mb]	1.26	1.36	1.46	1.56	1.73
Total 3L+4L $\sigma$ [mb]	1.26	1.36	1.46	1.56	1.73

Table 45: These are the results for the baseline upgrade which is a 6-Bin Finder, plus an upgraded linker, and Stereo Segment track rejection in SL7.

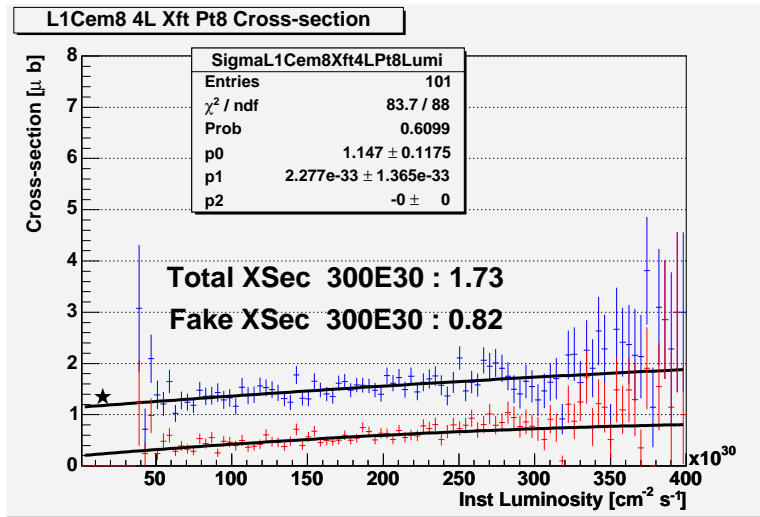


Figure 57: Simulated electron cross-section for 6-bin Finder plus upgraded linker, with stereo rejection from SL7. Only 4-layer tracks are included.

### 6.3 Summary of electron trigger rates

Many simulation scenarios were considered in terms of the trigger cross-section to high  $P_T$  electrons, which are defined as  $\geq 8$  GeV XFT tracks pointing to  $\geq 8$  GeV CEM clusters in events. Table 46 is a summary of the total trigger cross-sections for the scenarios outlined in this section.

Luminosity [ $1 \times 10^{32} \text{ cm}^{-2}\text{s}^{-1}$ ]	1.5	2.0	3.0
<b>Current 2 bin 3L</b>	<b>0.93</b>	<b>1.26</b>	<b>1.89</b>
<b>Current 2 bin 4L</b>	<b>1.90</b>	<b>2.23</b>	<b>3.11</b>
Current 2 bin 3L degraded	1.25	1.45	1.72
Current 2 bin 4L degraded	2.59	3.11	4.28
2 bin $ P_T  > 2.0$ 3L	1.19	1.68	2.77
2 bin $ P_T  > 2.0$ 4L	1.75	2.02	2.73
2 bin $ P_T  > 2.5$ 3L	1.18	1.69	2.91
2 bin $ P_T  > 2.5$ 4L	1.69	1.90	2.47
2 bin $ P_T  > 2.0$ 4L + Stereo	1.64	1.84	2.35
<b>2 bin <math> P_T  &gt; 2.5</math> 4L + Stereo</b>	<b>1.58</b>	<b>1.74</b>	<b>2.14</b>
6 bin Finder 3L	0.52	0.75	1.31
6 bin Finder 4L	1.59	1.74	2.13
6 bin Finder Degraded 3L	0.84	1.04	1.42
6 bin Finder Degraded 4L	1.98	2.27	2.95
6 bin Finder 3L + Stereo	0.20	0.27	0.42
6 bin Finder 4L + Stereo	1.51	1.64	1.97
6 bin Finder + Linker 4L	1.49	1.58	1.77
6 bin Finder + Linker 4L + Stereo (5,7)	1.44	1.53	1.67
<b>6 bin Finder + Linker 4L + Stereo (7)</b>	<b>1.46</b>	<b>1.56</b>	<b>1.73</b>

Table 46: Summary of trigger cross-sections for various upgrade scenarios, sorted by triggers from 3-Layer (3L) and 4-Layer (4L) XFT tracks. The scenarios in bold are the current device, the re-scoped upgrade, and the nominal baseline upgrade.

There is a significant fake rejection by only considering 4-layer tracks for both 2-bin and 6-bin options. At  $300\text{E}30 \text{ cm}^{-2}\text{s}^{-1}$ , eliminating 3-Layer tracks removes 40 % of events which are almost entirely fake.

The degraded COT scenario considered amounts to about a 20 % increase in fake electrons.

Electron trigger cross-sections using 3-Layer tracks actually increase for the 2-bin finder when the  $P_T$  threshold is raised, due to the replacing of a better quality low  $P_T$  track with a lower quality higher  $P_T$  track within the same linker slice.

Trigger cross-sections using the 2-bin finder with 4-layer tracks do decrease as expected when using a higher  $P_T$  threshold. This scenario has greater fake rejection at high luminosity.

The lowest rate expectedly belongs to a complete upgrade of 2-bin axial to 6-bin axial finder, 0-0-3-3-slope to 3-3-5-5-slope linker, plus the usage of 2 Stereo Layers for segment confirmation.

However, this also suffers from the lowest efficiency due to the necessary lack of a complete set of roads. More roads would flag more real electrons, but also more fake electrons.

The addition of 6-bin Stereo layers, the “re-scoped” XFT upgrade, represents a 31 % reduction in the trigger rate compared to a 44 % for the baseline upgrade at  $300\text{E}30 \times 10^{32} \text{ cm}^{-2}\text{s}^{-1}$ , and a 17 % reduction compared to a 23 % reduction at  $150\text{E}30 \times 10^{32} \text{ cm}^{-2}\text{s}^{-1}$ .

## 7 Conclusions

It is possible to meet the needs of CDF for high-luminosity running with a number of the XFT upgrade options presented here. The leading possibilities include upgrading the existing finder and linker boards in the XFT axial system to use six time bins of hit information (Option 2), adding stereo layers to the existing XFT axial system (Option 3), or upgrading both upgrading the existing axial system to six time bins and adding stereo layers (Options 2 + 3). Any of these options would meet the requirements of a factor of 3-4 reduction in the 7 GeV single-track trigger cross section and a factor of 2-4 reduction in the scenario C two-track trigger cross section. However, when one considers factors such as the risk of data loss due to commissioning difficulties and the amount of new hardware needed for the upgrade, the option of adding stereo layers to the current XFT axial system presents itself as the best choice.

Clearly, the option of doing both the 6-bin finder+linker axial upgrade plus the addition of a stereo XFT system provides the biggest performance boost. The roughly factor of five improvement in the single-track trigger cross section exceeds the goals of the upgrade and the factor of three improvement in the two-track trigger cross section fits comfortably in the desired range. However, it is interesting to note that these performance gains translate into only a factor of two improvement in the electron trigger rate, suggesting that these improvements are less significant when a high-purity trigger signal from another detector is combined with the XFT to produce a high- $p_T$  trigger. There is also evidence that the increased resolution of the linker upgrade means that a much larger set of roads is needed to maintain efficiency for high  $P_T$  tracks. Using a larger set of masks greatly increased the fake track rate, implying the same thing for the upgraded linker. Given the time remaining for completing the XFT upgrade, the complexity of simultaneously building and commission new axial and stereo hardware for the XFT makes this option unattractive.

Since both upgrading the existing axial XFT hardware and adding stereo coverage appears infeasible, the next best option is to do either the axial upgrade or the stereo upgrade by itself. Both options are predicted to yield similar XFT performance. The 6-bin finder + linker axial upgrade gives a factor of 3.3 improvement in the 7 GeV single-track trigger cross section, while the stereo upgrade provides a factor of 2.9 improvement. Both options give a factor of 2.5 improvement in the two-track trigger cross section. However, a main advantage of the stereo upgrade option is that it can be installed and commissioned without disrupting the operation of the current XFT system. The 6-bin axial upgrade option of the other hand, cannot be commissioned without interrupting current trigger operations. In addition, the stereo upgrade introduces a new aspect to the XFT track measurement—namely information about the three-dimensional trajectory of the track—that opens to door for new and unexplored trigger strategies that will not be available under the axial upgrade scenario. Although the current projections are based on the XFT stereo upgrade option using a higher minimum  $p_T$  threshold than the 6-bin finder + linker axial option, utilization of the three-dimensional tracking available with the stereo upgrade may make possible additional performance improvements that would allow a relaxing of this higher  $p_T$  threshold. Given that the performance of the two options is comparable, the stereo upgrade path proves clearly superior to the 6-bin axial upgrade. Table 47 provides a summary of the expected performance of the XFT stereo upgrade compared to the current XFT system.

	Efficiency	$p_T$ Resolution	$\phi_0$ Resolution	Single Track (7 GeV)	Scenario C Two-Track	CEM8 PT8
2-Bin (1.5 GeV) (Current System)	$p_T > 1.5$ GeV: 87.8% $p_T > 7$ GeV: 97.3%	2.3%/GeV	6.5 mRad	1.8 mb	1.5 mb	3.1 $\mu$ b
2-Bin + Stereo (2.5 GeV)	$p_T > 1.5$ GeV: 86.5% $p_T > 7$ GeV: 95.0%	2.2%/GeV	6.2 mRad	0.63 mb	0.65 mb	2.1 $\mu$ b

Table 47: A comparison of the predicted performance of the XFT stereo upgrade to the performance of the current XFT at a luminosity of  $3 \times 10^{32} \text{cm}^{-2} \text{s}^{-1}$ .

## References

- [1] J. Hoftiezer *et al.*, *XFT3D: A Proposal for Adding Stereo Segment Finding and 3D XFT Tracking in the Trigger*, CDF Note 4300 (1997).
- [2] J. Mueller and P. J. Wilson, *A 2 Track  $B^0 \rightarrow \pi^+\pi^-$  Trigger for Run II*, CDF Note 2665 (1994).